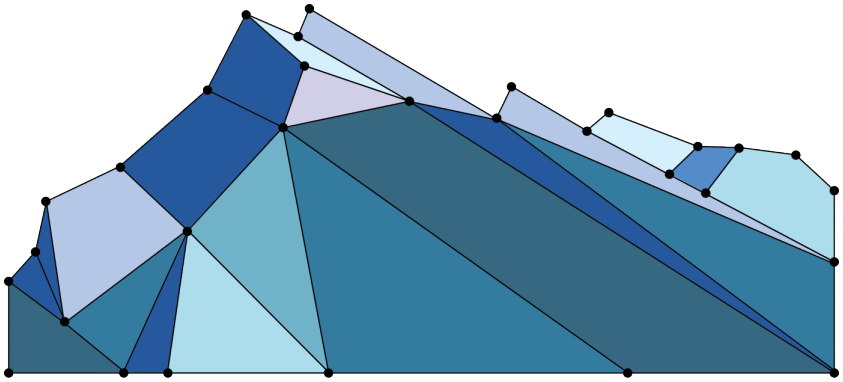

IUMAS8 June 11-16, 2023
Banff, AB Canada

Program

Overview

Conference: June 11 – 15, 2023

Kinnear Centre for Creativity & Innovation
Banff, AB, Canada

FIB SEM IUMAS CCEM Canadian Centre for Electron Microscopy MSC·SMC Promoting microscopy since 1972

SFR SYSTEMS FOR RESEARCH SOQUELEC JEOL

FULL MEETING OVERVIEW

Sunday, June 11, 2023

JSM-MSC Satellite Meeting: 4:55 – 9:40 pm
ZOOM Meeting ID: 812 8134 4380, Passcode: 102697

Monday, June 12, 2023

IUMAS & MAS Workshops / Welcome Reception

8:00	Registration		
8:45	MAS Workshop (KC 203)	9:00	IUMAS Workshop (KC 201)
10:40	Break	10:30	Break
11:00	MAS Workshop cont.		IUMAS Workshop cont'd
12:20	Lunch	12:30	Lunch
13:20	MAS Workshop cont'd	13:30	IUMAS Workshop cont'd
15:00	Break	15:00	Break
15:20	MAS Workshop cont'd	15:30	IUMAS Workshop cont'd
17:45	Registration/Welcome Reception		

Tuesday, June 13, 2023

IUMAS Meeting / FIB SEM Meeting / MSC Biological Sciences

8:30	Registration		
9:00	IUMAS Meeting (KC 203)	FIB SEM Meeting (KC 201)	
10:30	Break / Exhibition		
11:00	IUMAS Meeting cont'd	FIB SEM Meeting – Bio Focus	
12:30	Lunch / Exhibition / IUMAS Executive Meeting / MSC Executive Meeting		
14:15	IUMAS Meeting cont'd	FIB SEM Meeting cont'd	MSC – Bio Sciences (KC 101)
15:45	Break / Exhibition		
16:15	IUMAS Meeting cont'd	FIB SEM Meeting cont'd	MSC - Bio Workshop (KC 101)
18-21	Poster Session / Exhibition		

FULL MEETING OVERVIEW

Banquet:	KC 103	MSC Executive Meeting:	KC 202
Break / Exhibition:	KC 200 Galleria & KC 205	MSC Business Meeting:	KC 203
IUMAS Executive Meeting:	KC 206	Poster Session:	KC 200 Galleria & KC 205
Lunch:	Vistas Dining Room	Welcome Reception:	KC 200 Galleria & KC 205

Wednesday, June 14, 2023

Joint IUMAS & MSC Meeting / Banquet

9:00	Plenary Physical Sciences (KC 203 / 201)	
9:45	Plenary Biological / Materials Sciences (KC 203 / 201)	
10:30	Break / Exhibition	
11:00	TEM / STEM / Analytical (KC 203)	Biological Sciences (KC 201)
12:30	Lunch / Exhibition	
14:15	TEM / STEM / Analytical cont'd	Biological Sciences cont'd
15:45	Break / Exhibition	
16:15	Material Applications cont'd	Biological Sciences cont'd
18 – 22	Banquet	

Thursday, June 15, 2023

Joint IUMAS & MSC Meeting

9:00	Keynote Physical Sciences (KC 203 / 201)		
9:45	Keynote Biological Sciences (KC 203 / 201)		
10:30	Break / Exhibition		
11:00	Material Applications cont'd (KC203)		Biological Sciences cont'd (KC 201)
12:30	Lunch / Exhibition		
14:15	Spectroscopy/Spectromicro. (KC 203)	13:45	SEM/ESEM/in situ (KC201)
15:45	Break / Exhibition	15: 15	Break / Exhibition
16:15	Spectroscopy/Spectromicro. cont'd	15:45	Data Processing/Correlative (KC 201)
17:30	MSC Business Meeting (KC 203)		

PROGRAM

Sunday, June 11, 2023

4th Annual Joint Workshop Microscopical Society of Canada & Japanese Society of Microscopy
ZOOM Meeting ID: 812 8134 4380 Passcode: 102697
Hybrid meeting: virtual and in-person

Limits of electron and ion beam analysis and their application to nanoscience

Electrons and ions allow imaging, chemical and structural analysis at sub-nanometer scale in many materials of interest to physical and biological sciences. The practical limits can arise from the instrumentation, the interactions responsible for the measured signal and, ultimately, by radiation damage inflicted on the studied sample by the incident beam. Presentations in this year's symposium discuss the practical aspects of pushing the boundaries of electron and ion microscopy instrumentation, and the practical problems applying the electron and ion beam analysis to real-world samples in physical and biological sciences.

Time (Edmonton)	Time (東京)	Name	Title
16:55	7:55	Ken Harada; Marek Malac	Opening Remarks
17:00	8:00	Takehito Seki	Direct Electromagnetic Field Imaging at Defects by Differential Phase Contrast Scanning Transmission Electron Microscopy
17:30	8:30	Nadi Braidy	Encapsulation of dyes in carbon nanohorns
18:00	9:00	Cathal Cassidy	Gas-based charge compensation measured by off-axis holography in environmental TEM
18:30	9:30	Martin Coulliard	Disentangling EELS signals from optical modes in photonic and plasmonic nanoparticle dimers and trimers
19:00	10:00	Koudai Niitsu	Magnetic configurations of a skyrmionic vortex stabilized in FeGe nanoparticles
19:30	10:30	Nabil Bassim	Insights about Atomic-Scale Heteroepitaxy based on Correlative Electron Microscopy of Van der Waals Heterostructures
20:00	11:00	Makoto Schreiber	Lensing charged particles with the magnetic vector potential
20:30	11:30	Makoto Kuuwahara	Time-Resolved Measurement in TEM using a Semiconductor Photocathode
21:00	12:00	Alyssa Williams	Improved Visualization of Bone Ultrastructure in 3D FIB-SEM
21:30	12:30	Natalie Reznikov	The ultrastructure of bone in 3D: A twist of twists
22:00	13:00	Shigeo Mori,;Misa Hayashida	Closing Remarks

MAP

Banquet:	KC 103	MSC Executive Meeting:	KC 202
Break / Exhibition:	KC 200 Galleria & KC 205	MSC Business Meeting:	KC 203
IUMAS Executive Meeting:	KC 206	Poster Session:	KC 200 Galleria & KC 205
Lunch:	Vistas Dining Room	Welcome Reception:	KC 200 Galleria & KC 205

Ground Floor

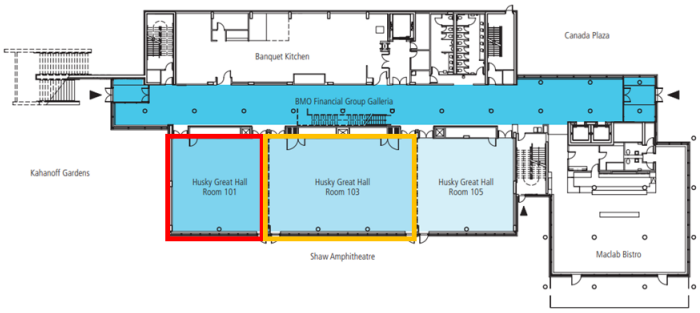

Second Floor

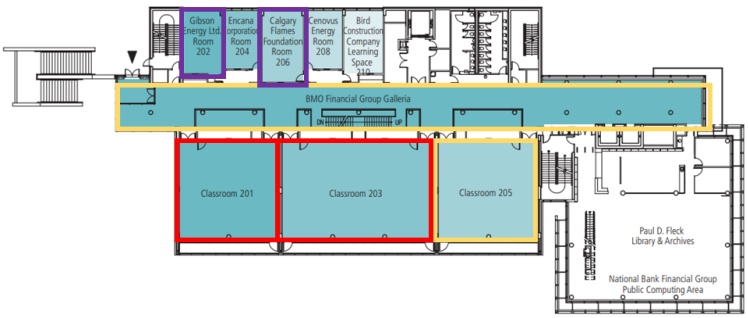

MSC·SMC
Promoting microscopy since 1972

SOQUELEC JEOL

HITACHI
Inspire the Next

The Japanese Society of Microscopy

PROGRAM

Monday, June 12, 2023

MAS Workshop: Open-Source Data Analysis (KC 203)

Organizers: Andy Herzing & Josh Taillon, National Institute of Standards and Technology
MAS is pleased to sponsor a topical workshop on Open-source software tools for microanalysis, taking place as part of IUMAS-8: The 8th Meeting of the International Union of Microbeam Analysis Societies in Banff, Alberta. This workshop will be highly interactive and aims to provide attendees with the skills necessary to feel comfortable running their own analyses using the various software packages and methods presented.

Time	Name	Title
8:45	Andy Herzing & Josh Taillon, National Institute of Standards and Technology	Welcome: Workshop Goals
9:00	Francisco de la Pena, Université de Lille	Hyperspy
10:00	Carter Francis, University of Wisconsin-Madison	Pyxem
10:40	Break	
11:00	Jonas Lähnemann, Paul Drude Institute for Solid State Electronics	LumiSpy
11:40	Hakon Anes, Norwegian University of Science and Technology	Kikuchipy
12:20	Lunch	
13:20	Colin Ophus, National Center for Electron Microscopy	py4DSTEM
14:20	Kevin Roccapriore, Oak Ridge National Lab	Machine Learning
15:00	Break	
15:20	Nicholas Ritchie, National Institute of Standards and Technology	NexL
16:00	Michael Jackson, BlueQuartz Software, LLC	DREAM.3D
16:40	Marcus Hanwell, Brookhaven National Laboratory	Tomography and Open-Source Software
17:20	Andy Herzing & Josh Taillon	Closing Remarks: Wrap -up
17:45	Welcome Reception	

IUMAS Workshop: Quantitative Microanalysis and Microfluorescence Imaging (KC 201)

Organizers: Gianluigi Botton, McMaster University and Canadian Light Source and Colin MacRae, CISRO
This full day workshop consists of two components. The first part of the workshop aims to cover the theory and practical aspects of microanalysis of complex materials where quantification is challenging due to the sensitivity of the samples to the electron beam interaction. The second part of the workshop covers the application of state-of-the-art microfluorescence imaging carried out within scanning electron microscopes, the comparison with EDS imaging in SEM, and the use of synchrotron light sources for macro-micro-nano scale imaging of a broad range of materials.

Time	Name	Title
9:00	Gianluigi Botton and Colin McRae	Overview of the Workshop
9:00	Nick Wilson, CISRO	Advanced Analysis of Minerals: sample preparation, cryo-microanalysis, quantification, matrix corrections, Soft XES for characterization of materials
9:45	Karsten Goemann, University of Tasmania	RE analysis using overlap corrections
10:30	Break	
11:00	Colin MacRae, CISRO	Cathodoluminescence and cryo-CL
12:30	Lunch	
13:30	Gianluigi Botton, McMaster University and Canadian Light Source	Overview of synchrotron techniques, combining photon and electron beam techniques
14:15	Andrea Somogyi, Synchrotron SOLEIL	X-ray optics for chemical imaging, detectors, X-Ray Fluorescence, X-Ray Absorption Spectroscopy imaging
15:00	Break	
15:30	Ibi Bondici, Canadian Light Source	Applications of Microfluorescence Imaging
16:00	Thomas Lam, Smithsonian Institution	Comparison of EDS and Microfluorescence Imaging in the SEM
17:00	All Speakers	Q&A Session on the workshop
17:45	Welcome Reception	

PROGRAM

Tuesday, June 13, 2023

Keynote Presentation (KC 203 & KC 201)

FIB SEM: Michael Phaneuf (9 AM – 9:45 AM)
An Imperfectly Recollected History of FIB in Canada (K01)

IUMAS Meeting (KC 203)

Time	ID	Name	Title
9:00	I01	Dale Newbury	Challenges in Low Beam Energy Electron-Excited X-ray Microanalysis with Energy Dispersive Spectrometry (EDS)
9:30	C01	Paul Carpenter	Advances in Quantitative EPMA Compositional Mapping Applied to Meteorites
9:45	C02	Colin MacRae	Measurement and correction of optical response in an EPMA
10:00	C03	Nicholas Ritchie	Comparing Direct-Fit and Filter-Fit k-ratios from EDS Spectra
10:15	ECS1	Alan Salek	Microstructural Study of Carbon Phases in Ureilite Meteorites using Electron Microscopy
11:00	I02	Nick Wilson	Cathodoluminescence and Soft X-ray Characterisation of Meteorite Samples using an EPMA
11:30	C04	Edward Vincenzi	Quantitative Assessment of X-ray Attenuation under Atmosphere to Vacuum Conditions
11:45	C05	Dawei Gao	Neural network-based MC X-ray for quantitative analysis of elements
12:00	I03	Karsten Goeman	Spectral cathodoluminescence and trace element mapping of apatite from the Ernest Henry deposit, Australia
14:15	I04	Philippe Jonnard	X-ray spectroscopy of lithium
14:45	C06	Khalil Hassebi	Detection of Li K Emission In Different Lithium Compounds
15:00	C07	Raynald Gauvin	Towards Quantitative Maps of Lithium in the Electron Microscope
15:15	C08	Yinuo Li	Quantitative Analyzation on Aluminum Alloys
15:30	C09	Jonas Lähnemann	Temperature-Dependent Generation Volume in Semiconductors Under Electron Beam Excitation
16:15	I05	Andrea Somogyi	Multilength-scale and multimodal scanning hard X-ray imaging and tomography of mesoscale samples
16:45	ECS2	Hadas Sternlicht	4D-STEM Characterization of Microstructural Transformations in Conductive Polymers Used for Li-ion Battery Anodes
17:00	ECS3	Juhyeok Lee	Advanced 3D Imaging via Multislice Electron Tomography using 4D-STEM
17:15	ECS4	Shenlan Yang	Micro-alloyed and ultralight elements in nano-scale precipitates in Al-Cu-Mg-Ag and Al-Cu-Li alloys revealed using atomic-resolution scanning transmission electron microscopy
17:30	C10	Robert Stroud	TESCAN TENSOR a 4D-STEM for Multimodal Characterization of Challenging and Interesting Specimens

FIB SEM Meeting (KC 201)

Time	ID	Name	Title
9:00	K01	Michael Phaneuf	An Imperfectly Recollected History of FIB in Canada
9:45	C11	Julia Deitz	Prospects of Full-scale Device Characterization via Ultra Short Pulsed Lasers with Dual Focused Ion Beams
10:00	C12	Guozhen Zhu	Controlling the Morphology of Rutile Nanowires by Focus-Ion-Beam Irradiation
10:15	C13	Bhaveshkumar Kamaliya	Beyond Direct Milling by FIB: Peculiar Self-Organization, Self-Assembly and Site-Specific Defect Engineering on the Surfaces
11:00	I06	Natalie Reznikov	The ultrastructure of bone in 3D: A twist of twists
11:30	C14	Alyssa Williams	Enhanced Visualization of Collagen Fibril and Mineral Ellipsoids in Bone Tissue Using FIB-SEM Nanotomography and Advanced Analysis Tools
11:45	C15	Mehdi Mosayebi	3D Reconstruction and Characterization of Lath Martensite in 13Cr-4Ni Stainless Steels Using PFIB-EBSD Serial Section Tomography
12:00	C16	Jiri Dluhos	FIB-SEM Tomography: Measuring Slice Thickness With Ga And Xe Ion Species FIBs And Stage Rocking
14:15	I07	Xiangli Zhong	Optimization, Minimising and Elimination of FIB Induced Defects
14:45	C17	Brenton Knuffman	High-Resolution FIB and SIMS with a Cesium Low Temperature Ion Source
15:00	C18	Jamie Ford	ToF-SIMS on a Plasma FIB: Dos and Don'ts
15:15	C19	Cheryl Hartfield	Novel LaserFIB Sample Preparation of Pillar Arrays For Synchrotron Imaging
15:30	C20	Jaroslav Kastyl	Automated preparation of high-quality lamellae using artificial intelligence assessed by 4D-STEM multimodal analysis
16:15	I08	Annalena Wolff	Scanning Transmission Helium Ion Microscopy – How Does It Compare to TEM?
16:45	ECS5	Maria Wątroba	Experimental analysis of plastic deformation in single-crystalline and ultrafine-grained Zn micropillars
17:00	C21	Rick Passey	Practical Applications of the Multi-Ion Species Plasma Focused Ion Beam
17:15	C22	Yang Yu	The next generation FIB source: GaBiLi ions for 2D and 3D ion microscopy
17:30	C23	Patrick Phillips	A new FIB/SEM for TEM sample preparation workflow

PROGRAM

Tuesday, June 13, 2023

MSC Biological Sciences (KC 101)

Time	ID	Name	Title
14:15	C24	Marc McKee	The Stenciling Principle for Extracellular Matrix Mineralization
14:45	C25	Ahmad Jomaa	The translating bacterial ribosome at 1.55 Å resolution by open access cryo-EM
15:15	C26	Jose Moran-Mirabal	Visualizing Cellulose Nanostructure with High Resolution Microscopy

MSC Biological Sciences Workshop (KC 101)

Organizers: Joey Davis, MIT; Joaquin Ortega, McGill University
This workshop will start by describing the cryoDRGN tool and capabilities for cryo-EM image classification. This introduction will be done by Dr. Joey Davis (MIT) who is part of the cryoDRGN developing team. The second hour of the workshop will be a discussion panel on currently available tools in image classification and how to deal with heterogeneous specimens.

Posters (Second Floor Galleria)

Session	ID	Name	Title
IUMAS	P01	James J. Dynes	Distribution and Speciation of Selected Elements in Insect Wings
IUMAS	P02	Joesph Stitsky	Exploring Phase in Soft X-ray Spectroptychography
FIB SEM	P03	Stéphanie Bessette	3D EDS-EBSD and segmentation of battery materials
Bio Sciences	P04	Khalid Al-Naemi	Low tension attachments are capable of chromosome capture
Bio Sciences	P05	Shannon Sim	Phosphoregulation of γ-tubulin regulates anti-parallel microtubule bundling through kinesin-5
Bio Sciences	P06	Eran Ittah	The Cornea Conundrum: How to Balance High Resolution and Context While Preserving Native Tissue Architecture
TEM / STEM / Analytical	P07	Sajad Shakerin	High-resolution characterization of additively manufactured bimetal using focus ion beam milling
TEM / STEM / Analytical	P08	Ken Harada	Observation of Magnetic Bubbles in $BaFe_{12-x-\delta}Sc_xMg_\delta O_{19}$ by Lorentz Microscopy and Electron Holography
TEM / STEM / Analytical	P09	Anitha Jose	Investigation of InGaN/GaN NW p-i-n junctions using Electron Holography

PROGRAM

Wednesday, June 14, 2023

Plenary Presentations (KC 203 / 201)

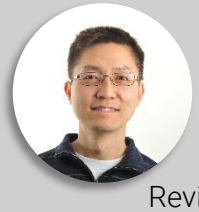

Physical Sciences: C. Shan Xu (9 AM – 9:45 AM)
Enable discoveries in life science using enhanced FIB-SEM (P01)

Biological / Material Sciences: Harald Hess (9:45 AM – 10:30 AM)
Review of Large Volume Imaging with Electrons and Cryo-Super-Resolution Microscopy (P02)

TEM / STEM / Analytical (KC 203)

Time	ID	Name	Title
11:00	I10	Maureen Lagos	Unveiling thermal properties of nanoscale cavities using electron spectroscopy
11:30	C27	Marek Malac	NanoMi: an Introduction to an Open-Source Electron Microscope
11:45	C28	Peter Neathway	Quantification of Entanglement Between Aloof Swift Electrons and Geometrically Fractal Nanoprisms
12:00	C29	John Donovan	The Holy Trinity of Microanalysis: Standards, K-ratios and Physics
1215	C30	Francisco de la Peña	Progress on applications of event-driven direct electron detectors to electron microscopy
14:15	I11	Vaso Tileli	Solid-liquid-gas interfacial phenomena and quantification of reaction product in liquid phase electron microscopy
14:45	ECS6	Gabriel T. Santos	Structural, chemistry, and electronic state of the interfaces of transparent conducting oxide and hematite applied in photoelectrocatalysis
15:00	C31	Carter Francis	A Method for Spatial Sampling of Metallic Glass Structure and Evolution Using 4-D STEM and Time Resolved 4-D STEM
15:15	C32	Kenneth Beyerlein	Watching Phase Transformations with a Dynamic Transmission Electron
15:30	C33	Arthur Blackburn	Sub-Ångström Resolution Imaging at 20 keV in a Scanning Electron Microscope from Ptychography with Integrated Projection Lens Distortion Correction

Materials Applications (KC 203)

Time	ID	Name	Title
16:15	I12	Marc Willinger	Applications of Environmental SEM as In-Situ Surface-Science Tool with Atomic Layer Sensitivity
16:45	C34	Venkata Kuppili	High Resolution X-ray Ptychography at the Cryo STXM endstation, Soft Xray Spectromicroscopy (SM) Beamline, Canadian Light Source
17:00	C35	Christian Vollmer	Functional chemistry of extraterrestrial organic matter revealed by high spatial resolution synchrotron spectroscopy – electron microscopy techniques
17:15	C36	Emmanuelle Brackx	Corium materials characterizations through electron microscopy and X-ray diffraction
17:30	C37	Nadi Braidy	Carbon Nanohorn Assembly and Structure Revealed by Aberration- Corrected Transmission Electron Microscopy

Biological Sciences (KC 201)

Time	ID	Name	Title
11:00	I12	Ian Dobbie	CryoSIM: the trials and tribulations of correlative super resolution cryo fluorescence imaging
11:30	C38	Jinyang Liang	Single-shot Photoluminescence Lifetime Imaging Microscopy using Compressed Sensing
11:45	C39	Polina Beskrovnaya	Outer membrane biogenesis in Acetonema longum
12:00	C40	Dominic Arpin	Cooperativity of ribosome associated GTPases in the assembly of the bacterial ribosome
12:15	I13	Joe Davis	Visualizing Massive Macromolecular Complexes in Motion with Cryo-EM, Cryo-ET, and Deep Learning
14:15	I14	Elitza Tocheva	Studies of the bacterial cell envelope using advanced imaging approaches
14:45	C41	Susanne Bechstedt	Multiscale imaging of microtubules
15:00	C42	Jackie Vogel	Interrogating the properties of a microtubule (+) endassociated nanoscale condensate in living cells using super-resolution microscopy
15:15	I15	William Hancock	From iSCAT to SCATTIRSTORM: Adventures in single-molecule microscopy
16:15	I16	Gili Naveh	Non-uniformity of the periodontal ligament: the dense collar in 3D
16:45	C43	Toni Tang	Lactation-induced changes in bone cellular and sub-cellular networks: indication for altered bone mineral transport
17:00	C44	Joaquin Ortega	RbgA Ensures the Correct Timing in the Maturation of the 50S Subunits Functional Sites
17:15	C45	Mouhanad Babi	Studying the hierarchical structure and nanoscale dislocations of bacterial cellulose using sr-CLEM
17:30	C46	Joseph Deering	The Three-Dimensional Structure of the Gecko Eggshell

PROGRAM

Thursday, June 15, 2023

Keynote Presentations (KC 203 / 201)

Physical Sciences: Takehito Seki (9 AM – 9:45 AM)
Advanced Phase Imaging in Scanning Transmission Electron Microscopy (K02)

Biological Sciences: Peijun Zhang (9:45 AM – 10:30 AM)
Multi-scale imaging by cryoEM: from cellular volumes to molecules at near-atomic resolution (K03)

Materials Applications (KC 203)

Time	ID	Name	Title
11:00	C47	Kodai Niitsu	Determination of magnetic exchange stiffness by measuring magnetic domain wall width
11:15	C48	Babafemi Agboola	Imaging and Spectroscopy of Kagome Lattice YCr_6Ge_6
11:30	C49	Jingyi Qu	Elucidating Structural and Chemical Modification of Ambient-Conditioned $LiNi_{0.8}Mn_{0.1}Co_{0.1}O_2$ with a Lithium Boron Carbon Oxide Coating with Analytical Electron Microscopy and X-ray Absorption Spectroscopy
11:45	C50	Robert Klie	Discovery of 1-dimensional TiO2 lepidocrocite
12:00	C51	Martin Couillard	Nanomineralogy in mining and environmental research
12:15	C52	Rodney Herring	Phase Imaging Dislocation Strain Annihilation at Crystal Surface Forming Pit

Spectroscopy / Spectromicroscopy (KC 203)

Time	ID	Name	Title
14:15	I17	Ann Chiaramonti	Atom Probe Tomography Using Wavelength-Tunable, Femtosecond-Pulsed Coherent Extreme Ultraviolet Radiation
14:45	C53	Ka Yin Lee	Hyperbolic Phonon Polaritons in Twisted Bilayers Revealed by Electron Energy Loss Spectroscopy
15:00	C54	Marcelo Martinho	Vibrational Spectroscopy of Single Molecular Nanocrystals in the Electron Microscope
15:15	C55	Pia Schweizer	Quantitative electron probe microanalysis of lithium in different materials including battery compounds
15:30	ECS7	Takahiro Ozawa	Isotope effect on lattice location of hydrogen in titanium hydride nanofilms revealed by Channeling NRA
16:15	C56	Heather Lowers	Cathodoluminescence Response of Barite at Room and Liquid Nitrogen Temperatures
16:30	C57	Isobel Bicket	Probing Near- and Far-Field Responses of the Magnetic Dipole Mode in a Plasmonic Split Ring Resonator
16:45	C58	Milenka Andelic	Investigation of structure and chemical properties of core/shell germanium/germanium-tin nanowires
17:00	C59	Bradley De Gregorio	EELS Characterization of Niobium Oxide Memristor Devices

Biological Sciences (KC 201)

Time	ID	Name	Title
11:00	I18	Monica Pillon	Defining How Ribonucleases Regulate Gene Expression
11:30	C60	Jingyu Sun	Dissecting the role of the universally conserved protein KsgA in the maturation process of 30S ribosomal subunit
11:45	C61	Amal Seffouh	Novel insights into the role of the YsxC GTPase in the assembly of the 50S ribosomal subunit revealed by Cryo-EM
12:00	C62	Ameena Hashimi	Cell Envelope Architecture of Chloroflexi Revealed by Cryo-Electron Tomography
12:15	I19	Matthew McCallum	Antigenic mapping with single particle cryoEM to reveal sites of vulnerability and immune evasion for SARS-CoV-2 variants

SEM / ESEM / in situ (KC 201)

Time	ID	Name	Title
13:45	I20	Erdmann Spiecker	Combining transmission diffraction and imaging in SEM: Prospects for in situ microscopy of thin films and 2D materials
14:15	C63	Moon Kim	Phase Transformation Study of 2D Materials by in-situ STEM
14:30	ECS8	Łukasz Rychłowski	Optimization of projection center based on EBSD Kikuchi band intensity profiles
14:45	C64	Yushun Liu	Real-time Slip Planes Monitoring during In-situ Nanoindentation Enabled by Hollow-cone Dark-field Imaging
15:00	C65	Ruth Birch	In Situ EBSD Studies of Blocky Grain Growth in Welded Zircaloy-4

Data Processing / Correlative (KC 201)

Time	ID	Name	Title
15:45	I21	James LeBeau	Direct Quantification of Short-Range Order in Materials by Combining STEM and Spatial Statistics
16:15	C66	Hrishikesh Bale	Investigation of stress corrosion cracking in CMSX-4 turbine blade alloys using Deep Learning assisted X-ray microscopy
16:30	C67	Robert Klie	Variational Convolutional Autoencoders for Anomaly Detection in Scanning Transmission Electron Microscopy
16:45	C68	Frédéric Voisard	Interpretation of serial section 3D EDX maps: multivariate analysis and deep learning hybrid approach
17:00	C69	Rasool Doostkam	Overcoming Phase Identification Ambiguity in the Analysis of SAED Patterns from Polymorphic Nanomaterials
17:15	C70	Ben Britton	Correlative energy dispersive X-ray spectroscopy (EDS/X) and electron backscatter diffraction (EBSD) analysis of

K01: An Imperfectly Recollected History of FIB in Canada

Michael W. Phaneuf
Fibics Incorporated, Ottawa, Ontario, Canada

In 1986 Melngailis estimated the worldwide population of focused ion beam (FIB) microscopes to be approximately 35 systems [1]. Thirteen years later, this author estimated the worldwide population to have grown to perhaps 25 times that number [2]. Proliferation of FIB and FIB-SEM microscope systems has continued at a fast pace and today the number of systems that have been installed in Canada alone is several times Melngailis' original number.

While the author admits to being an imperfect and undoubtedly biased historian, the return of the FIB SEM Meeting to Canada has provided the inspiration for this talk, which will endeavour to recount the history of FIB, as we know it, from the earliest systems in Canada. The first such system is believed to be a JEOL JIBL150 system installed at the National Research Council in 1989, predominantly for lithography-related applications (Figure 1, below). Four years later in 1993 the first FIB purchased by industry, a Micrion 9000, was installed at Northern Telecom Limited. Four years after that the first FIB capable of SEM-rivalling <5nm image resolution and many of the breadth of applications across multiple fields that we have come to expect of today's systems (not just semiconductor FIB) was installed at Fibics Incorporated (a Micrion 2500, installed in 1997). It is interesting to note all three of these early systems were installed in Ottawa.

This talk will draw on the recollection of some of those individuals involved in the early days of FIB in Canada. While the research institutes and universities that were early adopters of this technology typically had mandates to publish, the early work done by and for industry did not always see the light of day. A selection of "almost forgotten" or never published work from this period (drawing somewhat heavily from Fibics' archives) will be highlighted. Please note: A timeline of FIB installations in Canada will be presented and shared; to suggest system installation information for this timeline, please contact the author at mphaneuf@fibics.com.

References:
1. Melngailis, J., 1987. Critical Review: Focused ion beam technologies and applications. J. Vac. Sci. Technol., B. 5 (2), 469-495.
2. Phaneuf, M.W., 1999. Applications of focused ion beam microscopy to materials science specimens. Micron 30, 277-288.

Figure 1(Right): The first "true" FIB system in Canada, the JEOL JIBL150 Ion Beam Lithography system is "unveiled" at the Nation Research Council of Canada's Institute for Microstructural Sciences in February of 1990, after installation earlier in 1989. A direct-write LMIS machining application is shown. Please refer to the original newspaper article for complete details.

Heavens! 1,711 angels on a pin*point*

Ion beam machine is cutting edge in circuitry

By Jane Wilson
Citizen staff writer

Adding a new twist to an age-old question, scientists at the National Research Council have discovered how many angels can dance on the *point* of a pin.

The answer: 1,711.

Finding out how many angels could dance on the *head* of a pin would have taken too much time, said Ernie Kornelsen, manager of the NRC's new focused ion beam facility, the next generation in computer wizardry.

It's the first such machine in Canada and one of five in North America, putting researchers in Ottawa alongside AT&T and IBM in pursuing new developments in integrated computer circuitry.

The computerized machine can engrave such a small area with precision and speed that it drew 1,711 perfect little angels in a circular pattern on the point of a pin in 40 seconds flat.

The lines were 1/500th the size of a human hair.

All this expensive computer fire-power was unveiled with a flourish Tuesday. The NRC has set up the $2.5-million research facility with Bell-Northern Research, Northern Telecom and the Department of Communications sharing the $200,000 annual operating costs.

Faculty and graduate students from the University of Ottawa, Carleton and Queen's will have access to the equipment.

But the Japanese-made machine is not

(above) Drew Gragg, Citizen, (right) NRC photo
Above: Ernie Kornelsen with $2.5M machine; **Right:** Each angel is three millionths of a metre tall

Excerpted from *The Ottawa Citizen*, February 7th, 1990, page F7 (page 69).

K03:Multi-scale imaging by cryoEM: from cellular volumes to molecules at near-atomic resolution

Peijun Zhang[1,2]

[1] Division of Structural Biology, Wellcome Trust Centre for Human Genetics, University of Oxford, Oxford, OX3 7BN, UK

[2] Diamond Light Source, Harwell Science and Innovation Campus, Didcot OX11 0DE, UK

Structures of purified proteins and protein complexes are routinely determined to atomic or near-atomic resolutions using single particle cryoEM. Structures of macromolecular assemblies that are intrinsically flexible and dynamic, and often function in higher-order assemblies that are heterogeneous, have recently been analyzed to near-atomic resolutions using cryoET and subtomogram averaging (STA). The study of native complexes in cells using cryoET STA, coupled with cryoFIB/SEM and correlative and multiscale imaging, opens a new frontier in structural cell biology. I will present our recent multi-modal, multi-scale imaging of SARS-CoV-2 infection (1) and particulate methane monooxygenase (pMMO) in methanotrophic bacteria (2) to demonstrate the power of combining serial cryoFIB/SEM volume imaging with cell lamellae-based cryoET STA.

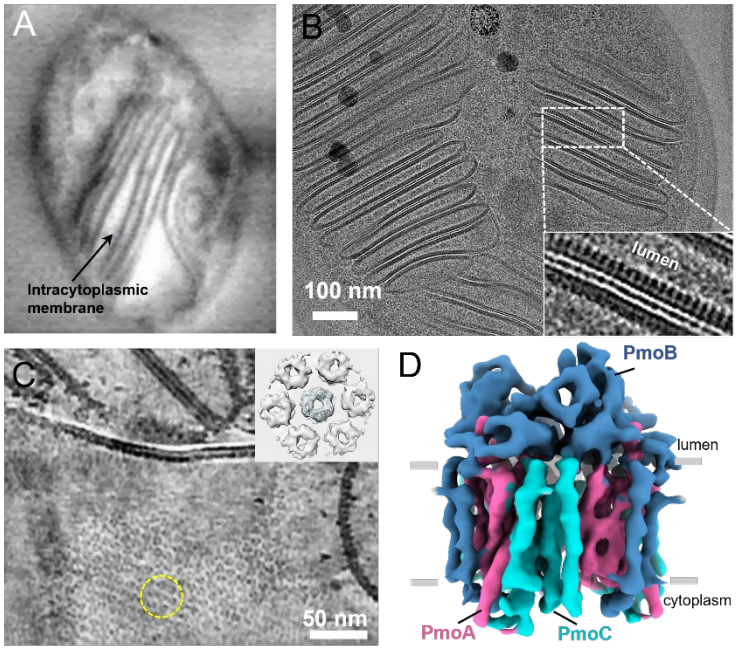

Figure 1. Native pMMO structure from methanotrophic bacteria. (A) Representative slices from serial cryoFIB/SEM volumes of methanotrophic bacteria. (B) An image of cryoFIB lamella of M. capsulatus. Inset, enlarged view of boxed area, displaying comb-like protein arrays. (C) A tomographic slice of M. capsulatus lamella displaying hexagonal arrays of particles. Inset, a subtomogram average of the 7-particle volume. (D) The pMMO trimer suntomogram averaging map at 4.8 Å resolution, consisting of PmoA (pink), PmoB (blue), and PmoC (cyan).

References:

1. Mendonça L, Howe A, Gilchrist JB, Sheng Y, Sun D, Knight ML, Zanetti-Domingues LC, Bateman B, Krebs AS, Chen L, Radecke J, Li VD, Ni T, Kounatidis I, Koronfel MA, Szynkiewicz M, Harkiolaki M, Martin-Fernandez ML, James W, Zhang P* (2021) Correlative multi-scale cryo-imaging unveils SARS-CoV-2 assembly and egress. Nat Commun. 12(1):4629.

2. Zhu Y, Koo CW, Cassidy CK, Spink MC, Ni T, Zanetti-Domingues LC, Bateman B, Martin-Fernandez ML, Shen J, Sheng Y, Song Y, Yang Z, Rosenzweig AC, Zhang P* (2022) Structure and activity of particulate methane monooxygenase arrays in methanotrophs. Nat Commun 13(1):5221.

P01:Enable discoveries in life science using enhanced FIB-SEM

C. Shan Xu[1]
[1] Department of Cellular and Molecular Physiology, Yale School of Medicine, New Haven, CT, USA

Isotropic high-resolution imaging of large volumes provides unique opportunities to study biology. Conventional Focused Ion Beam Scanning Electron Microscopy (FIB-SEM) offers high resolution (< 10 nm in x, y, and z) and robust image alignment. However, its prevailing deficiencies in imaging speed and duration cap the maximum possible image volume to less than 10^3 μm^3. To enable large volume high resolution imaging, we redesigned the system architecture and transformed FIB-SEM from a conventional system lacking long term reliability to a robust imaging platform with 100% effective reliability: capable of years of continuous imaging without defects in the final image stack [1].

This enhanced FIB-SEM technology has expanded the maximum imageable volume by more than 4 orders of magnitude, leading to several breakthrough discoveries in life science. Notably, the creation of the largest connectome to date was enabled with superior z resolution that facilitates automated tracing of neuronal processes while minimizing the time-consuming human proofreading effort [2]. Furthermore, this technology has facilitated the creation of the first open-access, 3D atlas of whole cells and tissues at an unprecedented isotropic resolution of 4-nm voxels [3]. These accomplishments demonstrate the immense potential of FIB-SEM technology in driving transformative advancements in life sciences research.

References

[1] Xu CS, et al. Enhanced FIB-SEM systems for large-volume 3D imaging. *eLife* 2017; **6**: e25916.
[2] Scheffer LK, et al. A connectome and analysis of the adult *Drosophila* central brain. *eLife* 2020; **9**: e57443.
[3] Xu CS, et al. An open-access volume electron microscopy atlas of whole cells and tissues. *Nature* 2021; **599** 147-151.

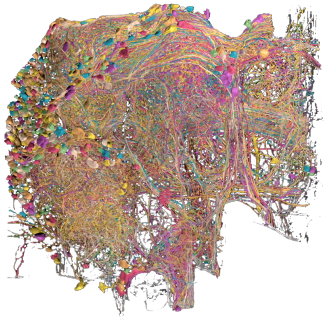

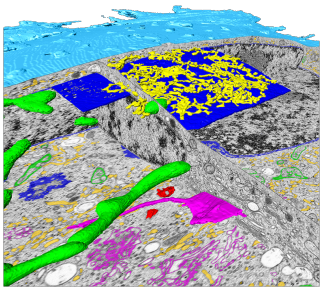

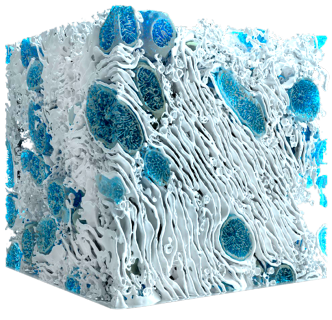

P02: Review of Large Volume Imaging with Electrons and Cryo-Super-Resolution Microscopy

Harald Hess
Janelia Research Campus, HHMI, Ashburn, Virginia, USA

Volume or 3D electron microscopy continues to expand its potential for imaging ever larger biological entities. Images from diamond knife cut sections launched the field of volume EM. An alternative of imaging the sequentially cut block face offered easier use and registration. FIB-SEM or Focused Ion Beam Scanning Electron Microscopy liberated the z resolution from the limits of minimal diamond section thickness and achieves a step edge resolution of 5-10 nm in the xy and most importantly the z directions. While this resolution is not up to the standards of TEM's, such resolution is of unique value when it encompasses whole cells and complete tissues. We will review the capabilities of FIB-SEM, which has imaged a complete fly brain and can routinely image 0.1 mm^3 sized volumes. Bigger volumes can be accessed by using thick (~20 microns thick) with a hot diamond knife followed by the finer FIBSEM imaging and milling. A cryogenic sample preparation protocol enables cryo-super-resolution microscopy to be paired with the FIB-SEM microscopy for correlative insight into biology. Examples are presented and prospects of future challenges are discussed. Finally, a MultiBeam imaging system which we call IBEAM-MSEM, Ion Beam Etching And Milling Multi Scanning Electron Microscope can image much larger volumes approaching 1.0 mm^3. It uses a hybrid cutting approach too, with samples cut into 100-1000 nm thickness and milled with an oblique ion or ion cluster beam followed by etching and wider area imaging with a 91 beam multiSEM.

I01:Challenges in Low Beam Energy Electron-Excited X-ray Microanalysis with Energy Dispersive Spectrometry (EDS)

Dale E. Newbury[1] and Nicholas W.M. Ritchie[1]
[1]National Institute of Standards and Technology, Gaithersburg, MD 20899 USA

Electron-excited X-ray microanalysis with energy dispersive spectrometry (EDS) following the standards-based protocol (using pure elements, stoichiometric compounds, etc.) can achieve a high level of analytical accuracy when the beam energy is selected in the "conventional range", e.g., $E_0 \geq 10$ keV. This choice enables excitation of suitable K, L, or M characteristic X-rays for all elements of the Periodic Table, except H and He, which do not produce characteristic X-rays. Typically, when challenge specimens of independently known composition and homogeneity are analyzed, the observed Relative Deviation from Expected Value, where RDEV= ([measured – known]/known) x 100%, is within than ±2.5% for 95% or more of analyses. When analysis is performed in the low beam energy regime, $E_0 \leq 5$ keV, achieving a similar level of accuracy is subject to several challenges: (1) The need to use less well characterized, low photon energy peaks for many elements, e.g., the Ti L-family instead of the Ti K-family and the Ba M-family instead of the Ba L-family. These lower energy peak families have lower fluorescence yield, which reduces the intensities relative to the continuum X-ray background, and extend over a wider range of energy, making peak fitting more challenging. Furthermore, the multi-edge structure of the L- and M- families can lead to dramatic self-absorption effects that depend subtly upon the material. (2) These families may overlap with the peaks of C and O, which are often present, further complicating peak fitting. (3) "Chemical effects": The relative intensity of the characteristic peaks of the L- and M- families may be altered by the chemical environment, which will affect peak fitting accuracy because of deviation from the peak reference model. (4) Every sample is layered. Surface layers that arise from oxidation and/or contamination are typically sufficiently thin relative to the total electron range so as to have a negligible effect for high beam energy analysis. At low beam energy, a shallow surface layer constitutes a much larger fraction of the electron range, which effectively means that two or more materials are simultaneously sampled. Multilayer analysis methods and Monte Carlo electron trajectory spectrum simulation are critical tools for analysis of such complex specimens. (5) As the beam energy is reduced below 5 keV, progressively more elements are effectively lost to analysis due to reduced or no excitation. The limits of detection at a given beam dose for a particular element become progressively poorer as the beam energy is reduced.

Estimating the accuracy of low beam energy analysis with the standards-based protocol requires careful consideration of all these challenges. The results for analysis at $E_0 = 5$ keV of EDS measurements made on a carefully curated set of 95 materials (including standard reference materials and stoichiometric compounds) containing 38 elements reveals a distribution of RDEV such that 95% of analyzed atomic concentrations fell within ±5% RDEV.

I02:Cathodoluminescence and Soft X-ray Characterisation of Meteorite Samples using an EPMA

Nick Wilson[1], Colin MacRae[1], Zsanett Pintér[1], Aaron Torpy[1], Dougal G. McCulloch[2], Alan G. Salek[2], Brenton A. Cook[2], and Andrew G. Tomkins[3]

[1] CSIRO Mineral Resources, Microbeam Laboratory, Clayton, Victoria Australia.
[2] Physics, School of Science, RMIT University, Melbourne, Victoria, Australia.
[3]School of Earth, Atmosphere and Environment, Monash University, Melbourne, Victoria, Australia

The addition of cathodoluminescence (CL) and soft x-ray emission spectrometers (SXES) to microprobes gives access to spectroscopies that provide sample information not available from wavelength dispersive or energy dispersive spectrometers. We have developed software and hardware to allow collection of the backscatter electron signal, WDS, EDS, SXES and CL spectral data simultaneously. This unique instrument enables us to avoid pixel misalignment and minimising electron beam induced damage artefacts associated with multiple pass mapping, in addition to that of the time saved. Fig. 1(a), shows a combination of CL and x-ray analysis, where the two carbon allotropes, lonsdaleite and diamond, are being distinguished using CL[1]. Spectra collected from the SXES detector also aid in the identification of the allotropes, and when combined with first-principles theoretical calculations of spectral shapes, they can give further insights into the material.

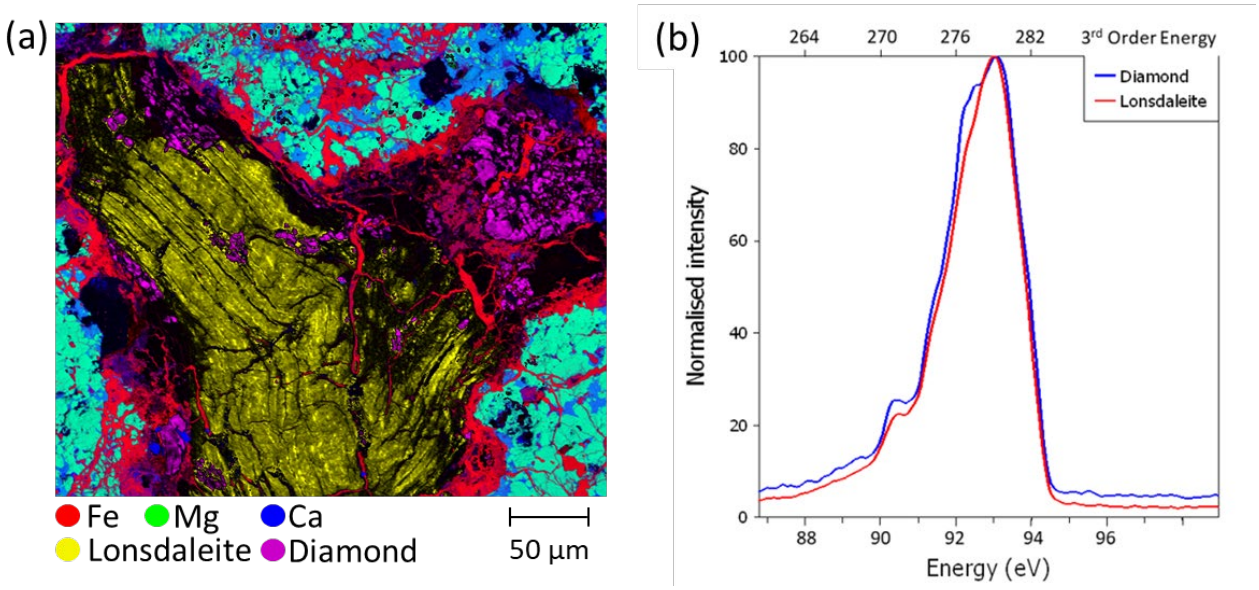

Figure 1. (a) Map showing lonsdaleite region within a ureilite (NWA 7983), (b) SXES spectra collected from diamond and lonsdaleite regions.

References

[1]Tomkins, A. G., Wilson, N. C., MacRae, C., Salek, A., Field, M. R., Brand, H. E. A., Langendam, A. D., Stephen, N. R., Torpy, A., Pintér, Z., Jennings, L. A., & McCulloch, D. G. (2022). Sequential Lonsdaleite to Diamond Formation in Ureilite Meteorites via In Situ Chemical Fluid/Vapor Deposition. PNAS, 119(38).

I03:Spectral cathodoluminescence and trace element mapping of apatite from the Ernest Henry deposit, Australia

Karsten Goemann[1], Jeffrey A. Steadman[2], Colin M. MacRae[3]

[1] Central Science Laboratory, University of Tasmania, Hobart, TAS, Australia
[2] Centre for Ore Deposit and Earth Sciences, University of Tasmania, Hobart, TAS, Australia
[3] CSIRO Mineral Resources, Clayton, VIC, Australia

Apatite [$Ca_5(PO_4)_3(OH,F,Cl)$] is an important petrogenetic indicator mineral in ore deposits, and panchromatic or colour cathodoluminescence (CL) images are often used to constrain formation and geological history of rocks, especially regarding fluid evolution and hydrothermal alteration [1,2]. Natural apatite contains trace elements including rare earth elements (REE) which substitute for Ca in the crystal lattice and produce characteristic sharp CL peak emission series (e.g. Nd^{3+}, Sm^{3+}, Dy^{3+}) or broader emissions (Mn^{2+}, Eu^{2+}, Ce^{3+}), see e.g. [2,3].

Hyperspectral CL maps with a spectral range of 200-1000 nm were acquired using a JEOL JXA-8530F Plus electron microprobe equipped with a JEOL xCLent V CL spectrometry system. A range of natural apatite crystals from drill holes within a 5 km radius around the Ernest Henry iron oxide copper gold (IOCG) deposit (NW Queensland, Australia) were mapped, both within and outside the ore zone [4]. The resulting CL maps show a wide range of textural and spectral features. The CL spectra are complex, requiring the fitting of up to over 40 different sharp and broad pseudo-Voigt peaks for a complete spectral description. By comparing the spectra with available literature data (e.g., [2,3]) a range of commonly occurring peaks can be assigned with good confidence to Nd^{3+} (peak cluster at 867-923 nm), Sm^{3+} (peaks at 600, 643, 705 nm), Dy^{3+} (578, 483, 753 nm), Mn^{2+} (broad emission centered at 565-570 nm), and Ce^{3+} on the Ca(I) site (broad emissions at 350 and 375 nm), with small shifts of the peak centres of up to a few nm observed between samples. Several additional small sharp peaks can be assigned to Gd^{3+} (312 nm), Er^{3+} (540 nm), Yb^{3+} (975 nm), Tb^{3+} (435, 415, 385 nm), however in this case the identification often relies only on a single weak peak and/or fitting is compromised by strong underlying broad emissions not related to these elements. Additional broad emissions observed at 405-445 and 465-485 nm can potentially be due to either Ce^{3+} on the Ca(II) site or Eu^{2+} [2,3].

After CL spectrometry the same apatite grains were mapped by laser ablation inductively coupled plasma mass spectrometry (LA-ICPMS). The elemental information from both techniques generally corresponds well with each other, supporting CL peak assignments, but there are also significant differences. For example, some ore zone apatite grains exhibit regions very enriched in As (up to 7 wt% As_2O_5) in EPMA-WDS and LA-ICPMS maps. These high-As zones coincide with a marked reduction of the overall CL emission, which has in the past been described as quenching of the CL emission by As [5], but may be in fact related to the structural modification caused by As substituting P.

1. F Bouzari et al. (2016), *Econ. Geol.* **111**, 1397.
2. U Kempe, J Götze (2002), *Mineral. Mag.* **66**, 151.
3. M Gaft, R Reisfeld, G Panczer (2015), Modern Luminescence Spectroscopy of Minerals and Materials, 2nd ed. Springer Mineralogy, 606p.
4. JA Steadman et al. (2022), *Frontiers Earth. Sci.* 926114.
5. E-A Perseil, P Blanc, D Ohnenstetter (2000), *Can. Mineral.* **38**, 101.

I04:X-ray spectroscopy of lithium

Philippe Jonnard[1]

[1]Laboratoire de Chimie Physique – Matière et Rayonnement, Sorbonne Université – CNRS, Paris, France

Lithium is a light metal which is nowadays very important for applications, in particular in the energy domain. Thus, characterization and quantification of lithium, that is to say determination of the chemical state, location and number of Li atoms in a sample, is of high interest. If x-ray spectroscopy of lithium could be implemented efficiently in scanning electron microscopes (SEM) or electron microprobe analyzers (EPMA), then one could expect to use the standard processes and quantification tools to study the electronic structure and determine the weight fraction of lithium in solid samples. Thus, SEM and EPMA could be used at all the stages of the production and use of lithium, from the characterization of geologic samples to battery devices.

Owing the atomic number of lithium equal to three, its electronic structure is very simple: two *1s* core electrons and one valence electron with *n=2* principal quantum number. In consequence the Li x-ray emission spectrum is also quite simple: it consists in the $K\alpha$ emission band corresponding to the *2p – 1s* electron transition. Following the low binding energy of the Li *1s* core level, the Li $K\alpha$ emission band lies in the ultra-soft x-ray or extreme ultraviolet spectral range, at photon energies around 50 eV (25 nm).

However, despite the development of new dispersive elements, optimized periodic multilayers and variable line spacing gratings, the spectroscopy of lithium is still, for both emission and detection reasons, a difficult to obtain on both SEM and EPMA.

- First, in the ultra-soft x-range there is no transparent materials. The strong attenuation of the radiation makes the analyzed thickness quite shallow, from a few tens of nanometers to a maximum of hundred of nanometers, so that few lithium atoms contribute to the emission. In addition, the Li *1s* fluorescence yield is extremely low, leading to a quite low emitted intensity. Regarding the possible quantification, attenuation coefficients are not well known in this spectral range. Moreover, Li $K\alpha$ being an emission band the position of its maximum and its shape depend on the chemical state of the emitting lithium atom. So, standard process relying on the determination of the intensities from the height of the considered emission cannot be used.
- Second, from the experimental point of view, any window in the spectrometer will lead to a strong loss of photons. Owing to the long wavelength, crystals cannot be used to disperse the radiation. Thus, periodic multilayers or gratings must be used, both having limited reflectance. In both cases, the used spectrometers have small solid angles of collection, making necessary to use large incident electron currents, of the order of a few hundreds of nA, in the SEM and EPMA. This is not harmless, since these currents, focused in spots of micrometer size, can lead to the damaging of the sample or to the migration of the lithium atoms.

We shall review the different points mentioned above.

I05:Multilength-scale and multimodal scanning hard X-ray imaging and tomography of mesoscale samples

Andrea Somogyi, Kadda Medjoubi
Nanoscopium beamline, Synchrotron Soleil, 91192 Saint-Aubin, France

Non-invasive multi-scale and multimodal 2D/3D characterization of heterogeneous or hierarchically structured mesoscale samples is crucial to address complex scientific problems and to link nanoscale features and functionalities to properties and functionalities emerging at larger scales. This triggers an ever-increasing demand for new analytical tools capable of providing spatially resolved multi-scale information on intact samples. Scanning synchrotron based hard X-ray imaging and tomography techniques are ideally suited to tackle this challenge due to their large penetration depth and inherently multimodal nature, where complementary simultaneous information can be obtained on the elemental distribution, morphology, crystalline structure. Furthermore, scanning techniques provide straightforward access to multiple-length scale experiments.

Thanks to recent developments in fast continuous scanning, data acquisition, and the high flux of modern hard X-ray nanoprobes[1,2], scanning 2D multimodal imaging has become routinely available for user experiments. Amongst the scanning techniques, high analytical sensitivity of X-ray Fluorescence (XRF) imaging provides unique possibilities in several scientific fields to study the role and fate of trace elements. Moreover, emerging scanning XRF tomography provides information on the internal elemental distribution within the studied specimen. In this presentation I will provide some examples on the possibilities provided by these analytical tools.

References

1. Medjoubi, K. et al. Development of fast, simultaneous and multi-technique scanning hard X-ray microscopy at Synchrotron Soleil. J. Synchrotron. Rad. 20, 293–299 (2013).

2. Somogyi, A. et al. Optical design and multi-length-scale scanning spectro-microscopy possibilities at the Nanoscopium beamline of synchrotron soleil. J. Synchrotron. Radiat. 22, 1118–1129 (2015).

I06: The ultrastructure of bone in 3D: A twist of twists

Daniel J. Buss[1], Roland Kroeger[2], Marc D. McKee[1,3], Natalie Reznikov[1,3,4]*

[1]Department of Anatomy and Cell Biology, Faculty of Medicine and Health Sciences, McGill University, Montreal, Quebec, Canada; [2]Department of Physics, University of York, Heslington, York, United Kingdom; [3]Faculty of Dental Medicine and Oral Health Sciences, McGill University, Montreal, Quebec, Canada; [4]Department of Bioengineering, Faculty of Engineering, McGill University, Montreal, Quebec, Canada
*natalie.reznikov@mcgill.ca

Structural hierarchy of bone – observed across multiple scales and in three dimensions – is essential to its mechanical performance. While the mineralized extracellular matrix of bone consists predominantly of carbonate-substituted hydroxyapatite, type I collagen fibrils, water, and noncollagenous organic constituents, it is largely the 3D arrangement of these inorganic and organic constituents at each length scale that endow bone with its exceptional mechanical properties. Based on recent volumetric imaging studies of bone using FIB-SEM tomography [1] and STEM tomography [2], and earlier works spanning scales up to the level of whole bones, we illustrate the self-similarity of nested structural motifs across several orders of magnitude and link the hierarchical organization of bone to the ubiquity of spiral structure in Nature. We discuss the omnipresence of twisted, curved, sinusoidal, coiled, spiraling, and braided motifs in bone in at least nine of its twelve hierarchical levels – a visualization undertaking that has not been possible until recently with advances in 3D imaging technologies. We hypothesize that the twisting motif occurring across each hierarchical level of bone is linked to enhancement of function, rather than being simply an energetically favorable way to assemble mineralized matrix components. We propose that attentive, further consideration of twists in bone tissue and in the skeleton at different scales will likely enhance our understanding of structure–function relationships in bone.

Acknowledgment: Object Research Systems Inc., Natural Sciences and Engineering Research Council of Canada

References:

[1] Buss et al., Journal of Structural Biology X, Vol. **6**, (2022), 100057.
[2] Reznikov et al., Science, Vol. **360**, (2018), eaao2189.

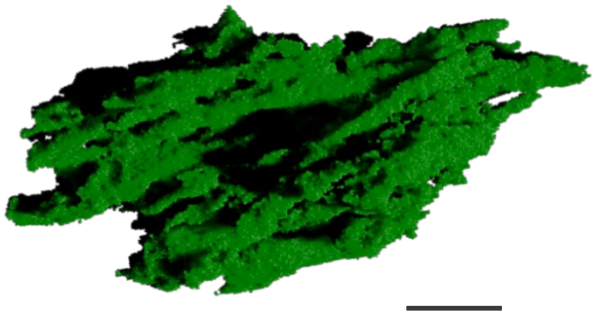

Fig. 1. This figure shows a micrometer-size mineral tesselle – a typical space-filling motif in mature bone, imaged by FIB-SEM Slice&View tomography. The spindle-shaped tesselle shows a gentle longitudinal twist following the texture of co-aligned collagen fibrils in bone. Scale bar equals 500 nm.

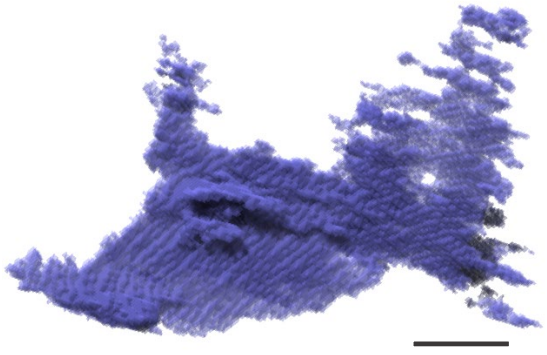

Fig. 2. This figure shows a few hundred nanometer-sized aggregate of bone mineral crystallites, imaged by STEM tomography. The layers of merging and splitting crystallites also subtly twist, and the overall shape of the mineral aggregate is similar to that of the tesselle in Fig 1. Scale bar equals 50 nm.

I07: Optimization, Minimising and Elimination of FIB Induced Defects

Xiangli Zhong[1], Xiaorong Zhou[1], Philp J Withers[1], Sarah Haigh[1], Lucille A Giannuzzi[2], Joseph R Michael[3], Ping Xiao[1], Grace Burke[1]

[1] Department of Materials, University of Manchester, Manchester, UK
[2] L.A. Giannuzzi & Associates LLC, Fort Myers, FL, USA
[3] Sandia National Laboratory, PO Box 5800, Albuquerque, NM, USA

Since the first Dual beam Focused Ion Beam (FIB) – Scanning Electron Microscope (SEM) system (herein after refers to FIB) was built in 1993, it has become one of the most important type of microscope in electron microscope (EM) labs in addition to SEM and TEM. The FIB, as a 'lab in a machine' with both processing and imaging capabilities in a single machine, has dominated the Transmission Electron Microscopy (TEM), Atom Probe (ATP) and nano Computational Tomography (nanoCT) sample preparations and local cross-sectional analysis. FIB applications have been extensively extended to 3D analysis for chemical, crystallographic, and material information. The combined sample preparation and 2D/3D analysis capabilities has made it a non-disposable to many materials and recently become an increasing important tool in biological sciences. However, due to its nature of complexity, it often induces critical defects including damages and contaminations which negatively affect the precise analysis of TEM, ATP, nanoCT, 3D EBSD/EDS/SE/BSE images. The defects are commonly due to the results of ion beam milling/imaging, electron beam imaging, in-situ CVD process etc. The FIB induced defects are a spectrum of damages and contaminations. Optimization, minimization, and elimination of FIB induced defects are critical for 'true' analysis of a sample. However, despite the exponentially increasing applications, there are very limited research in this area and no comprehensive study of the spectrum of defects in the open literature so far. This study tries to present a relatively full picture of FIB induced defects and proposed solutions including procedures and methods to tackle the problem taking into consideration seven aspects of the defects: 1) contaminations from FIB CVD process and solutions[1], 2) ion beam induced damages on soft materials and solutions[2], 3) ion beam induced chemical artefact and solutions[3], 4) ion beam induced defects on hard materials and solutions[4][5], 5) ion beam induced phase transformation of austenitic steel[6], 6) solutions of ion beam induced phase transformation of austenitic steel, 7) optimization of FIB for large area 2D and 3D analysis [7].

References

[1] X. L. Zhong, S. Schilling, N. J. Zaluzec, and M. G. Burke, "Sample preparation methodologies for in situ liquid and gaseous cell analytical transmission electron microscopy of electropolished specimens," *Microsc. Microanal.*, vol. 22, no. 6, pp. 1350–1359, 2016, doi: 10.1017/S1431927616011855.

[2] X. Zhong *et al.*, "Multi-modal plasma focused ion beam serial section tomography of an organic paint coating," *Ultramicroscopy*, vol. 197, no. November 2017, pp. 1–10, 2019, doi: 10.1016/j.ultramic.2018.10.003.

[3] X. Zhong *et al.*, "Comparing Xe+pFIB and Ga+FIB for TEM sample preparation of Al alloys: Minimising FIB-induced artefacts," *J. Microsc.*, vol. 282, no. 2, pp. 101–112, 2021, doi: 10.1111/jmi.12983.

[4] X. L. Zhong, S. J. Haigh, X. Zhou, and P. J. Withers, "An in-situ method for protecting internal cracks/pores from ion beam damage and reducing curtaining for TEM sample preparation using FIB," *Ultramicroscopy*, vol. 219, 2020, doi: 10.1016/j.ultramic.2020.113135.

[5] M. G. B. X. L. Zhong, S. A. McDonald P.J Withers, "Novel focused ion beam in-situ methods for stressed and cracked TEM sample preparation," in *European Microscolical Congress*, 2016, pp. 487–488.

[6] J. R. Michael, L. A. Giannuzzi, M. G. Burke, and X. L. Zhong, "Mechanism of FIB-Induced Phase Transformation in Austenitic Steel," *Microsc. Microanal.*, vol. 28, no. 1, pp. 70–82, 2022, doi: 10.1017/S1431927621013738.

[7] I. S. C. X. L. Zhong, P.J Withers, Y Guo, X.R. Zhou, "Insights to Crystallographic and Topographic Characteristics of Local Corrosion Attack on Zinc Xiangli Zhong," *Corros. Sci.*, vol. xx, p. xx, 2023.

I08: Scanning Transmission Helium Ion Microscopy – How Does It Compare to TEM?

Annalena Wolff[1,2], Rebecca Fieth[2]

[1] California Institute of Technology, Kavli Nanoscience Institute, Pasadena, CA, USA
[2] Central Analytical Research Facility, Queensland University of Technology, Brisbane, QLD, Australia

Since its initial release a decade ago, the Helium Ion Microscope (HIM) has established itself as a tool of choice for many imaging as well as nanofabrication applications [1]. This work explores the HIM's analysis capabilities of unstained biological samples using a self-built dark field scanning transmission ion microscopy holder. For thin enough samples, such as thin sections of biological specimen on TEM grids, the high energy helium ions can penetrate through the sample. The deflection angle of the transmitted ions can be determined using Monte Carlo simulations (SRIM). This effect can be used to design a dark field scanning transmission ion microscopy holder (DF-STIM). The holder design is based on a previously reported experiment [2]. In principle, ions,

which are deflected by a specific angle hit a metal conversion plate, which is mounted at a specified distance h below the sample where they create a secondary electron signal which can be collected by the HIM's Everhart-Thonley Detector. Ions which are deflected less than the acceptance angle enter a hole in the holder which his located directly below the specimen. This hole acts as a Faraday cup. For this case, no secondary electron signal is created. For biological samples, areas with higher carbon density create signal while areas with lower carbon density create less signal and can this be distinguished in the DF STIM image. The DF STIM holder is tested by imaging stained and unstained biological samples and the results are compared to TEM measurements (Figure 1). The measurements show that the in house designed DF-STIM holder can be used in the HIM to record high signal to noise images of unstained biological samples, revealing nanosized internal features such as collagen fibres. This technique outperformed the TEM imaging capabilities for the unstained biological specimen used in the experiment.

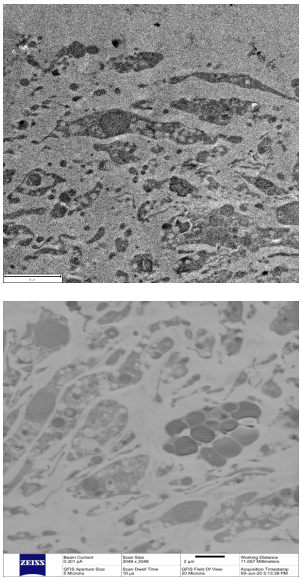

Figure: TEM (top) and DF-STIM micrograph (bottom) of an unstained biological sample.

References

[1] Allen FI. A review of defect engineering, ion implantation, and nanofabrication using the helium ion microscope. Beilstein J Nanotechnol. 2021 Jul 2;12:633-664. doi: 10.3762/bjnano.12.52. PMID: 34285866; PMCID: PMC8261528.

[2] Emmrich D, Wolff A, Meyerbröker N, Lindner JKN, Beyer A, Gölzhäuser A. Scanning transmission helium ion microscopy on carbon nanomembranes. Beilstein J Nanotechnol. 2021 Feb 26;12:222-231. doi: 10.3762/bjnano.12.18. PMID: 33728240; PMCID: PMC7934706.

Dr. Crystal Cooper is thanked for the many useful discussions and the sample preparation suggestions

I10: Unveiling thermal properties of nanoscale cavities using electron spectroscopy

Joaquin E. R. Gonzalez [1], Ka Yin Lee[1], Babafemi S. Agboola[1], Marcelo D. Martinho[1] Connor Wong[1], Nabil D. Bassim[1,2], Yao-Wen Yeh[3], Philip E, Batson[3], Peter Rez[4], Maureen J. Lagos[1,2]*

[1] Department of Materials Science and Engineering, McMaster University, Hamilton, ON, Canada

[2] Canadian Centre for Electron Microscopy, McMaster University, Hamilton, ON, Canada
[3] Department of Physics and Astronomy, Rutgers University, Piscataway, NJ, US
[4] Department of Physics, Arizona State University, Phoenix, AZ, US

Nanoscale cavities offer unique opportunities to explore novel physical and chemical properties in extremely confined spaces. For instance, surface phonon polaritons can be sustained within a dielectric cavity and they drive heat transfer processes within the cavity walls [1]. Understanding the complex behavior of these surface phonon polaritons requires the use of local spectroscopy probes with nanoscale sensitivity. We will discuss spatially-resolved high energy resolution EELS studies [2] in nanoscale dielectric cavities subjected at different temperatures. Our work focus on understanding the role of temperature in the behavior of surface phonon coupling and inelastic electron scattering.

Cavities with gaps raging between 5 and 150 nm were fabricated, and they were subjected to temperatures between 300 – 1000 K. A large variety of coupled phonon polariton modes were detected within the cavity indicating the existence of several available channels for heat transfer processes. The spatial distribution of inelastic scattering across the cavity nanogaps was also determined revealing a strong temperature-dependent behavior, which suggest a complex interplay between thermal and vibrational behavior. The scattering probability across the gap exhibits a parabolic distribution which is strongly dependent on both the gap distance and the temperature profile across the gap. Temperature of the cavity was measured locally with high precision [3]. We developed a theoretical model for inelastic electron scattering from phonons sustained in objects at different thermal states. Our work represents progress towards interpretation of temperature-dependent EELS data and understanding of the interplay between thermal and phonon properties of coupled nanostructures.

References

[1] J. Cuevas and F. Garcia-Vidal, ACS Photonics 5 (2018) 10.
[2] M. J. Lagos *et al*., Microscopy 71 (2022), i174.
[3] M. J. Lagos and P. E. Batson, Nano Letters 18 (2018), 4556.
[4] We acknowledge NSERC for providing funding under a Discovery Grant, CCEM for access to microscopy facilities, and Philip Batson for access to the Rutgers microscopy facilities.

I11: Solid-liquid-gas interfacial phenomena and quantification of reaction product in liquid phase electron microscopy

Vaso Tileli[1]
[1] Institute of Materials, Ecole Polytechnique Federale de Lausanne, Lausanne, Vaud, Switzerland

Surface and interface sensitive operando characterization methodologies are required to unlock electrochemical and electrocatalytic processes. Liquid phase electrochemical transmission electron microscopy (TEM) can provide the sensitivity and selectivity at single particle level. In this talk, I will describe the advancements of ec-LPTEM towards studying the solid-liquid-gas interfacial processes occurring on Co-based oxygen evolving oxide catalysts [1]. By performing real-time measurements, we can associate the potential-dependent variation of the local contrast to the effects that precede the electrocatalytic reaction such as electrowetting and redox-induced reactions. Further, through optimization of the microcell, we report on the direct probing of the evolution of molecular oxygen by *operando* electron energy loss spectroscopy (EELS). Similar experiments on IrO_2 particles indicate the capability to separate the contribution of different components in the EEL spectra, providing qualitative maps of O_2 and liquid electrolyte [2]. I will also discuss preliminary results on the quantification of the gaseous products inside the liquid-cell enclosures demonstrating key considerations for performing and interpreting electrocatalytic experiments in liquid phase electron microscopy.

References

[1] T.-H. Shen, L. Spillane, J. Peng, Y. Shao-Horn, and V. Tileli, Nature Catalysis **5**, 30 (2022)
[2] T.-H. Shen, R. Girod, J. Vavra, and V. Tileli, under review

I12: Applications of Environmental SEM as In-Situ Surface-Science Tool with Atomic Layer Sensitivity

Marc Willinger

[1] Department of Chemistry, TUM School of Natural Sciences, Technical University of Munich, Garching b. München, Germany

Methodological developments and the availability of commercial tools for in situ electron microscopy have extended our ability to observe materials beyond the thermodynamically isolated state of static atomic arrangements in vacuum. Observing how (functional) materials react and interact with a defined (chemical) environment at high resolution and over different length and time scales is key to an atomistic understanding of processes relevant to materials science, chemistry and biology. Fascinated by the ability to resolve structures at the most fundamental, atomic scale, the electron microscopy community has largely focused on in-situ TEM. As a very local method, it should be complemented by methods capable of providing information on larger scale dynamics, where processes involving collective motion of many atoms and effects related to heat and mass transfer can be observed. In recent years, we have therefore complemented in-situ TEM with experiments performed inside the chamber of an environmental scanning electron microscope (ESEM). In doing so, we have realised the fascinating potential of in-situ and operando SEM, which seems to have been partially overlooked by the growing in-situ TEM community. The aim of my talk is to highlight some of the capabilities of in-situ SEM, in particular the high surface sensitivity that can be achieved, and the important role that in-situ SEM can play in bridging the gap between fundamental UHV-based surface science studies of model systems on the one hand, and studies of complex structured functional materials under application relevant conditions on the other. Examples range from temperature induced phase transformations to chemical reactions and growth processes. [1-3].

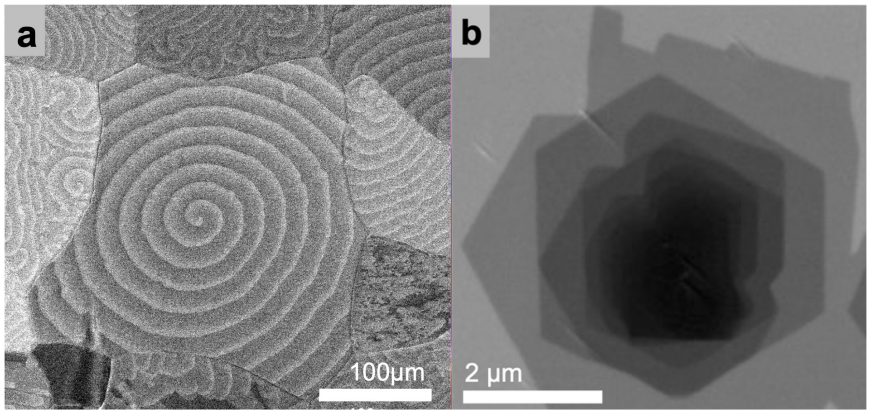

Figure 1 | Spirals: a) In-situ SEM image recorded during NO_2 hydrogenation on a polycrystalline platinum foil showing propagating reaction fronts on different grains [2]. b) Spiral growth of multi-layer graphene imaged during CVD growth on a platinum substrate inside the SEM chamber at ~ 1000 °C [3].

References:

[1] Cao J. *et al. Nat Commun* **11,** 3554 (2020). https://doi.org/10.1038/s41467-020-17346-7
[2] Barroo C. et al. Nat Catal 3, 30–39 (2020).
[3] Wang, Z.-J *et al. Adv. Mater. Interfaces* **5**, 1800255 (2018).

I12: CryoSIM: the trials and tribulations of correlative super resolution cryo fluorescence imaging.

Ian Dobbie
John Hopkins University

We have developed a super resolution cryo-fluorescence optical microscope in order to perform correlative imaging with the cryo Soft X-ray Tomography (SXT) beamline at the Diamond Light Source. Using Structured Illumination Microscopy (SIM) the microscope generates images at almost twice the achievable conventional optical resolution in 3 dimensions. By reducing the gap between the resolution in optical fluorescence images and the X-ray tomography significantly more information can be extracted from the correlated image sets. However, there are many barriers to reliably produce high quality fluorescence images of 3D samples in cryo while preserving the sample integrity. The sample must be kept cold, condensation must be avoided on both the sample and the optics, sample position must be highly stable and light must be collected at as high a numerical aperture as possible. We have open source control software providing a simple interface with high speed control of the wide range of hardware involved as well as a high degree of flexibility to provide a range of experimental options. Despite, these challenges we have been able to reliably produce images with sub 200 nm resolution and achieve correlative alignment at sub 100 nm. The CryoSIM and cryoSXT instruments are available for open access via peer revied applications.

I13: Visualizing Massive Macromolecular Complexes in Motion with Cryo-EM, Cryo-ET, and Deep Learning

Joseph H. Davis
Department of Biology, Massachusetts Institute of Technology, Cambridge, MA

Macromolecular machines such as the ribosome undergo massive structural changes as they assemble and function. While we have long appreciated such structural changes exist, experimentally visualizing and analyzing large ensembles of these structures is challenging. Here, I briefly describe cryoDRGN, a software package we developed to analyze structural heterogeneity in protein complexes visualized by cryo-electron microscopy (cryo-EM). This approach, which uses a purpose-built neural network based on a variational autoencoder, maps individual particle images to a low-dimensional latent space, effective sorting particles based on their structure. Moreover, users can generate ensembles of hundreds-to-thousands of three-dimensional structures from this latent space using the trained networks, which facilities are more comprehensive understanding of the structural states accessible to the protein complex of interest. I will detail our application of cryoDRGN to understand bacterial ribosome biogenesis, highlight a series of vignettes where we have found the expressive capacity of this deep learning approach particularly informative in characterizing the extensive heterogeneity in the datasets. I additionally describe our recent development of tools to automate thorough analyses of cryoDRGN models, and how we have used these automated tools to reveal key assembly events that couple r-protein binding and rRNA folding, and to layer rRNA helical folding maps onto classical r-protein association maps established by Nomura, Nierhaus, and colleagues. Finally, I describe our work to deploy analogous methods aimed at analyzing structural heterogeneity in situ via cryo-electron tomography, which we believe will allow us to visualize the molecular events guiding ribosome biogenesis in situ.

I14:Studies of the bacterial cell envelope using advanced imaging approaches

Danielle Sexton[1], Ameena Hashimi[1], Polina Beskrovnaya[1], Elitza I. Tocheva[1]*

[1] Department of Microbiology and Immunology, The University of British Columbia, Vancouver, BC, Canada

Cryogenic preservation of biological samples, especially bacteria, has proven advantageous when studying systems *in situ*. In particular, membrane preservation and overall arrangement of major macromolecular assemblies are kept in their native state. Generating 3-dimentional models of whole bacterial cells using cryo-electron tomography (cryo-ET) further provides cellular context at unprecedented (2-4μm) resolution. For samples that are thicker than 1μm in diameter, approaches such as cryo-focused ion beam milling (cryo-FIB) can be applied and combined with cryo-ET. Lastly, in order to identify features of interest within cells, we can combine the above approaches with fluorescence light microscopy (fLM).

Here, we present a super-resolution cryo-correlative light and electron microscopy (cryo-CLEM) method, and combined it with cryo-FIB milling to structurally characterize the bacterium *Deinococcus radiodurans* [1]. Subsequent cryo-electron tomography (cryo-ET) revealed an unusual diderm cell envelope architecture with a thick layer of peptidoglycan (PG) between the inner and outer membranes, an additional periplasmic layer, and a proteinaceous surface S-layer. Cells grew in tetrads, and division septa were formed by invagination of the inner membrane (IM), followed by a thick layer of PG. Cytoskeletal filaments, FtsA and FtsZ, were observed at the leading edges of constricting septa. Numerous macromolecular complexes were found associated with the cytoplasmic side of the IM. Altogether, our study revealed several unique ultrastructural features of *D. radiodurans* cells, opening new lines of investigation into the physiology and evolution of the bacterium.

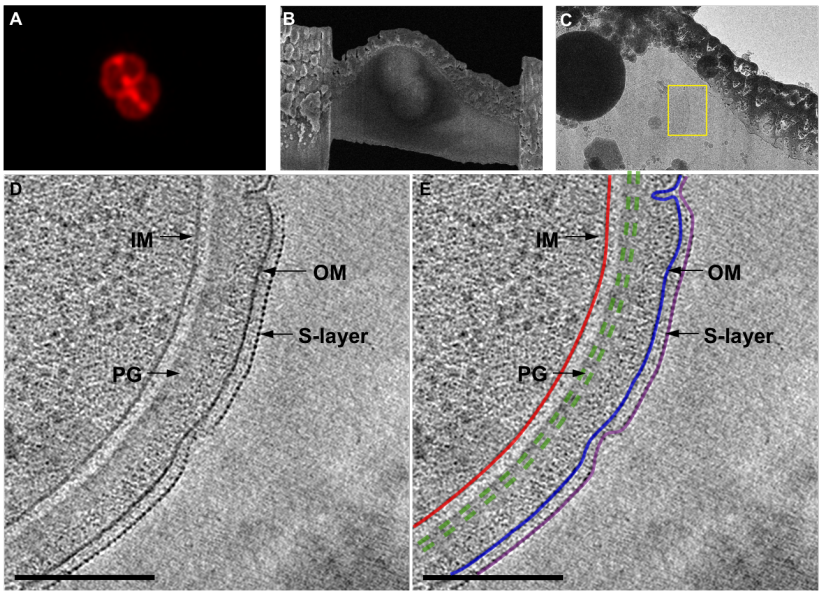

Fig. 1. Advanced imaging approaches to study the cell envelope of *D. radiodurans*. A) Membrane dye used to stain cells, fLM. B) Labella overview post cryo-FIB milling. C) A section of the lamella used for cryo-ET. D) Tomographic slice through a cell. E) Annotated cell envelope layers.

References

1 Sexton, D. L. *et al.* Ultrastructure of Organohalide-Respiring Dehalococcoidia Revealed by Cryo-Electron Tomography. *Appl Environ Microbiol* **88**, e0190621, doi:10.1128/AEM.01906-21 (2022).

I15: From iSCAT to SCATTIRSTORM: Adventures in single-molecule microscopy

William O. Hancock[1]

[1] Department of Biomedical Engineering, Pennsylvania State University, University Park, PA 16802

I will describe our work on the design and application of two multi-modal microscopes for single-molecule microscopy. The first system combines Interferometric Scattering (iSCAT) microscopy, developed by Philipp Kukura's lab, together with Total Internal Reflection Dark-Field (TIRDM). By labeling kinesin-1 motors on one head with a 30-nm gold nanoparticle, we were able to track motor stepping at 1 kHz temporal resolution and 1-2 nm spatial precision. This allowed us to clarify previously uncovered features of kinesin stepping. We extended this system to understanding microtubule dynamics by labeling tubulin dimers with 20-nm gold nanoparticles and observing these tubulin reversibly binding at the plus-ends of growing microtubules. These tools have the potential to be applied broadly to single-molecule studies to increase the temporal resolution beyond what is traditionally accessible by fluorescence, while still maintaining the spatial resolution provided by point-spread function fitting. I will also describe our work developing a multi-modal microscope to study the mechanism of cellulose degradation by cellulases for bioenergy applications. In particular, we have optimized the ability to combine Interference Reflection Microscopy (IRM) to image cellulose micro- and nanofibers with TIRF to simultaneously image fluorescently-labeled cellulase enzymes degrading the cellulose.

I16: Non-uniformity of the periodontal ligament: the dense collar in 3D

Andy Lee[1], Han Xu[1], Gili R.S Naveh[2,3]*

[1] Department of Oral Medicine Infection and Immunity, Harvard School of dental Medicine, Boston, MA, USA

[2] Department of Biomedical Engineering, Tufts University, Medford, MA, USA
[3] Department of Orthodontics, Tufts University, Boston, MA, USA

Teeth function under high repetitive loads in various directions. Unlike bones, teeth do not have a remodeling capacity and therefore any structural damage might lead to tooth failure. One of the most important strategies for tooth survival is through the ability of the tooth to move inside the bone. The periodontal ligament (PDL) is a soft tissue that connects the tooth to the jaw bone. Being the only soft tissue in the tooth-bone complex, the PDL has a central role in tooth movement and survival. Since the PDL is a non-uniform structure, unravelling the structure-function relations of the PDL while preserving 3D context of the tissue is crucial. To do so we used a top-down approach avoiding sectioning and fixation to preserve the 3D structure and function. Using a humidity chamber coupled with a loading system inside a microCT, AFM, bone clearing and optical imaging we studied the structure and function of the PDL in its 3D context (1-4). We discovered a unique region closest to the oral cavity, the dense collar. This area, has dense collagenous network, low vascularization and poroelasticity and has a central role in the PDL function. By impairing the dense collar structure, we studied the changes in the PDL function both mechanically and biologically. We hypothesize that this region not only contributes to the mechanical properties of the PDL but has a role in preventing bacterial invasion to the PDL as well. In periodontal disease destruction of the periodontal tissues leads to uncontrolled inflammation, bone resorption and increased tooth mobility. Identifying early stage structural changes that precede the onset of the disease will enable better control and the ability to restore the PDL structure for better clinical outcomes.

References

1. Connizzo, B.K., et al., *Nonuniformity in Periodontal Ligament: Mechanics and Matrix Composition.* J Dent Res, 2020. **0**(0): p. 22034520962455.
2. Connizzo, B.K. and G.R.S. Naveh, *In situ AFM-based nanoscale rheology reveals regional non-uniformity in viscoporoelastic mechanical behavior of the murine periodontal ligament.* J Biomech, 2020. **111**: p. 109996.
3. Naveh, G.R.S., et al., *Nonuniformity in ligaments is a structural strategy for optimizing functionality.* PNAS, 2018. **115**(36): p. 9008.
4. Xu H, Lee A, Naveh GRS. 3D imaging of PDL collagen fibers during orthodontic tooth movement. JoVE 2021 DOI: 10.3791/62149.

I17: Atom Probe Tomography Using Wavelength-Tunable, Femtosecond-Pulsed Coherent Extreme Ultraviolet Radiation

Ann Chiaramonti[1], Benjamin Caplins[1], Jacob Garcia[1], Luis Miaja-Avila[2], and Norman Sanford[2]*

[1] Material Measurement Laboratory, National Institute of Standards and Technology, Boulder, CO, USA

[2] Physical Measurement Laboratory, National Institute of Standards and Technology, Boulder, CO, USA

As the non-regulatory National Metrology Institute of the United States, the mission of the National Institute of Standards and Technology (NIST) is to promote U.S. innovation and industrial competitiveness by advancing measurement science, standards, and technology. From supporting the industrial revolution with standards for light bulbs and fire hose screw threads to promoting cutting-edge metrology research in areas of advanced communication, quantum science, forensics, and biomaterials, NIST has always focused research efforts and measurement services in addressing contemporary societal needs. Through a combination of metrology labs, technology labs, and National User Facilities, NIST can drive innovation in a variety of areas important to materials characterization research.

In this talk, I will discuss a world-first research program dedicated to the goal of identifying the 3D spatial location and chemical (isotopic) identity of "any atom in any solid." This program uses extreme ultraviolet (EUV) light to perform 3D atom probe tomography (APT). Ionizing radiation in the EUV region of the electromagnetic spectrum ($E \approx$10 eV to 100 eV, λ= 124 nm to 12 nm) offers potential new ionization and desorption pathways for APT that are not available using current state of the art commercial near-ultraviolet (NUV; E=3.5 eV, λ=355 nm) and more recently, deep-ultraviolet (DUV; E= 4.8 eV, λ=257 nm) light sources.

Instrument design and experimental results from the world's first EUV radiation-pulsed atom probe microscope will be presented. This instrument uses wavelength-tunable femtosecond-pulsed coherent EUV radiation from phase-matched high harmonic generation in a hollow-core capillary waveguide. I will show data from a variety of materials systems that demonstrate successful EUV-triggered field ion emission. Time-independent background levels, delayed evaporation tails, peak widths, charge state ratios, multiple hit counts, and the relative number of cluster ions will be compared with NUV experiments on the same samples and specimens. The myriad possible ionization and desorption mechanisms potentially operating in EUV APT will be discussed.

I18: International Union of Microbeam Analysis Societies Joint with the Annual Microscopical Society of Canada and FIB SEM Meetings Defining How Ribonucleases Regulate Gene Expression

Justin A. Gee[1], Jason G. Williams[2], Monica C. Pillon[1]*

[1] Department of Biochemistry and Molecular Biology, Baylor College of Medicine, Houston, Texas, USA

[2] Epigenetics and Stem Cell Biology Laboratory, National Institute of Environmental Health Sciences, Research Triangle Park, North Carolina, USA

Dysregulated gene expression is a hallmark of human disease. A determinant of gene expression is mRNA abundance, which is fundamentally a balance between mRNA synthesis and decay. Groundbreaking work has defined mechanisms by which diseases hijack mRNA synthesis (ex. oncogenic Myc transcription factors), yet comparatively little is known about how RNA decay pathways contribute to gene dysregulation and disease progression. Ribonucleases are the centerpiece to RNA decay pathways and their dysregulation has been associated with a wide variety of pathologies including cancer and neurological dysfunction. Many of the >125 known human ribonucleases influence RNA abundance, but their mechanism of action in RNA processing and decay pathways remain to be elucidated. We mounted a multidisciplinary research program focused on revealing the molecular rules controlling understudied ribonucleases. Using cutting-edge biophysical techniques such as single particle cryo electron microscopy with enzymology and cell biology, we are building a comprehensive understanding of the structural architecture and regulation of ribonucleases in the absence and presence of its RNA targets and auxiliary factors. By uncovering the molecular cues orchestrating ribonuclease specificity, function, and regulation, our program is building a foundation of knowledge for how ribonucleases support human health and how their dysregulation can contribute to complex disease.

I19: Antigenic mapping with single particle cryoEM to reveal sites of vulnerability and immune evasion for SARS-CoV-2 variants

Matthew McCallum[1], Anna De Marco[2], Nadine Czudnochowski[3], Alex Chen[3], Kaitlin R Sprouse[1], M Alejandra Tortorici[1], Mary-Jane Navarro[1], Alexandra C Walls[1], Matteo Samuele Pizzuto[2], Davide Corti[2], and David Veesler[1]

[1] Department of Biochemistry, University of Washington, Seattle, WA, USA
[2] Humabs Biomed, Vir Biotechnology, Bellinzona, Switzerland
[3] Vir Biotechnology, San Francisco, CA, USA

The SARS-CoV-2 spike glycoprotein contains a receptor-binding domain (RBD) targeted by most neutralizing antibodies in COVID-19 patient plasma. Little was known about neutralizing antibody binding outside the RBD and their contribution to protection. We isolated human monoclonal antibodies derived from memory B cells which recognize the SARS-CoV-2 S N-terminal domain (NTD) and show that a subset of them neutralize SARS-CoV-2[1]. Using Single particle cryoEM, we defined an antigenic map of the SARS-CoV-2 NTD and identified a single 'supersite' recognized by all of the neutralizing antibodies[1]. Subsequent to this analysis, worldwide SARS-CoV-2 transmission led to the recurrent emergence of variants, including Alpha, Beta, Gamma, Delta, Kappa, Epsilon, and Omicron. We showed that these variants dampen the potency of vaccine-elicited serum antibodies and provided a structural framework for describing the impact of individual mutations[2-4]. Notably, we found every variant of concern had a dramatically mutated NTD supersite facilitating neutralizing antibody evasion[2-4].

References

1. McCallum, M.*, Bassi, J.*, de Marco*, Chen, A.*, Walls, A.C.*, di Iulio, J., Tortorici, M.A., Navarro, M. Silacci-Fregni, C., Saliba, C., Sprouce, K. R., Agostini, M., Pinto, D., Culap, K., Bianchi, S., Jaconi, S., Cameroni, E., Bowen, J.E., Tilles, S.W., Pizzuto, M.S., Guastalla, S.B., Bona, G., Pellanda, A.F., Garzoni, C., Van Voorhis, W.C., Rosen, L.E., Snell, G., Telenti, A., Virgin, H.W., Piccoli, L., Corti, D., and Veesler, D. 2021. SARS-CoV-2 immune evasion by variant B.1.427/B.1.429. *Science*. 373(6555): 648-654.
2. McCallum, M.*, Czudnochowski, N. *, Rosen, L.E., Zepeda, S.K., Bowen, J.E., Walls, A.C., Hauser, K., Joshi, A., Stewart, C., Dillen, J.R., Powell, A.E., Croll, T.I., Nix, J., Virgin, H.W., Corti, D., Snell, G., and Veesler, D. 2022. Structural basis of SARS-CoV-2 Omicron immune evasion and receptor engagement. *Science*. 375(6583): 864-868.
3. McCallum, M., Walls, A. C., Sprouse, K. R., Bowen, J. E., Rosen, L., Dang, H. V., de Marco, A., Franko, N., Tilles, S. W., Logue, J., Miranda, M. C., Ahlrichs, M., Carter, L., Snell, G., Pizzuto, M., S., Chu, H. Y., Van Voorhis, W. C., Corti, D., and Veesler, D. 2021. Molecular basis of immune evasion by the delta and kappa SARS-CoV-2 variants. *Science*. 374(6575): 1621-1626.
4. McCallum, M.*, de Marco, A.*, Lempp, F., Tortorici, M.A., Pinto, D., Walls, A.C., Beltramello, M., Chen, A., Liu, A., Zatta, F., Zepeda, S., di Iulio, J., Bowen, J.E., Montiel-Ruiz, M., Zhou, J., Rosen, L.E., Bianchi, S., Guarino, B., Fregni, C.S., Abdelnabi, R., Foo, S.C., Rothlauf, P.W., Bloyet, L.M., Benigni, F., Cameroni, E., Neyts, J., Riva, A., Snell, G., Telenti, A., Whelan, S.P.J., Virgin, H.W., Corti, D., Pizzuto, M.S., and Veesler, D. 2021. N-terminal domain antigenic mapping reveals a site of vulnerability for SARS-CoV-2. *Cell*. 184(9): 2332-2347.

I20:Combining transmission diffraction and imaging in SEM: Prospects for in situ microscopy of thin films and 2D materials

Erdmann Spiecker[1], Peter Denninger[1], Christian Dolle[1,2], Peter Schweizer[1,3]

[1] Institute of Micro- and Nanostructure Research & Center for Nanoanalysis and Electron Microscopy (CENEM), University of Erlangen-Nürnberg, Germany
[2] now at: Microscopy of Nanoscale Structures & Mechanisms (MNM), KIT Karlsruhe, Germany
[3] now at: National Center for Electron Microscopy (NCEM), LBNL, Berkeley

In situ (S)TEM is a powerful tool for studying processes and properties of thin films like, e.g., solid state dewetting [1] and plastic deformation [2]. Even though SEM instruments are much more widespread and the lower electron energies provide advantages, in particular for 2D materials, transmission imaging and diffraction for in situ studies of thin films in SEM is still in its infancy.

In this contribution we present in situ studies in SEM carried out over the past years at CENEM in Erlangen. We report on in situ mechanical cleaning of monolayer graphene [3] and manipulation of basal dislocations in bilayer graphene (Fig. 1a) [4,5]. We discuss an in situ study of metal-induced layer exchange in a Ag/a-Si film stack providing deep insight into the early stages of the process. We introduce a method [6] which modifies our LEND setup [7] to enable simultaneous acquisition of images and diffraction patterns and correlate texture evolution and grain coarsening in a Au film (Fig. 1b). Finally, we discuss perspectives of in situ microscopy of thin films in SEM.

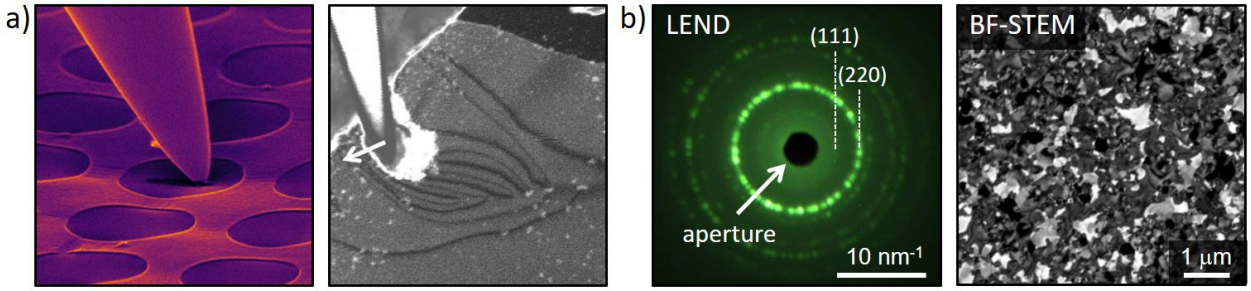

Figure 1: a) In situ mechanical cleaning of graphene [3] and in situ manipulation of dislocations in bilayer graphen [4,5]. b) Simultaneous transmission diffraction and imaging in SEM [6] enabling correlation of texture evolution and grain coarsening during annealing of a gold film.

References

[1] F. Niekiel, P. Schweizer, S.M. Kraschewski, B. Butz, E. Spiecker, The process of solid-state dewetting of Au thin films studied by in situ scanning TEM, Acta Mater. 2015, 90, 118.
[2] J.P. Liebig, M. Mačković, E. Spiecker, M. Göken, B. Merle, Grain boundary mediated plasticity: A blessing for the ductility of metallic thin films?, Acta Mater. 2021, 215, 117079.
[3] P. Schweizer, C. Dolle, D. Dasler, G. Abellán, F. Hauke, A. Hirsch, E. Spiecker, Mechanical cleaning of graphene using in situ electron microscopy, Nat. Commun. 2020, 11, 1743.
[4] P. Schweizer, C. Dolle, E. Spiecker, In situ Manipulation and Switching of Dislocations in Bilayer Graphene, Sci. Adv. 2018, 4, eaat4712.
[5] E. Spiecker, S.H. Oh, Z.W. Shan, Y. Ikuhara, X. Scott, Insights into fundamental deformation processes from advanced in situ transmission electron microscopy, MRS Bull. 2019, 44, 443.
[6] P. Denninger, P. Schweizer, E. Spiecker, Parallel Acquisition of Real and Reciprocal Space Data in Transmission SEM, Microsc. Microanal. 2022, 28 (S1), 2500-2503.
[7] P. Schweizer, P. Denninger, C. Dolle, E. Spiecker, Low energy nano diffraction (LEND) – A versatile diffraction technique in SEM, Ultramicroscopy 2020, 213, 112956.

I21: Direct Quantification of Short-Range Order in Materials by Combining STEM and Spatial Statistics

James M. LeBeau, Michael Xu, Shaolou Wei, Cemal C. Tasan

[1] Department of Materials Science & Engineering, Massachusetts Institute of Technology, Cambridge, MA USA

Short-range chemical and structural order can be a key tool to govern material properties ranging from mechanical behavior to dielectric response. The analysis of such short-range order (SRO) has typically relied on diffraction methods, either X-ray or neutron, where the Bragg peaks provide the global structure while diffuse scattering captures the nature of local chemical or structural order. These approaches, however, lack the spatial resolution necessary to directly connect SRO to local phenomena and interaction with extended defects. Instead, direct investigations of SRO at the atomic scale are possible using scanning transmission electron microscopy (STEM), which offers insights down to the single atom column level. Because this approach averages informational along the beam direction, analysis of nanoscale SRO with STEM imaging is limited by projection of the three-dimensional sample. Statistically significant spatial correlations between the structure and chemistry determined from these two-dimensional datasets thus remains challenging.

In this presentation, we will discuss how applying methods commonly used in Geographic Information Systems (GIS) can be used to quantify the spatial correlation between measures of local chemistry and structure from atomic-resolution STEM imaging of a compositionally complex systems. Specifically, we will demonstrate that by using measures such as the Moran's I statistic, chemical and structural order can be identified and quantified using a near-neighbor shell approach similar to the Warren-Cowley parameter, yet formulated for a two-dimensional real space image. To test this methodology, we will first consider the relaxor Pb(Mg1/3Nb2/3)O3 (PMN) where we will determine the type of ordering present and to quantify the spatial variation of chemical order, oxygen octahedral distortions, and oxygen octahedral tilts [1]. The extent of autocorrelation and inter-feature correlation among these short-range ordered regions will then be evaluated through a spatial covariance analysis, showing correlation as a function of distance. Taking the approach a step further, we will examine extremely local (<2 nm) SRO in the refractory high entropy Ti38V15Nb23Hf24 alloy [2] where the mix of heavy and light elements makes directly measurement of SRO challenging. Through GIS methods, we are then able to show that a non-random, sublattice-based order between (TiV) and (NbHf) is found and is consistent with predicted site occupancies and bond preferences. With the addition of Al, a small but statistically significant enhancement of short-range ordering will also be demonstrated. Overall, the results demonstrate that integrating GIS tools for analyzing microscopy datasets can serve to unravel subtle relationships among chemical and structural features in complex materials that can be hidden when ignoring their spatial distributions.

References

1. Xu M, Kumar A, LeBeau JM (2023) Correlating local chemical and structural order using Geographic Information Systems-based spatial statistics. *Ultramicroscopy*, 243:113642. doi:10.1016/j.ultramic.2022.113642
2. Xu M, Wei S, Tasan CC, LeBeau JM (2023) Determination of Local Short-Range Order in TiVNbHf(Al). *arXiv*:2302.03502. doi:10.48550/ARXIV.2302.03502

ECS1: Microstructural Study of Carbon Phases in Ureilite Meteorites using Electron Microscopy

Alan Salek[1], Andrew G. Tomkins[2], Colin MacRae[3], Nick Wilson[3] and Dougal McCulloch[1]*

[1.] Physics, School of Science, RMIT University, Melbourne, Victoria 3001, Australia
[2.] School of Earth, Atmosphere and Environment, Monash University, Melbourne, Victoria 3800, Australia
[3.] CSIRO Mineral Resources, Microbeam Laboratory, Victoria 3169, Australia
* Corresponding author: alan.salek@outlook.com

Ureilites are primitive achondrite meteorites that result from fractional melt extraction from deep within the ureilite parent body [1]. These meteorites contain up to 7% carbon and exhibit a range of carbon phases, including amorphous carbon, graphite, diamond, and diamond-like structures [2-4]. The hexagonal form of diamond, lonsdaleite, has also been reported, despite recent speculation that it may not exist [5]. In this study, we used optical petrography, electron probe microanalysis (EPMA), and electron microscopy to investigate the carbon phases present in several ureilite meteorites. The key to our study was the use of EDS and CL spectroscopies in the EPMA to produce maps of polished sample surfaces that distinguish between different carbon phases as shown in figure 1(a). These were then targeted for TEM analysis by preparing site specific specimens using a focused ion beam (FIB). In addition to graphite and diamond, we find well-ordered lonsdaleite crystallites up to ~0.5 µm in diameter (figure 1(b)), proving beyond doubt that lonsdaleite can exist as a distinct phase of carbon under ambient conditions. Furthermore, the textures in meteorites indicate that polycrystalline lonsdaleite replaced and preserved the shape of pre-existing graphite, implying that a pathway exists for manufacture of shaped ultrahard tools, given predictions that lonsdaleite has superior mechanical properties to diamond.

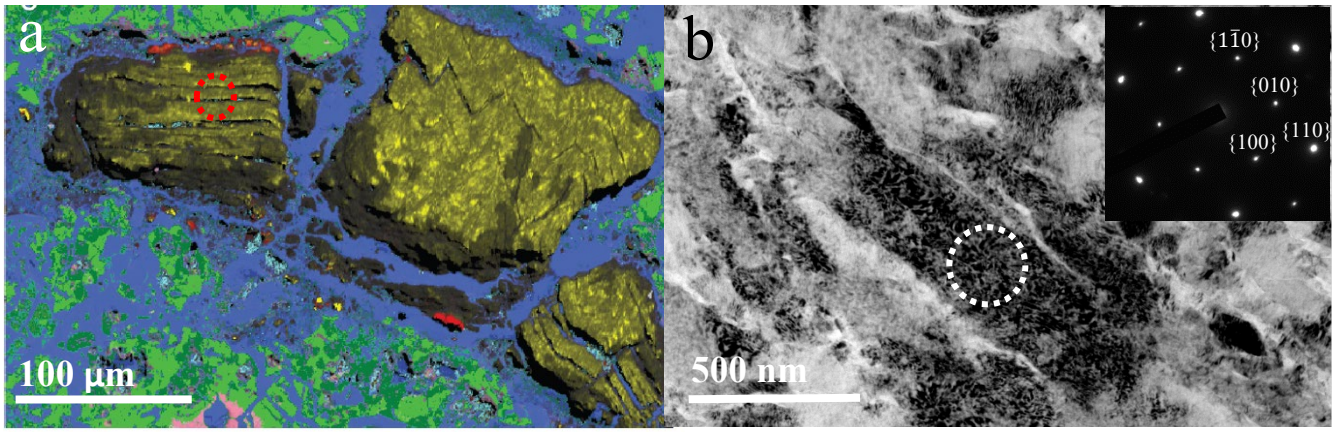

Figure 1. a) Cathodoluminescence map of polished cross-section from ureilite NWA 7983 showing olivine and pyroxene as green, other iron silicates as blue, diamond as red and lonsdaleite as yellow. b) TEM image from a lonsdaleite region indicated by the red circle in a) with an inset of the diffraction pattern (white circle) which was indexed to the <001> zone of lonsdaleite.

References:
[1] Collinet, M. and Grove, T. L., Meteoritics and Planetary Science **vol. 55** (2020)
[2] Grady, M. M. and Wright, I. P., Space Science Reviews **vol. 106** (2003)
[3] Goodrich, C. A., et al., Meteoritics and Planetary Science **vol. 50** (2014)
[4] Nestola, F., et al., Proceedings of the National Academy of Science **vol. 117** (2020)
[5] Nemeth, P., et al., Proceedings of the National Academy of Science **vol. 119** (2022)

ECS2: 4D-STEM Characterization of Microstructural Transformations in Conductive Polymers Used for Li-ion Battery Anodes

Hadas Sternlicht[1,2], Tianyu Zhu[1], Benjamin H. Savitzky[1], Colin Ophus[1], Gao Liu[1] and Andrew M. Minor[1,2]

[1] Lawrence Berkeley National Laboratory, Berkeley, CA, United States
[2] Materials Science and Engineering, University of California, Berkeley, CA, United States

Conductive polymer binders are used in composite anodes for Li-ion batteries, since they provide electronic conductivity, mechanical support, improved capacity retention, and moderate volume changes during electrochemical cycling [1,2,3]. Promising polymer binders include poly(9,9-dioctylfluorene-*co*-fluorenone-*co*-methylbenzoic ester), abbreviated as PFM [4]. Selective removal of bulky alkyl side chains upon annealing, resulting in hierarchically ordered structures in the polymer based on π-π stacking, was assumed to be responsible for the enhanced properties.

In this work, spin-coated TEM samples of PFM were characterized using four-dimensional scanning transmission microscopy (4D-STEM) to address the structure of the polymer chains at the nanometer length-scale at different annealing and acquisition conditions. Using 4D-STEM, the complete reciprocal space information was captured and analyzed, while allowing for the practical evaluation of applied dose, addressing the challenges associated with the characterization of soft materials [5]. In the diffraction patterns, we could discern between a rotationally homogeneous ring, oriented lobes of low-q scattering, and oriented arcs, indicating a gradual amorphous to semi-crystalline microstructural transition, associated with the formation of π-π stacking between the polymer chains. All of the features that appear in the diffraction patterns were directly correlated to the structure of the polymer, and were tracked as a function of temperature, allowing for the mapping of polymer chain orientation to reveal a granular morphology, where in this context a grain is defined as a region of continuous single orientation of the π-π stacking, which does not change abruptly. Variations in the characteristic spacings were demonstrated, together with changes in the grain size of the polymer, and the probabilities of defined relative orientations, as a function of radial distances. The implication of the grain morphology will be discussed in terms of electrochemical behavior and compared to results acquired by X-ray diffraction.

Beyond determining the characteristics of the "bare" polymer, PFM was also studied as part of an organic-inorganic composite with SiO_x particles, *i.e.* SiO_x-PFM, accounting for full anode samples. The transition to the semi-crystalline phase was detected regardless of the proximity to SiO_x particles. This quantitative approach for the characterization of PFM and PFM based anodes, significantly enhances the ability to design promising polymer-based anodes with enhanced mechanical robustness and ionic-electronic transport for exceptional electrochemical performance in practical battery systems.

References
[1] G Liu et al., Advanced Materials **23** (2011), p. 4679.
[2] H Zhao et al., Nano Letters **14** (2014), p. 6704.
[3] T Zhu and G Liu, Journal of The Electrochemical Society **168** (2021), p. 050533.
[4] T Zhu et al., Nature Energy (2023).
[5] O Panova et al., Nature Materials **18** (2019), p. 860.

ECS3: Advanced 3D Imaging via Multislice Electron Tomography using 4D-STEM

Juhyeok Lee[1], Moosung Lee[1,2], YongKeun Park[1,2,3], Colin Ophus[4], and Yongsoo Yang[1]
[1.] Department of Physics, Korea Advanced Institute of Science and Technology (KAIST), Daejeon, Korea.

[2.] KAIST Institute for Health Science and Technology, Daejeon 34141, Korea.

[3.] Tomocube, Inc., Daejeon 34051, Korea.
[4.] National Center for Electron Microscopy, Molecular Foundry, Lawrence Berkeley National Laboratory, Berkeley, California 94720, United States.

Electron tomography provides invaluable three-dimensional structural insight that surpasses that of two-dimensional imaging techniques. It has advanced to the point of resolving atomic-level details using a specialized microscopy technique called annular dark field scanning transmission electron microscopy (ADF-STEM) combined with aberration correction [1-9]. However, ADF-STEM-based tomography has some limitations, including a high requirement for electron dose, poor contrast for light elements, and the potential for artifacts from nonlinear image contrast [10-11]. In this study, we propose a new method called MultiSlice Electron Tomography (MSET) that uses a 4D-STEM tilt series (4D-STEM refers to 2D diffraction images of a converged electron beam at each point in a 2D STEM raster [12-13]). Our simulations show that MSET can reduce undesirable artifacts arising from nonlinear contrast, increase sensitivity for light elements, and decrease the required electron dose. We believe that MSET has the potential to be widely applied to materials that were previously challenging to study, such as radiation-sensitive specimens and materials containing light elements whose 3D atomic structures have remained unknown due to electron dose limitations or nonlinear imaging contrast.

References

[1] S. Van Aert et al., Nature **470** (2011), p. 374-377.
[2] R. Xu et al., Nat. Mater. **14** (2015), p. 1099–1103.
[3] Y. Yang et al., Nature **542** (2017), p. 75–79.
[4] J. Zhou et al., Nature **570** (2019), p. 500–503.
[5] X. Tian et al., Nat. Mater. **19** (2020), p. 867–878.
[6] Y. Yang et al., Nature **592** (2021), p. 60–64.
[7] J. Lee, C. Jeong, and Y. Yang, Nature Commun. **12** (2021), 1962.
[8] J. Lee et al., Nano Lett. **22** (2022). p. 665-672.
[9] H. Jo et al., Nature Commun. **13** (2022), 5957.
[10] O. Krivanek et al, Nature **464** (2010), p. 571–574.
[11] M. Treacy and J. Gibson, Ultramicroscopy **52** (1993), p. 31-53.
[12] C. Ophus et al, Microscopy and Microanalysis **20** (2014), p. 62-63.
[13] C. Ophus, Microscopy and Microanalysis **25** (2019), p. 563-582.

ECS 4: Micro-alloyed and ultralight elements in nano-scale precipitates in Al-Cu-Mg-Ag and Al-Cu-Li alloys revealed using atomic-resolution scanning transmission electron microscopy

S.L. Yang[1], X.J. Zhao[2], H.W. Chen[2], B.D. Esser[1,3], S.D. Findlay[4], J. Etheridge[1,3], N. Wilson[5], J.F. Nie[1]

[1.] Department of Materials Science and Engineering, Monash University, Clayton, VIC, Australia
[2.] College of Materials Science and Engineering, Chongqing University, Chongqing, PR China
[3.] Monash Centre for Electron Microscopy, Monash University, VIC, Australia
[4.] School of Physics and Astronomy, Monash University, Clayton, VIC, Australia
[5.] CSIRO Mineral Resources, Clayton, VIC, Australia

Al-Cu-Mg-Ag and Al-Cu-Li alloys have excellent mechanical properties due to a dense and uniform distribution of nano-scale **Ω** (in Al-Cu-Mg-Ag alloys) and T_1 (in Al-Cu-Li alloys) precipitate plates on $\{111\}_\alpha$ planes of the α-Al matrix [1]. Due to the challenge of precisely determining the positions of Ag, Mg and Li inside the precipitates, debates remain regarding the structures and formation mechanisms of **Ω** and T_1. Atomic-resolution high-angle annular dark-field (HAADF) scanning transmission electron microscopy (STEM) is effective in revealing atomic columns of heavy elements, but cannot unambiguously distinguish Mg from Al (or Ag from Cu), or detect the ultralight element Li. Therefore, we used HAADF-STEM and atomic-resolution energy dispersive X-ray spectroscopy (EDX) to reveal the positions of Ag and Mg inside precipitates in an Al-Cu-Mg-Ag alloy [2], Figures 1(a-b), and we found a hexagonal precursor phase designated **Ω′**. In the study of T_1 in an Al-Cu-Li alloy, we used atomic-resolution annular bright-field (ABF) STEM and electron energy-loss spectroscopy (EELS) STEM to directly visualize Li atomic columns inside T_1, Figures 1(c-d). Our work demonstrates the importance of advanced imaging techniques in the study of challenging metallurgical problems [3].

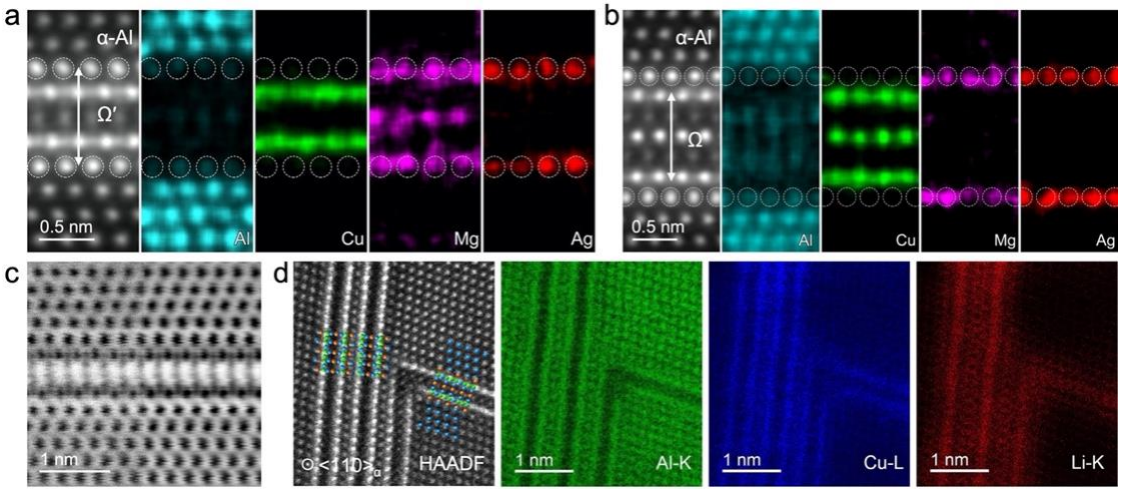

Figure 1. (a-b) Fourier filtered HAADF-STEM and EDX-STEM images of (a) **Ω′** and (b) **Ω** precipitate plates in an Al-Cu-Mg-Ag alloy, viewed along $<110>_\alpha$. (c) ABF-STEM image of an edge-on T_1 precipitate plate in an Al-Cu-Li alloy, viewed along $<110>_\alpha$. (d) HAADF-STEM image and corresponding EELS-STEM maps of T_1 precipitates in an Al-Cu-Li alloy.

References:
[1] J.F. Nie in "Physical Metallurgy", ed. D.E. Laughlin, K. Hono, (Elsevier, Oxford) p. 2031.
[2] S.L. Yang et al., Acta Mater. **225** (2022), p. 117538.
[3] The authors acknowledege funding from the Australian Research Council, and the use of the Electron Microscopy Centre of Chongqing Univeristy and Monash Centre for Electron Microscopy. The presenter acknowledges the ECS award provided by the Australian Microbeam Analysis Society.

ECS5: Experimental analysis of plastic deformation in single-crystalline and ultrafine-grained Zn micropillars

M. Wątroba[1], W. Bednarczyk[2], C. Tian[1], K. Pratama[1], J. Michler[1], J. Schwiedrzik[1]

[1] Empa Swiss Federal Laboratories for Materials Science and Technology Laboratory for Mechanics of Materials and Nanostructures, Thun, Switzerland

[2] Warsaw University of Technology, Faculty of Materials Science and Engineering, Warsaw, Poland

Zinc (Zn) shows great potential for biomedical applications owing to its unique biodegradability and biocompatibility [1]. Although Zn suffers from low mechanical strength and brittleness, high-strength Zn alloys have been recently developed [2,3]. The strengthening effect typically results from grain size, texture, grain boundary types, solute elements, or intermetallic phases in a microstructure. Due to a high c/a ratio of the HCP lattice, Zn exhibits strong anisotropy of mechanical properties, which depends on the initial texture and critical resolved shear stresses (CRSS) of specific deformation modes [4]. The paramount intention of this work was to gain insights into the effect of size and crystallographic orientation on the deformation mechanisms and strengthening in Zn micropillars. Since many micropillar compression studies follow the principle *smaller is stronger*, meaning the decrease in specimen size entails strain hardening and flow stress increase, the interplay with micropillar diameter and intrinsic grain size was included to understand strengthening effects at a small-length scale. Single-crystalline and ultrafine-grained Zn micropillars were prepared from annealed and electrodeposited states via FIB milling. EBSD analysis was used for basal- and prismatic slip-oriented grain selection in the annealed sample and characterization of grains in the electrodeposited sample. Activation of a slip system was predicted based on the Schmid Factor calculations, further used for CRSS evaluation. Compression tests conducted using an *in situ* nanoindentation system in SEM showed an increased CRSS with a decreased micropillar size. Deformation behavior and strain hardening were different depending on the activated slip system. Compression of the single-crystalline micropillars at different strain rates did not result in significant CRSS variation and deformation mode change. Ongoing analysis of the polycrystalline micropillars indicated an evident effect of intrinsic grain size on their mechanical response. *Post-mortem* SEM-EBSD analysis showed a lack of twinning. Slip trace analysis confirmed only basal or prismatic slip activation in single-crystalline micropillars. Overall, the results are a basis for simulating the mechanical behavior of 3D-architected Zn metamaterial structures currently under development. Furthermore, the CRSS results can serve as input data to predict the mechanical properties and plastic deformation of bioresorbable Zn implant materials.

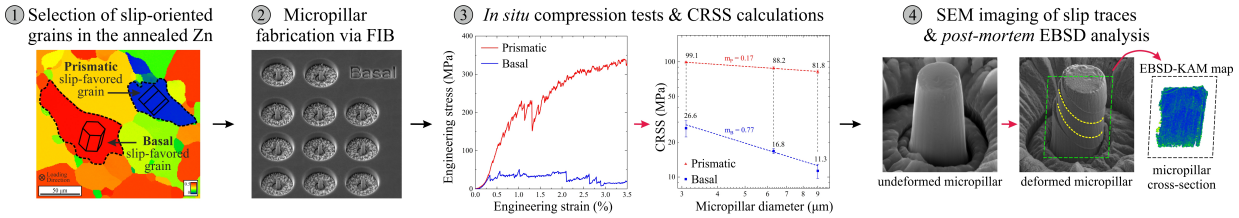

Fig. 1 Experimental steps for *in situ* Zn micropillar compression and *post-mortem* analysis

References:

[1] H. Kabir, et al., Recent research and progress of biodegradable zinc alloys and composites for biomedical applications: Biomechanical and biocorrosion perspectives, Bioact. Mater. 6 (2021) 836–879.

[2] H. Yang, et al., Alloying design of biodegradable zinc as promising bone implants for load-bearing applications, Nat. Commun. 11 (2020) 401.

[3] M. Wątroba, et al., Fine-tuning of mechanical properties in a Zn–Ag–Mg alloy via cold plastic deformation process and post-deformation annealing, Bioact. Mater. 6 (2021) 3424–3436.

[4] L. Cauvin, et al., Multi-scale investigation of highly anisotropic zinc alloys using crystal plasticity and inverse analysis, Mater. Sci. Eng. A. 729 (2018) 106–118.

ECS6: STRUCTURAL, CHEMISTRY, AND ELECTRONIC STATE OF THE INTERFACES OF TRANSPARENT CONDUCTING OXIDE AND HEMATITE APPLIED IN PHOTOELECTROCATALYSIS

Gabriel T. Santos[1,2], Karen Bedin[2], Paulo F.P. Fichtner[1], Flávio Souza[2], Jefferson Bettini[2]

[1] Engineering school, Federal University of Rio Grande do Sul (UFRGS), RS, Brasil
[2] National Nanotechnology Laboratory (LNNANO/CNPEM), Campinas, SP, Brasil

Climate urgency has challenged the development of green power generation systems, in which photoelectrocatalysis (PEC) devices are the holy grail. The design of PEC devices applied to water-splitting reactions is critical to enhancing their performance. At the nanoscale, the efficiency of the device is driven by interface boundary conditions. Changes in chemical concentration or structural arrangements at the interface regions result in unique physical properties that can improve device performance. Knowledge on the structural, chemical, and electronic state of heterogeneous interfaces can contribute to the development and enhancement of PEC devices, being typically assessed at the nanoscale by high-resolution transmission electron microscopy (HRTEM) images, in addition to electron energy loss spectroscopy (EELS) and energy dispersive spectroscopy (EDS) coupled to a scanning mode microscope (STEM). In this study, we investigated the interface of hematite with 3% Zr deposited on fluorine-doped tin oxide (FTO). The samples were prepared by deep coating and annealing in order to crystallize hematite. After crystallization, we added a NiFeOx solution to form a layer of co-catalytic material (Ni). Samples were prepared for TEM using a focused ion beam (FIB). We obtained chemical and electronic state characterization at the FTO/Hematite interface via STEM-EELS-EDS maps, processed using multivariate analysis calculations (PCA and NLLS). The results show a 2.5-nm thick interface region containing a Fe-Sn-O mixture. Structural analysis of the interface region by HRTEM imaging and HRTEM simulations showed that Hematite and FTO exhibit lattice distortions, and stress field images were obtained via Geometric phase analysis (GPA). The concentration map revealed that Zr segregated at the grain boundaries of the hematite and in the mixing region of the interface and that Ni is deposited on the free surface of the hematite, not FTO. Zr acts in grain size control and interface adjustment and Ni is a co-catalyst, improving the efficiency of the PEC device. The energy maps show a shift towards Sn+4 to Sn+2 and Fe+3 to Fe+2 for both FTO and Hematite grain boundaries, caused by the loss of oxygen from the system.

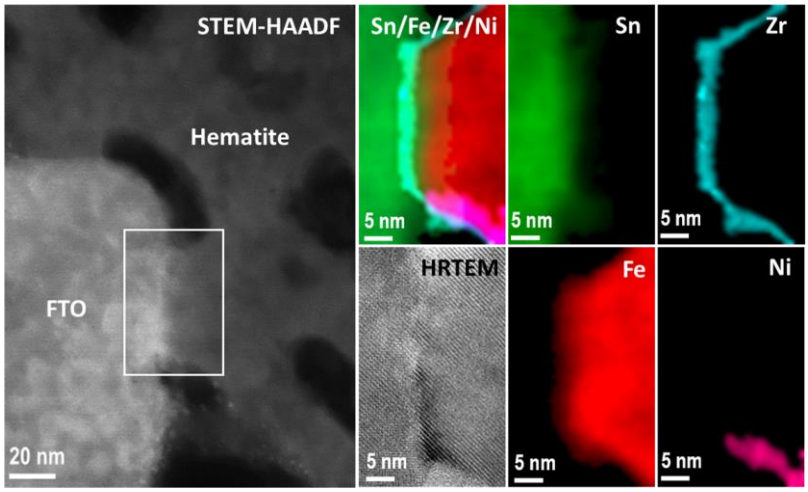

Figure 1: STEM - HAADF image of the hematite/Zr/Ni region on the FTO substrate. Interface where the concentration maps were performed with the average of the EELS and EDS

ECS7: Isotope effect on lattice location of hydrogen in titanium hydride nanofilms revealed by Channeling NRA

Takahiro Ozawa[1], Natsuko Kishi[2], Daiichiro Sekiba[2], Yuya Komatsu[3], Ryota Shimizu[3], Taro Hisotugi[3,4], Kunihiko Yamauchi[5], Ikutaro Hamada[5], Katsuyuki Fukutani[1,6]

[1] Institute of Industrial Science, The University of Tokyo, Meguro, Tokyo, Japan
[2] Graduate School of Pure and Applied Sciences, University of Tsukuba, Tsukuba, Ibaraki, Japan
[3] School of Materials and Chemical Technology, Tokyo Institute of Technology, Tokyo, Japan [4] Department of Chemistry, The University of Tokyo, Bunkyo, Tokyo, Japan
[5] Graduate School of Engineering, Osaka University, Suita, Osaka, Japan
[6] Advanced Science Research Center, Japan Atomic Energy Agency, Tokai, Ibaraki, Japan

Hydrogen (H) has a possibility to modify the electronic properties of host materials such as superconductivity and metal-insulator transition. Identification of H lattice location is an important first step to reveal the mechanism behind these phenomena. Combining the ion channeling effect with nuclear reaction analysis with $^{1}H(^{15}N, \alpha\gamma)^{12}C$, structure analysis of H was realized, which is called Channeling NRA. Furthermore, the energy analysis of the emitted γ-ray allows for the simultaneous detection of H and D atoms from one sample. We report the structure analysis of titanium hydride by Channeling NRA and the theoretical calculation of the site energy for hydrogen.

An epitaxial thin film of $TiH_{0.60}D_{1.0}(110)$ with a thickness of ~100 nm was fabricated on a MgO(110) substrate by reactive magnetron sputtering. Channeling NRA was performed around the normal incidence with an energy of 6.45 MeV. Figure 1 shows line scan profiles of normalized

NRA yields for (a) H and (b) D. Increases in the H-NRA yield equally at (001), (111) and $(1\bar{1}\bar{1})$ plane channelings revealed that most H atoms occupy the tetrahedral (T) site while ~5 atom% of H are located at the octahedral (O) site. On the other hand, the increase in the D-NRA yield was prominent at (001), indicating that D atoms solely occupy the T site. Theoretical calculations revealed that the zero-point energy is larger at T site than at O site, and therefore, the T site is stabilized with respect to the O site for D rather than H due to the mass effect. We also discuss the influence of lattice distortion on site energy.

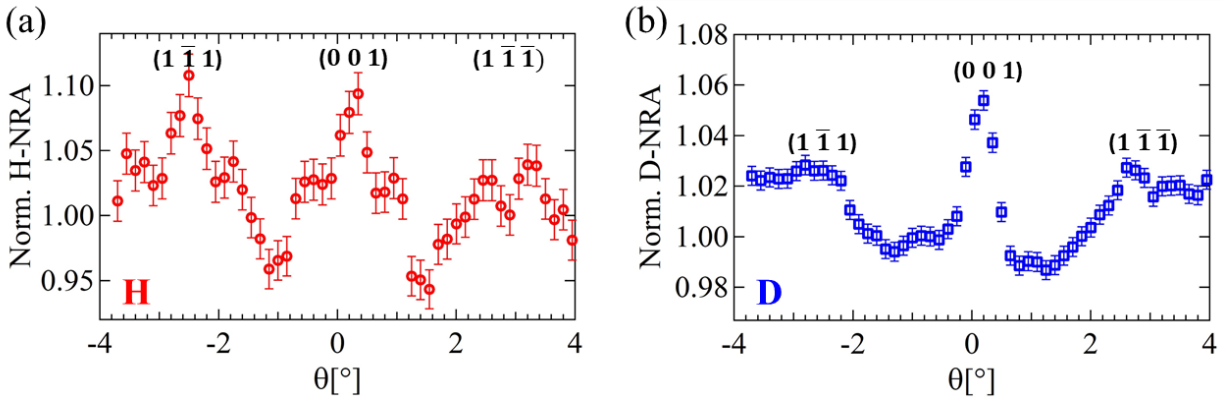

Figure 1 NRA line profiles of (a) H and (b) D for $TiH_{0.60}D_{1.0}(110)$ epitaxial nanofilm.

ECS8: Optimization of projection center based on EBSD Kikuchi band intensity profiles

Łukasz Rychłowski[1], *Tomasz Tokarski*[1], *Grzegorz Cios*[1], *Aimo Winkelmann*[1], *Gert Nolze*[2], *Piotr Bała*[1]

[1] Academic Centre of Materials and Nanotechnology, AGH University of Science and Technology, Kraków, Poland

[2] Federal Institute for Materials Research and Testing (BAM), Berlin, Germany

Accurate positioning of the projection center (PC) is necessary for a variety of electron backscatter diffraction (EBSD) analysis techniques. Methods such as high-resolution EBSD, phase identification, and misorientation determination are especially sensitive to the incorrect PC position. Considering that the main limitation during any EBSD analysis is the necessity of a defined diffracting phase - a method for the determination of the projection center is proposed that is based on the analysis of band intensity profiles of a single Kikuchi pattern. Compared to the currently most common techniques for calculating PC described in detail in [1] the proposed methodology allows the derivation of the projection center without prior knowledge about the diffracting lattice or alteration of the EBSD measurement setup.

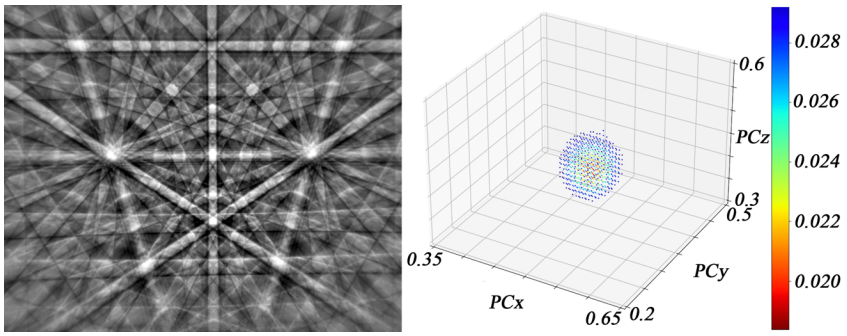

Figure 1. Si backscattered diffraction pattern (left) and corresponding PC scan (right). Each point defines a specific PC position. Color scale based on std. deviation of the calculated lattice parameter.

Kikuchi patterns used to determine PC were registered using FEI Versa3D with Oxford Instruments Symmetry S2 EBSD camera at a 20 kV accelerating voltage, a 16 nA probe current, and are processed by CALM software [2], where crystallographic plane traces and intensity profiles of the bands are derived. Simulated and corrected by the dynamical theory of electron diffraction [3] Kikuchi patterns were used to determine the precision of the method.

References

[1] Dingley D and Randle V 1992 *J. Mater. Sci.* **27** 4545-4566

[2] Nolze G, Tokarski T, Rychlowski L, Cios G and Winkelmann A 2021 *J. Appl. Cryst.* **54** 1012-1022

[3] Winkelmann A, Trager-Cowan C, Sweeney F, Day A P and Parbrook P 2007 *Ultramicroscopy* **107** 414-421

C01: Advances in Quantitative EPMA Compositional Mapping Applied to Meteorites

P. K. Carpenter[1], A.J. Irving[2], C.J.-K Yen[1], and B.L. Jolliff[1]

[1]Dept. of Earth and Planetary Sciences and McDonnell Center for the Space Sciences, Washington University, Saint Louis, MO, USA

[2]Dept. of Earth & Space Sciences, University of Washington, Seattle, WA, USA.

Meteorites are important samples of planetary materials, and electron-probe microanalysis (EPMA) is fundamental to their characterization, classification, and petrologic interpretation. We discuss meteorite research using quantitative EPMA quantitative compositional mapping with full matrix correction at each pixel, resulting in elemental and mineral stoichiometric data used to calculate the area fraction of minerals for modal recombination analysis. These methods have been applied to martian nakhlite NWA 14369, a cumulate igneous rock with early-crystallized olivine followed by crystallization of zoned Ca-pyroxene (pigeonite and augite), with interstitial feldspathic glass and/or plagioclase [1]. A complete analysis is obtained at each pixel, and mineral stoichiometry on a 24-oxygen basis is used to identify the mineral for classification and further calculations. Cation sums of 18, 16, and 15 represent olivine, pyroxene, and plagioclase, respectively. Cluster analysis of chemically zoned minerals makes phase identification com-plicated and stoichiometric screening simplifies this step. It is then possible to further calculate forsterite (Fo) and fayalite (Fa) olivine end-member components.

Analysis of a zoned olivine from nakhlite 14369 is shown in Fig. 1. The phase classification of olivine, pyroxene, and plagioclase is made using segmentation of the cation sum histogram as shown graphically in Fig. 1B. Pixels classified as olivine are used to generate the blue region of Fig. 1A. Further calculation of Fo and Fa content is used to construct the olivine histogram shown in Fig. 1C, and in Fig. 1D the quantitative olivine Fa content is color encoded. A line traverse of extracted olivine fayalite content is also shown in Fig. 1D. The core and rim olivine compositions are valuable in discussions of evolution of the nakhlite parent magma.

References

[1] Carpenter P.K. et. al. *53rd LPSC.*, # 2690, 2022.

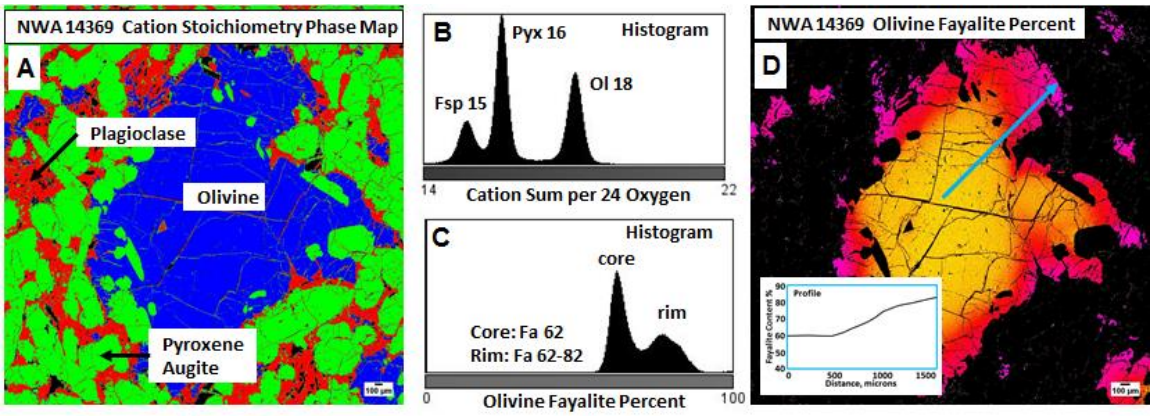

Figure 1. A. Phase classification based solely on mineral cation sum using histogram data in. Fig. **1.B**. **Figure 1 C.** Calculated olivine fayalite composition for all pixels classified as olivine with histogram showing homogeneous core and progressively zoned rim. **D.** Resulting phase map for olivine with color scale for fayalite content 62-82 percent and inset line profile for core-rim traverse extracted from map data set.

C02: Measurement and correction of optical response in an EPMA

Colin M. MacRae[1], N.C. Wilson[1], A. Torpy[1], Z. Pinter[1] and C.J. Davidson[1]

[1] CSIRO Mineral Resources, Microbeam Laboratory, Victoria 3169, Australia
* Corresponding author: Colin.MacRae@csiro.au

Cathodoluminescence (CL) collection in parallel with x-ray analysis provides a quick and easy tool to identify crystal structures and often minor-to-trace element activators can be detected and identified by examining the spectral emission lines [1]. While we have a luminescence database [2] which contains both emission lines and spectra, the identification of emission centers is not always straight forward as different collection systems produce different spectral shapes. For example, fig. 1, shows CL spectra collected at 20kV from emerald and quartz corrected and uncorrected. The quartz spectra show a peak at 2.77eV due to the presence of trace Ti which shifts to 2.87eV when corrected for the optical response [3]. The emerald spectra contains a broad peak at 1.67eV due to Fe^{3+} and a narrower peak at 1.81eV due to Cr^{3+}. When a correction is applied these spectra change due to the combination of the optical response of the spectrometer (CCD and grating) and the absorption in components in the optical path (fiber, mirrors, and lenses). In the case of the collection of cathodoluminescence through the optical assembly of the electron microprobe (EPMA) we have many optical components each adding a different spectral convolution. By inserting a light source into the EPMA we can measure the transmission response of the optical components and by similarly the spectrometers response can be determined by measuring a well characterized light source. Once these corrections are applied to the collected spectra then emission centers can be determined with less risk of misidentification. The luminescence database (https://luminescence.csiro.au/luminescence) maintained by CSIRO is currently being updated.

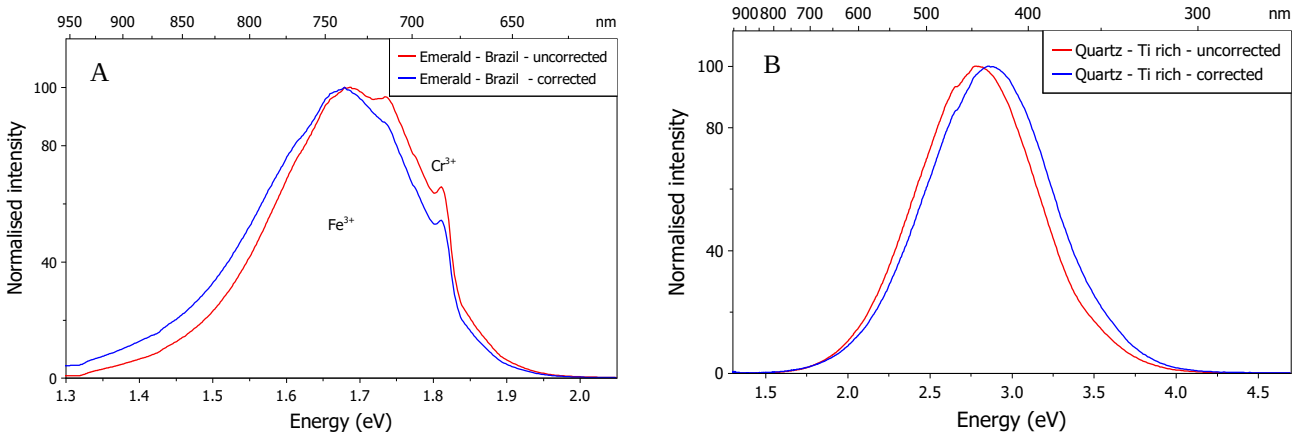

Figure 1. a) Cathodoluminescence spectra from emerald (beryl) from Brazil and b) CL spectra from a synthetic Ti enriched quartz. The effect of correcting for transmission and collection efficiency of the optics and spectrometer are clearly visible in both shape and peak position movements.

References:
[1] MacRae, C.M., Wilson, N.C. & Torpy, A. Mineralogy and Petrology 107, 429–440, 2013
[2] CM MacRae and NC Wilson. Microscopy and Microanalysis 14 (2), 184-204, 2008
[3] Gotze et al. American Mineralogist (in submission)

C03: Comparing Direct-Fit and Filter-Fit k-ratios from EDS Spectra

Nicholas W. M. Ritchie[1], *Dale E. Newbury*[1]

[1] National Institute of Standards and Technology, Materials Measurement Science Division, Gaithersburg, MD 20899, USA

In either energy dispersive spectrometry (EDS) or wavelength dispersive spectrometry (WDS), the fundamental quantity measured in an X-ray microanalysis measurement is X-ray intensity. If we can attribute the X-ray intensity to a characteristic X-ray line, we can measure this intensity on a material of unknown composition and a material of known composition (the 'standard'). The ratio of these two intensities is called the k-ratio. Regardless of how the intensity from the known material is determined (model as in "standardless analysis" or measurement as in "standard-based analysis"), the k-ratio serves as the starting point for the computation of the unknown material's composition. Accurately determining the k-ratio is thus critical.

For either EDS or WDS, the process is complicated by the presence of both continuum and characteristic X-rays which are practically indistinguishable at the characteristic X-ray energy. Extracting the k-ratio from WDS measurements is typically performed using a two or more proximate background measurements and one on-peak measurement. For EDS, the k-ratio emerges from the process of fitting peak shape references to the unknown and standard. However, this process is complex and requires a mechanism to discount the contribution from the continuum. Two possible mechanisms are direct-fit and filter-fit. Filter-fit applies a medium-pass `top-hat` filter to the raw spectrum data and fits the resulting processed spectra using a linear-least squares algorithm. Direct-fit models the continuum and subtracts its contribution to the raw spectra before performing a linear-least squares algorithm. Our experience suggests that neither algorithm is clearly better than the other in most situations. The k-ratios produced by either are typically comparable to the level of accuracy achievable by the technique. However, there are situations which favor one over the other like hard to model continuum measurements or low energy X-ray lines.

C04: Quantitative Assessment of X-ray Attenuation under Atmosphere to Vacuum Conditions

Edward P. Vicenzi[1], Thomas Lam[1], and Nigel Kelly[2]

[1] Museum Conservation Institute, Smithsonian Institution, Suitland, MD, USA
[2] Bruker Nano Analytics, Denver, CO, USA

X-ray spectra are typically collected under vacuum conditions that allow for optimized compositional sensitivity. Some X-ray fluorescence (XRF) measurements are performed in atmosphere by necessity given oversized targets, or the need to use portable instrumentation outside of a laboratory setting. In such cases, high pressure conditions cause attenuation of low to moderate energy X-rays owing to atmospheric absorption effects [1]. To quantitatively evaluate the magnitude of such effects we have measured K line intensities for F through S in binary compounds using two models of Bruker benchtop μXRFs at differing pressures, in addition to SEM chamber measurements conducted under low and high vacuum conditions. Soft X-rays (F, Na, and Mg) suffer disproportionate attenuation of their signals relative to P and S (Figure 1). Moreover, all elements examined demonstrate an intensity drop even for small differences in pressures from high vacuum to low vacuum conditions of < 3 mb by 6 % for Na and 2.5 % for S. By quantifying these intensity changes, we can conduct He flow displacement experiments under ambient conditions to determine the equivalent vacuum condition for a given He flow rate; thereby constraining the sensitivity of an atmospheric XRF analysis for non-metallic materials that contain elements with low to moderate X-ray energies.

References

1. Seibert, J.A. and J.M. Boone, Journal of nuclear medicine technology **33**(2005), p. 3-18

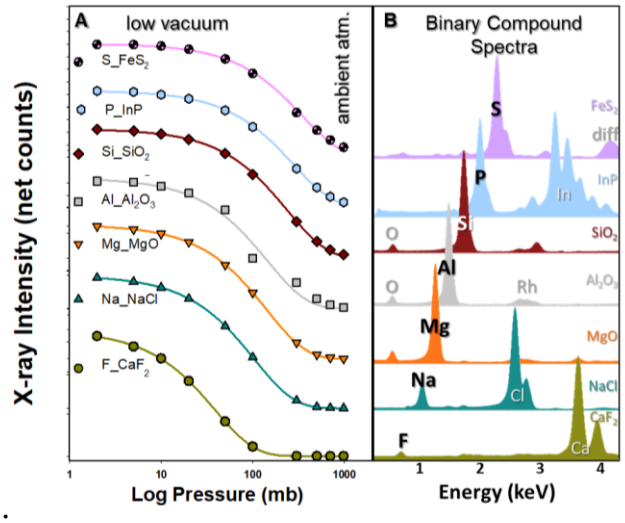

Figure 1. XRF generated X-ray intensities as a function of pressure. A) Scaled net intensities for F (0.68 keV) to S (2.31 keV) K line X-rays under atmospheric pressure to low vacuum conditions for a thin window detector system where solid lines represent fits to the data. B) Low vacuum (2 mb) X-ray spectra for seven binary compounds examined highlighting the F, Na, Mg, Al, Si, P, and S peaks tracked in A.

C05: Neural network-based MC X-ray for quantitative analysis of elements

Dawei Gao[1], Yu Yuan[1], Raynald Gauvin[1], Nicolas Piché[2]

1.Department of Mining and Materials Engineering, McGill University, Montreal, Quebec, Canada.

2.Object Research Systems. Montreal, Canada.

Energy dispersive X-ray spectroscopy (EDS) is an analytical technique that allows for the elemental analysis of materials. It produces a spectrum in which the intensity of the signal can correspond to the concentration of the element. However, this quantitative analysis capability requires access to a large database of standard elements, which is costly. So, we combine neural networks and Monte Carlo simulations to solve this problem.

Monte Carlo Simulation [1] is an outstanding program to predict electron solid interactions. This process can be achieved through calculating the trajectories of a large number of electrons striking a sample at once as well as the generated X-ray between each collision. Over the decades, different software based on the Monte Carlo Simulation program has been developed, such as CASINO[2], Win X-ray[1], MC X-ray[3] and Penelope[4], of which MC X-ray and Penelope are currently two of the most powerful ones due to their ability to simulate the complete EDS spectrum of samples with different shapes and compositions. To validate the reliability of the MC X-ray, we compare the simulation results between MC X-ray and Penelope from three perspectives: X-ray depth distribution, K-ratio with the Pouchou database [5] and spectrums with experimental data. The results have shown that the simulation results of MC X-ray and Penelope from different aspects are very close. However, under the same simulation conditions, the average time Penelope takes to process is 90 times longer than the time MC X-ray takes. Therefore, we use different concentrations and the corresponding spectrums rapidly and accurately generated by MC X-ray as the training set for the deep learning model, thus the concentrations can be predicted when the spectrum produced by EDS is input to this trained model. This model addresses the huge expense of obtaining a standard EDS database.

References

1. Gauvin R, Lifshin E, Demers H, et al. Win X-ray: A new Monte Carlo program that computes X-ray spectra obtained with a scanning electron microscope[J]. Microscopy and Microanalysis, 2006, 12(1): 49-64.

2. Hovington P, Drouin D, Gauvin R. CASINO: A new Monte Carlo code in C language for electron beam interaction—Part I: Description of the program[J]. Scanning, 1997, 19(1): 1-14.

3. Gauvin R, Michaud P. MC X-ray, a new Monte Carlo program for quantitative X-ray microanalysis of real materials[J]. Microscopy and Microanalysis, 2009, 15(S2): 488-489.

4. Llovet X, Salvat F. PENEPMA, A Monte Carlo code for the simulation of X-ray emission spectra using PENELOPE[C]//Workshop Manual, Madison, Wisconsin. 2006.

5. Pouchou J L, Pichoir F, Heinrich K F J, et al. Electron probe quantitation[J]. 1991.

C06: Detection of Li K Emission In Different Lithium Compounds

Khalil Hassebi[1], Nicolas Rividi[2], Anne Verlaguet[3], Alexei Erko†[4], Juergen Probst[5], Heike Loechel[5], Thomas Krist[5], Philippe Jonnard[1]

[1] Laboratoire de Chimie Physique—Matière et Rayonnement, Faculté des Sciences et Ingénierie, Sorbonne Université, UMR CNRS, 4 Place Jussieu, , 75252 Paris Cedex 05, France

[2]Service Camparis, UMS 7154—CNRS, OSU Ecce Terra, Sorbonne Université, 4 place Jussieu, 75005 Paris, France

[3]Sorbonne Université, CNRS-INSU, Institut des Sciences de la Terre de Paris, ISTeP UMR 7193, F 75005 Paris, France

[4] Institut fuer Angewandte Photonik e. V., Rudower Chaussee 29-31, D-12489 Berlin, Germany

[5]Nano Optics Berlin GmbH, Krumme Str 64, D-10627 Berlin, Germany

Soft x-ray emission spectroscopy (XES) is a technique used to study the electronic structure of materials. It measures the energy spectrum of emitted x-rays from a sample. It is performed by irradiating the sample with ionizing particles (electrons in our case) and measuring the energy distribution of the x-rays that are subsequently emitted. The emitted x-rays are characteristic of the electronic states of the sample, thus, the presence of an element can be detected, and could be also used to perform quantitative analysis.

Reflection zone plates (RZP) can be used in XES as a wavelength-dispersive element [1]. They consist of a series of concentric zones, each with a slightly different thickness. When x-rays are incident on the zone plate, the different zones act as diffraction gratings, causing the x-rays to diffract and interfere with one another while focusing them at the same time. They have higher spectral resolution and cover wider energy ranges compared to other optical elements such as periodic multilayers. RZPs allow to the reach of energy resolutions as low as 0.49 eV at the Al $L_{2,3}$ line (around 72 eV) [2]. With parallel detection of x-rays in contrast to conventional wavelength dispersive spectroscopy (WDS) spectrometers with a dispersive crystal (or multilayer) based on Rowland mounting they do not have a scanning mechanism.

In this work, we demonstrate the use of a Fresnel (RZP) implemented in an electron microprobe for the detection of Li K (around 50-55 eV) emission in different lithium compounds. Li K emission is a characteristic emission band produced when Li 1s levels are ionized inside the material. However, it can be challenging to detect this emission due to its low fluorescence yield, re-absorption effects, and the presence of other spectral lines in the same energy range. We report on our measurements of the Li K emission bands in several lithium compounds with an RZP spectrometer. Our results demonstrate this approach's potential for various applications in the field of x-ray spectroscopy.

Acknowledgment: This research was funded by Agence Nationale de la Recherche in the framework of the SQLX Project (ANR-20-CE29-0022).

References

[1] A. Erko *et al.*, *Opt. Express*, vol. 22, no. 14, p. 16897, Jul. 2014, doi: 10.1364/OE.22.016897.

[2] A. Hafner *et al.*, O*pt. Express*, vol. 23, no. 23, p. 29476, Nov. 2015, doi: 10.1364/OE.23.029476.

C07: Towards Quantitative Maps of Lithium in the Electron Microscope

Raynald Gauvin[1*] and Nicolas Brodusch[1]

[1.] Department of Materials Engineering, McGill University, Montréal, Québec, Canada, H3A 0C5.
[*] raynald.gauvin@mcgill.ca

This paper will present where we are to perform quantitative EDS and EELS maps of Lithium based materials in the electron microscope. State of the art results acquired with the SU-9000 dedicated STEM will be shown. This microscope has EELS capabilities that allows Li detection [1]. It is also equipped with the Extreme EDS system from Oxford Scientific that can detect the K_α line of Lithium [2]. The SU-9000 has a resolution of 0,22 nm in bright field STEM without aberration correctors and it allows lattice imaging. Figure 1 shows an EELS spectrum of Li_2FeSiO_4 taken with the Hitachi SU-9000 at 30 keV. Even if the X-ray K_α line was not seen for this material with the Extreme EDS detector, the ionization edges are clearly visible for Fe, Li and Si. Figure [2] shows a Li EELS jump ratio map of an Al 2099 alloy taken with the Hitachi SU-9000 at 30 keV. This map shows δ precipitates (Al_3Li) which are spheres between 5 to 20 nm and T_1 plates (AlCuLi) that have thicknesses between 2 to 6 nm. The fact that the edges are always ionized is a strong advantage for EELS since it does not matter if there is or not an electron transition leading to X-Ray emission, where is often the case that there are no Li K_α line with oxides cathode-based materials. Also, the emission rate in EELS is greater than about 10 000 than that of EDS owing to the fluorescence factor. The downside of EELS is the need for a transparent specimen and beam damage can also be an issue. Results obtained with a cryo-holder to minimize beam damage are underway and will be presented.

References:
[1] N. Brodusch, H. Demers, A. Gellé, A. Moores and R. Gauvin (2019), Ultramicroscopy, 203, pp.1-36.
[2] P. Hovington, V. Timoshevskii , S. Burgess, H. Demers, P. Statham, R. Gauvin, K. Zaghib (2016), Scanning, 38, 6, pp. 571 – 578.
[3] R. Gauvin *et al.* (2021), Microscopy and Microanalysis, 27, pp. 1868

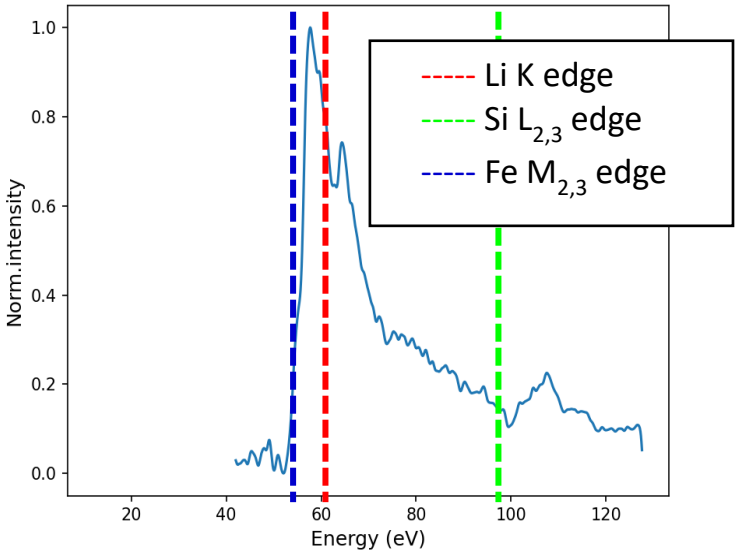

Figure 1. EELS spectrum of Li_2FeSiO_4 taken with the Hitachi SU-9000 at 30 keV.

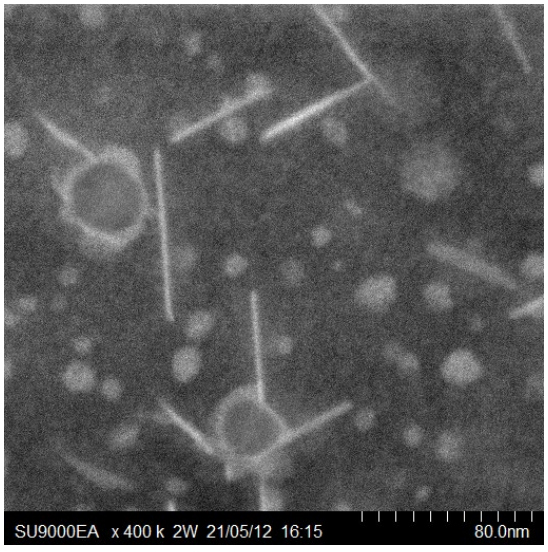

Figure 2. Li EELS jump ratio map of an Al 2099 alloy taken with the Hitachi SU-9000 at 30 keV.

C08: Quantitative Analyzation on Aluminum Alloys

Yinuo Li[1], Sabrina Clusiau[2], Pascal Gauthier[3], Nicolas Piché[4], Raynald Gauvin[5]
[1,2,5] Materials Engineering, McGill University, Montreal, Quebec, Canada
[3] Rio Tinto, Montreal, Quebec, Canada
[4] ORS, Montreal, Quebec, Canada

Aluminum alloys are widely used in the aerospace and automotive industry because of their extraordinary properties. Sample material Al 5182 is mainly applied to fabricate vehicle parts, which has magnesium (Mg) and manganese (Mn) as minor elements with some Iron (Fe) addition [1]. Alloying aluminum with Mn additions provides an increase in low-cycle fatigue resistance, while Mg can improve the strength and hardness of the material [2]. Al 5182 contains many intermetallic compounds such as Mg_2Si and $Al_6(MnFe)$ that result in a strengthening effect [1]. Those precipitations in its microstructure can have a significant influence on the mechanical properties, and therefore will be analyzed quantitatively in this research.

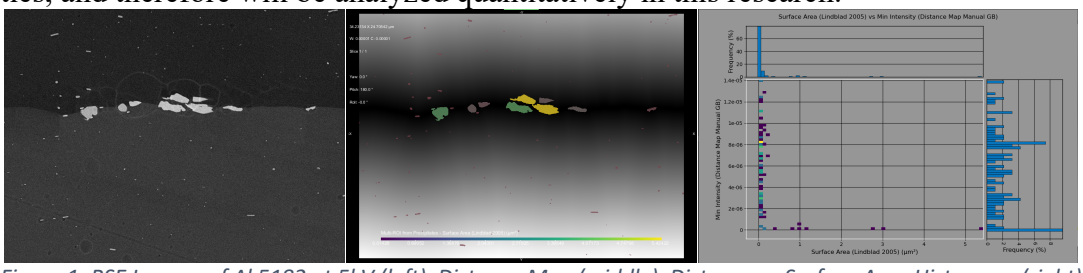

Figure 1: BSE Images of Al 5182 at 5kV (left), Distance Map (middle), Distance vs Surface Area Histogram (right)

Composition of the alloy was determined with energy dispersive spectroscopy (EDS) and its phase distribution was captured by scanning electron microscopy (SEM). High efficiency automation process can be potentially employed on the SEM to acquire large volume of microstructure data obtaining more general results with higher accuracy. Precipitate distributions within grains and on grain boundaries is an important factor featuring its microstructure that could play an overall impact on the material's performance, which has not been widely studied in previous research. Precipitate distribution as well as type, size and fraction of the precipitates will be analyzed quantitatively using Dragonfly software. Distance map can be produced for direct visualization and inspection as shown above with precipitates color coded in terms of surface area. A more detailed statistical analysis of the precipitates can then be done. Histogram in figure 1 is generated to determine the relationship between size and distribution, illustrating a uniform distribution of smaller precipitates throughout the grains (conclusion drawn from points on the left side of the histogram) and the tendency of larger dispersoids formation on or close to the grain boundaries (from points on the very bottom of the histogram). This relation could differ from alloy to alloy with its influence on mechanical properties of alloys to be further determined.

References

[1] E. Aryshenskii, J. Hirsch, and S. Konovalov, "Investigation of the Intermetallic Compounds Fragmentation Impact on the Formation of Texture during the as Cast Structure Thermomechanical Treatment of Aluminum Alloys," Metals, vol. 11, no. 3, 2021.
[2] A. Fortini, M. Merlin, E. Fabbri, S. Pirletti, and G. L. Garagnani, "On the influence of Mn and Mg additions on tensile properties, microstructure and quality index of the A356 aluminum foundry alloy," Procedia Structural Integrity, vol. 2, 2016.

C09: Temperature-Dependent Generation Volume in Semiconductors Under Electron Beam Excitation

J. Lähnemann, U. Jahn, V.M. Kaganer, C. Pfüller,
C. Chèze, K. Biermann, R. Calarco, O. Brandt
Paul-Drude-Institut für Festkörperelektronik,
Leibniz-Institut im Forschungsverbund Berlin e.V., Berlin, Germany

The attainable spatial resolution of analytical techniques based on electron beam excitation such as in a scanning electron microscope is governed by elastic and inelastic scattering of the primary high-energy electrons. The resulting cascade of scattering events leads to a variety of excitations in the sample, such as excited atomic shell electrons, plasmons, and hot electron-hole pairs within a generation volume that strongly depends on the energy of the impinging primary electrons. An accurate knowledge about the spatial distribution of generated carriers is necessary to assess the spatial resolution and perform quantitative analyses for any electron-beam-induced measurements. Commonly employed Monte-Carlo programs such as CASINO [1] simulate this scattering cascade and are generally assumed to represent the generation volume. In the present work, we carry out an experimental determination of the generation volume relevant for cathodoluminescence spectroscopy [2], comparing the results with those simulated using CASINO. Contrary to common belief, the generation volume is found to strongly depend on temperature.

The lateral distribution of generated carriers for sample temperatures between 10 and 300 K is obtained from cathodoluminescence intensity profiles measured across single (In,Ga)N quantum wells embedded in thick GaN layers. Additional, thin (Al,Ga)N barriers inhibit carrier diffusion to the quantum well, which would broaden the profiles. The experimental cathodoluminescence profiles are found to be systematically wider than the energy loss distributions calculated by means of CASINO. This effect becomes more pronounced for both decreasing sample temperatures as well as higher acceleration voltages and is confirmed for analogous GaAs/(Al,Ga)As quantum well structures. We show that this broadening can be explained by the quasi-diffusive expansion of the hot carrier distribution during cooling that takes place prior to the diffusion of thermalized carriers at the band edges and subsequent carrier recombination. This process is controlled by electron-phonon scattering and results in an increasing carrier spread with decreasing temperatures. The dependence on acceleration voltage is a mathematical result of the heavy-tailed nature of the initial scattering volume as calculated by CASINO. Finally, we present a phenomenological approach to simulate the carrier generation volume that can be used for the investigation of the temperature dependence of carrier diffusion. Apart from cathodoluminescence spectroscopy, these results should be directly relevant for electron-beam induced current measurements. Our study shows that the paradigm of a generation volume independent of temperature is not applicable to all SEM-based techniques.

References
[1] D. Drouin *et al.*, Scanning **29**, 92 (2007).
[2] U. Jahn *et al.*, Phys. Rev. Applied **17**, 024017 (2022).

C10: TESCAN TENSOR a 4D-STEM for Multimodal Characterization of Challenging and Interesting Specimens

Robert Stroud[1]
[1]TESCAN USA, 765 Commonwealth Dr #101, Warrendale, PA 15086, USA

The methodology and design behind TESCAN TENSOR - the world's first Integrated, Precession-assisted, Analytical 4D-STEM will be presented. An advanced (electron diffraction) microscope, with STEM, 4D-STEM and STEM Tomography applications, TESCAN TENSOR will be shown to be the solution of choice for a range of nanoscale applications. These include multimodal characterization of functional materials, semiconductor thin films, and submicron, synthetic and natural particle crystals. Examples including results from battery and semiconductor device applications will be presented.

Designed from the ground up, to provide quality, throughput, and robustness of 4D-STEM acquisition, analysis, and processing, TESCAN TENSOR has been optimized with state-of-the-art technologies, such as Precession Electron Diffraction (PED), 4D-STEM computing and visualization, electrostatic beam blanking, and ultra-high vacuum at the specimen area. Additionally, TESCAN TENSOR features near real-time, automated data analysis and processing, whereby on-the-fly processing presents first results during acquisition. As a result, TESCAN TENSOR allows the operator to focus on data acquisition and analysis, rather than time consuming manual microscope alignments.

4D-STEM phase and orientation analysis of lithium-ion battery anode materials. A precession-assisted, analytical 4D-STEM, TESCAN TENSOR, provides a solution for nanoscale phase and orientation mapping of phase separations and crystallographic ordering.

Precession-assisted 4D-STEM was used to produce maps of $LiTi_2(PO_4)_3$, TiO_2 and $LiTiOPO_4$ phases present in spindle-like battery anode particles. 4D-STEM phase analysis will be presented showing that TiO_2 nanoparticles form a network at the $LiTi_2(PO_4)_3$ sub-particle boundaries, which may provide a more effective diffusion pathway for lithium ions at higher cycling rates.

Multimodal phase and orientation analysis of complex semiconductor devices. For semiconductor manufacturers, it is desired to have comprehensive analytical capabilities, with the ability to measure chemical and structural properties, complementary to specimen morphology, down to the sub-nanometer scale. This is generally addressed using Energy Dispersive X-Ray (EDX) mapping, defect analysis through diffraction measurements, crystal orientation and phase mapping, and critical dimension imaging. These capabilities are important as the electrical performance of devices depends strongly on the type and distribution of crystalline phases in individual layers. Analytical electron microscopy, incorporating EDX, and phase/orientation analyses is therefore crucial for both process development and failure analysis.

While EDX maps are useful for rapid evaluation of elemental distributions, they cannot be used to conclusively determine phase distributions or segregations, this is instead investigated using precession electron diffraction assisted 4D-STEM.

TESCAN TENSOR provides a solution for robust, multimodal, nano-characterization of complex semiconductor devices made up of multiple phases with real-time data analysis and processing for the benefit of process development and failure analysis.

C11: Prospects of Full-scale Device Characterization via Ultra Short Pulsed Lasers with Dual Focused Ion Beams

Julia I. Deitz[1,], Daniel L. Perry[1], Andrew T. Polonsky[1], Timothy J. Ruggles[1], Katherine L. Jungjohann[2], Katharine L. Harrison[1], Josefine D. McBrayer,[1] Shannon Boettcher[3], and Joseph R. Michael[1]

[1.] Sandia National Laboratories, PO Box 5800, MS 0886, Albuquerque, NM 87185-0886
[2.] National Renewable Energy Laboratory, Golden, CO 80401
[3.] University of Oregon, Eugene, OR 97403

Characterization of entire devices is vital to establishing the inherent structure-property relationships that govern failure and performance. Particularly, the ability to characterize features in the associated large areas/volumes with nanoscale resolution – chemical impurities, stress voiding, structural defects - provides critical information on interfacial phenomena. Such challenges are frequently tackled via use of conventional Ga^+ focused ion beams (FIB), where slice-and-view milling can give a 3D reconstruction of volumes. However, milling rates associated with the Ga^+ FIB limit the achievable volume to at most 40x40x40 μm^3. Alternatively, Xe^+ plasma FIBs can routinely characterize volumes up to 200x200x200 μm^3, but applications such as battery coin cells and capacitors with relevant features on the order of millimeters in length require larger volumes to get to the features of interest.

Nanoscale characterization of volumes up to 2000x2000x1000 μm^3 became possible with the introduction of the Thermo Fisher Scientific laser Xe^+ FIB. [1] In this contribution, we present 2D and 3D opportunities/challenges with the laser Xe^+ FIB for full-scale device characterization. Specifically we highlight cryogenic work of with battery cells, [2] [3] and electrolyzers. Additionally, we highlight the potential for even larger cross-sectioning with a commercial tantalum capacitor component in original packaging shown in Figure 1. This was achieved by combining multiple laser-cutting operations through automation packages to dimensions more than 4 mm wide. Development of optimized slice and view imaging protocols to enable 3D reconstructions for a wide variety of materials/devices will be discussed.

Figure 1. Composite image of a tantalum capacitor from serial sectioning with the femtosecond laser.

References:

[1] McLean P. Echlin *et. al*, (2020) *COSSMS* 24(2) 100817.
[2] Katherine L. Jungjohann *et. al*, (2021) *ACS Energy Lett.* 6 2138–2144.
[3] Katharine L. Harrison *et.* al, (2021) *Iscience* 24(12) 103394.

C12: ontrolling the Morphology of Rutile Nanowires by Focus-Ion-Beam Irradiation

*Zhina Razaghi[1], Ming-hui Lin[1], Guo-zhen Zhu[1]**

[1] Department of Mechanical Engineering and Manitoba Institute of Materials, University of Manitoba, Winnipeg, MB, R3T 2N2, Canada

Ion beam irradiation has been widely applied as a doping technique for tuning local compositions of thin films and nanostructures. While injecting high-energy ions into the material, crystal defects like vacancies and dislocations form, likely causing local volume expansion and subsequent ion-induced deformation. The ion-induced bending behaviors of nanowires have been discussed under varying conditions such as different ion energies and ion doses for nanowires with different diameters. [1,2] However, how ion-induced bending changes with the shape of nanowires is rarely considered. Herein, single-crystal rutile nanowires with bead-like and prismatic shapes were investigated under a 30 keV Ga^+ ion beam using a TEScan FIB-SEM. An ion dose of 4.32×10^8 cm^{-2} was scanned and thus induced noticeable bending of nanowires, particularly for prismatic nanowires (see the yellow lines). As predicted from the Monte Carlo simulation (IM3D, Irradiated Microstructures in 3D), ion-irradiated region was confined within the depth of ~40 nm from the facet surfaces of nanowires, considering the current irradiation conditions such as the multifaceted morphology of nanowires and consequent changing angle of incidence and shadowing effect. This was additionally supported by ion-damaged regions observed in nanowires using transmission electron microscopy. Accordingly, a finite element model, considering local volume expansion, was employed and successfully predicted the bending effect. Compared to prismatic nanowires, the ion-induced volume expansion can be largely released in bead-like nanowires, and thus, the bending of bead-like nanowires can be suppressed. Such bending effect can be reversed by ion irradiation in the opposite direction.

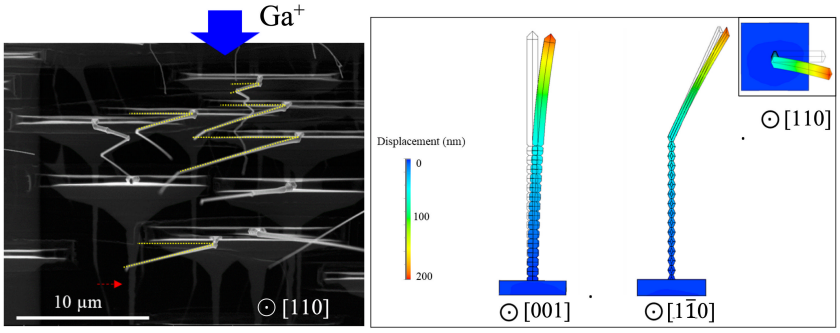

Figure 1 Ion-induced bending of rutile nanowires [3]. Left: SEM image of rutile nanowires under a Ga+ ion beam. These nanowires consist of bead-like part (vertical) and prismatic part (inclined). Right Figure: Finite-Element (FE) simulation (Ansys) of the displacement profile of nanowires, with volume expansion predicted by the implantation profile calculation from IM3D simulations.

References

[1] Chaudhary, Y.S., Khan, S.A., et al., Thin Solid Films, 492(2005): 332-226.
[2] Doan, N., Martin, G., Physical Review B, 67(2003): 134107.
[3] Razaghi, Z., D.Y. Xie, et al., RSC Advance, 12(2022):5577-5586.

C13:Beyond Direct Milling by FIB: Peculiar Self-Organization, Self-Assembly and Site-Specific Defect Engineering on the Surfaces

Bhaveshkumar Kamaliya[1], Morvarid Ghorbani[1,] Angela Cleri[2], Adrian Kitai[1], Jon-Paul Maria[2], Jing Fu[3], Rakesh Mote[4], Nabil Bassim[1]

[1] Materials Science and Engineering, McMaster University, Hamilton, ON, Canada
[2] Materials Science and Engineering, Pennsylvania State University, University Park, PA, USA [3] Mechanical and Aerospace Engineering, Monash University, Clayton, Victoria, Australia
[4] Mechanical Engineering, Indian Institute of Technology Bombay, Mumbai, Maharashtra, India

Precise nanoscale control on the atomistic structure progression of the material surface during FIB irradiation attained unconventional nano-polygons [1] and superior complexities in 3D morphologies [2]. These periodic nanostructures, which protruded from the surface and evolved from an array of circular FIB-spots, demonstrated the peculiar capability of FIB. The experimental attempts lack a complete understanding of the mechanism behind the formation of these unusual nanostructures; thus, molecular dynamics (MD) simulations are essential for robust atomistic insights. Generally, the MD simulations (being computationally extensive) for FIB-materials interactions are carried out with single-spot FIB-impingement [1] in the simulation domain; this approach limits the understanding towards the formation of 3D nanostructures. Hence, modified MD simulations were carried out with multi-spot FIB-impingement (periodically in a square grid manner) over the surface of the Ge-crystal to investigate the kinetics of thermalization, crystallographic damage, and morphology transition. The physical effects, such as site-specific thermalization, atomic stresses, atomic diffusion, and site-specific lattice transformation, were investigated. Further, the kinetics of the viscous-fingering process was investigated for nanoscale-control on phase transformation and site-specific self-organization. This study advances the operation and understanding of peculiar self-organization by FIB-material interactions, and it provides novel theoretical insights into controlling the morphologies at the nanoscale.

The next part of the talk focuses on the defect engineering in Cadmium Oxide (CdO) and Silicon Carbide (SiC) P-I-N Junction for enhancing its optoelectrical properties owing to the capacity of FIB for site-specific ion-implantation in nanoscale precision. Site-specific carrier concentration modification in CdO can result in the fabrication of laterally-patterned optical metamaterials with an all-FIB process without requiring a layer-by-layer material deposition to form heterojunction constituents. Tailoring the site-specific defects in Silicon Carbide (SiC) P-I-N Junction results in improved photoluminescence properties of the device. These defect engineering attempts provide the pathway towards unconventional optoelectronic devices and photonic properties.

References

[1] B. Kamaliya, V. Garg, A. C. Y. Liu, Y. (Emily) Chen, M. Aslam, J. Fu, and R. G. Mote, *Tailoring Surface Self-Organization for Nanoscale Polygonal Morphology on Germanium*, Adv. Mater. **33**, 2008668 (2021).
[2] B. Kamaliya and R. G. Mote, *Nanofabrication Using Focused Ion Beam*, in *Advanced Machining Science*, edited by V. K. Jain (CRC Press, 2022), pp. 229–248.

C14: Enhanced Visualization of Collagen Fibril and Mineral Ellipsoids in Bone Tissue Using FIB-SEM Nanotomography and Advanced Analysis Tools

Alyssa Williams[1,2], Tengteng Tang[3], Aurélien Gourrier[4,5], Michael W. Phaneuf[2], Nabil Bassim[1,3,6], Kathryn Grandfield[1,6]

[1.] School of Biomedical Engineering, McMaster University, Hamilton, Ontario, Canada
[2.] Fibics Incorporated, Ottawa, Ontario, Canada
[3.] Department of Materials Science and Engineering, McMaster University, Hamilton, ON, Canada
[4.] Univ. Grenoble Alpes, LIPHY, F-38000, Grenoble, France.
[5.] CNRS, LIPHY, F-38000, Grenoble, France
[6.] Canadian Centre for Electron Microscopy, McMaster University, Hamilton, ON, Canada

Bone architecture is founded on the arrangement of mineral and organic content. At the nanoscale, collagen fibrils and ellipsoidal-shaped mineral-rich regions create the building blocks of bone and indicate nanoscale bone processes [1–3]. 3D visualization of these features is challenging in mineralized tissue due to the requirements of high-resolution imaging across a large volume[4]. In this work, we used focused ion beam-scanning electron microscopy (FIB-SEM) nanotomography and image analysis to enhance the 3D visualization of collagen fibrils in the context of mineral ellipsoids in human tibial cortical bone tissue. FIB-SEM nanotomography acquisition alongside tools such as deep learning and fast Fourier transform (FFT) and inverse FFT analysis were optimized and implemented for clear visualization of the collagen fibril 67nm D-banding periodicity and mineral ellipsoids in orthogonal planes. FFT analysis highlights the ubiquitous presence of fibrils both in and around mineral ellipsoids and 3D visualization clearly shows fibrils co-aligned with the ellipsoids' major long axis. 3D analysis also shows fibrils crossing over towards the center of the ellipsoids (Figure 1E- white arrow). Thereby, experiencing twisting at the fibril level. This study is the first to segment collagen fibrils in association with mineralized cortical bone tissue from FIB-SEM and the utilization of inverse FFT analysis to enhance the visualization of collagen fibrils in/around mineral ellipsoids. Thereby, elucidating the interwoven connection between these two distinctive hierarchical features of nanoscale bone architecture.

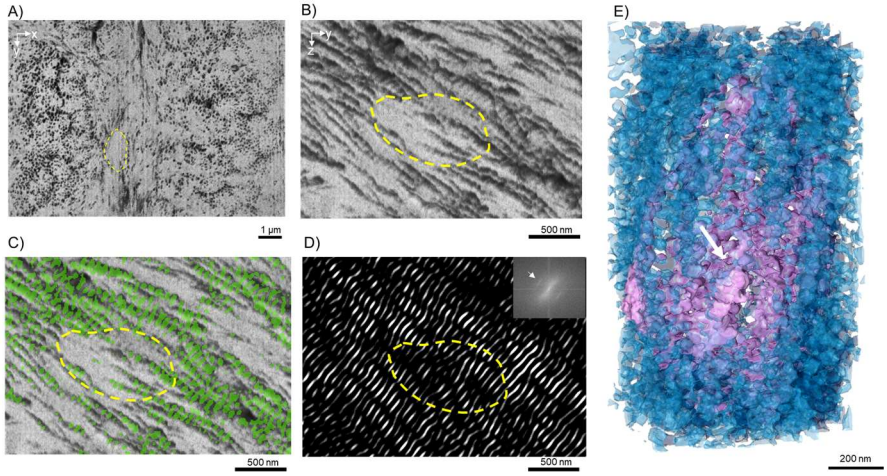

Figure 1. A) Bone FIB-SEM view with ellipsoids present (yellow outline). B) Ellipsoid structure with visible collagen fibrils. C) Fibril segmentation D) IFFT analysis of fibril periodicity. E) 3D fibrils in (pink) and outside (blue) of the ellipsoid

References

[1] Binkley et al. J Struct Biol (2020) 107615.
[2] Buss et al. J Struct Biol 212 (2020) 107603.
[3] Katz et al. Connect Tissue Res 21 (1989) 149–158.
[4] Raguin et al. Ssrn Electron J (2020).

C15: 3D Reconstruction and Characterization of Lath Martensite in 13Cr-4Ni Stainless Steels Using PFIB-EBSD Serial Section Tomography

Mehdi Mosayebi[1], Daniel Paquet[2], Pierre-Antony Deschênes[2,3], Nabil Bassim[1,4]

[1] Materials Science and Engineering Department, McMaster University, Hamilton, ON, Canada.
[2] Hydro-Québec, Institut de recherche d'Hydro-Québec, Varennes, QC, Canada.
[3] Mechanical Engineering Department, École de technologie supérieure, Montreal, QC, Canada.
[4] Canadian Centre for Electron Microscopy, McMaster University, Hamilton, ON, Canada.

Lath martensite in steel is well known to show a hierarchical microstructure consisting of packets, blocks, sub-blocks, and laths. Since this complex microstructure affects the toughness and strength of steels, clarifying the characteristics of morphology and crystallography of martensite is of great importance [1,2]. 3D characterization techniques have demonstrated great potential to provide important insights into the 3D morphology of complicated microstructures. In this regard, serial section tomography with Xe+ plasma FIB (PFIB) offers the ability to collect data from sufficiently large volumes to be representative of the behavior of the bulk material while maintaining sufficient spatial resolution to observe all relevant features of a complex microstructure [3].
In this study, PFIB serial section tomography was employed for large-volume 3D EBSD characterization of low-carbon 13Cr-4Ni martensitic stainless-steel. The results of crystallographic and morphological analysis revealed that each martensitic packet can be decomposed into clusters of martensitic blocks such that blocks with specific variants can adapt unique morphological arrangements in 3D. Figure1 presents real examples of these morphological arrangements including: **(i)** parallel arrangement of three distinct variants sharing ~60°@[011] orientation relationship, **(ii)** T-shape arrangement of two distinct variants sharing ~10°@[011] orientation relationship, and **(iii)** Triangular arrangement of three distinct blocks sharing ~10°@[011], ~50°@[011], and ~60°@[011] orientation relationships.

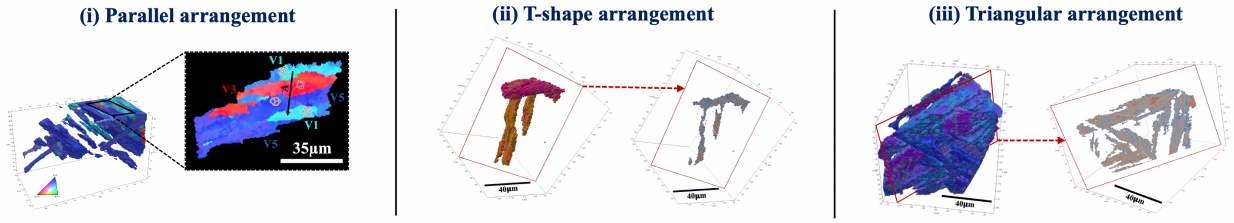

Figure 1. 3D reconstruction of three different morphological arrangements observed for martensitic blocks in 13Cr-4Ni martensitic stainless-steel using PFIB-EBSD tomography.

References

[1] Kitahara, Hiromoto, et al. "Crystallographic features of lath martensite in low-carbon steel." *Acta materialia* 54.5 (2006): 1279-1288.
[2] Morito, Shigekazu, et al. "Quantitative analysis of three-dimensional morphology of martensite packets and blocks in iron-carbon-manganese steels." *Journal of Alloys and Compounds* 577 (2013): S587-S592.
[3] Burnett, T.L., et al. "Large volume serial section tomography by Xe Plasma FIB dual beam microscopy." *Ultramicroscopy* 161 (2016): 119-129.

C16: FIB-SEM Tomography: Measuring Slice Thickness With Ga And Xe Ion Species FIBs And Stage Rocking

*V. Ondračka[1], J. Dluhoš[2], M. Joens[3], J. Kaštyl[1]**
[1] TESCAN Brno s.r.o., Brno, Czech Republic
[2] TESCAN ORSAY HOLDING a.s., Brno, Czech Republic
3TESCAN USA Inc., Warrendale, Pennsylvania, USA

During a FIB-SEM tomography data volume reconstruction, the voxel size is of great importance. While the x and y voxel sizes are validated by SEM calibration during the microscope setup, the z voxel size, i.e., slice thickness, is affected by factors such as stage stability, sample thermal drift, stage movement precision, and drift correction algorithm precision.

In this study we obtained the actual slice thickness by measuring the shift per slice of prepared surface structures, see Figure 1., similar to the one used by Jones, Mingard and Cox [1].

Figure 1: Two ruler-structure images, one in green and one in red channel, overlayed. The images are separated by 20 slices, illustrating the shift in the angled ruler lines that is measured and used for the slice thickness calculation. A new angled line can be seen appearing on the right side.

Three measurements were performed, one for Ga beam, Xe beam, and Ga beam with added stage "rocking movement" during the slicing step. Image analysis using an ImageJ macro based on ROI image correlation confirmed stable slicing with a random error around the nominal slice thickness. All the measurements contained more than 1500 slices, running automatically for at least 2 days, and the overall slicing stability was also confirmed by visual inspection of the reconstruction.

Having available the data from drift correction, its quality and raw images, we can draw conclusions regarding the right drift correction acquisition conditions and correlation marks. The data acquired shows that TESCAN's FIB-SEM Tomography yields stable slicing and relevant results if FIB drift correction is used and best practices are followed, without having to rely on slice thickness measurement procedures that require flat samples, additional acquisition time, resolution, and postprocessing.

References

[1] H.G. Jones, K.P. Mingard, D.C. Cox; *Investigation of slice thickness and shape milled by a focused ion beam for three-dimensional reconstruction of microstructures;* Ultramicroscopy 139 (**2014**), pp. 20-28.

C17:High-Resolution FIB and SIMS with a Cesium Low Temperature Ion Source

Brenton Knuffman, Andrew Schwarzkopf, Adam V. Steele
zeroK NanoTech Corporation, Gaithersburg, MD, USA

We present the latest results from focused ion beam and secondary ion mass spectrometry systems employing a Cs+ Low Temperature Ion Source (LoTIS)[1]. The Cs+ LoTIS provides a high-brightness beam of ions that extends the capabilities of modern FIB and SIMS systems. For FIB applications, LoTIS provides a smaller probe size at picoampere currents for nanomachining applications when compared to the Ga+ LMIS and sufficient current for preparing cross sections. For SIMS applications, LoTIS provides order-of-magnitude smaller probe sizes across a range of currents enabling the highest available spatial resolution when compared to other reactive species ion sources for SIMS. The SIMS:ZERO instrument developed at zeroK in collaboration with the Luxembourg Institute of Science and Technology (LIST) synergizes the advantages LoTIS brings to FIB and SIMS, enabling users to enhance SIMS microscopy techniques with FIB sample preparation and FIB nanofabrication with real-time SIMS analysis for process control.

(A)

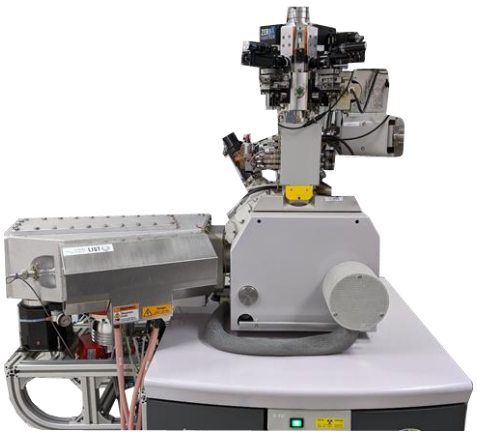

(B)

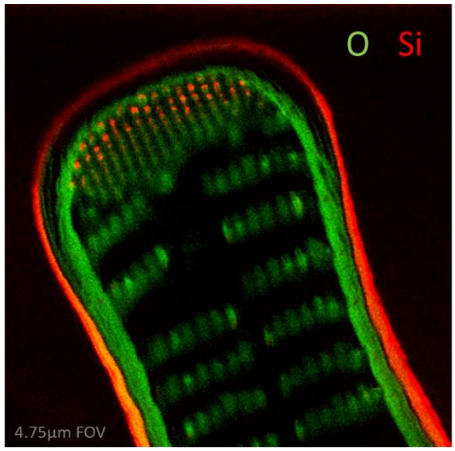

(C)

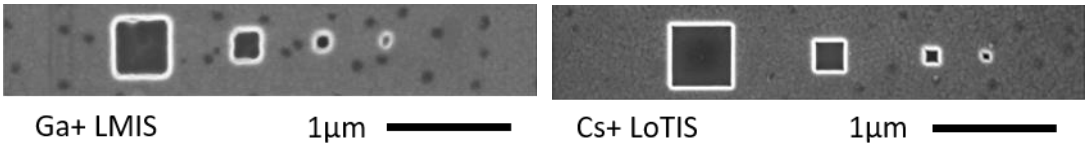

(A): FIB/SIMS instrument "SIMS:ZERO" equipped with a Cs+ Low Temperature Ion Source and a compact magnetic sector mass spectrometer for SIMS; ***(B)*** SIMS image of oxygen and silicon distributions in a diatom. Acquired with SIMS:ZERO – credit J. Audinot & O. de Castro, Luxembourg Institute of Science and Technology; ***(C)*** Comparison of FIB milling in Au film by a Ga+ LMIS (***Left***) and a Cs+ LoTIS (***Right***) – credit T. Loeber, Technical University Kaiserslautern

References

[1] A. V. Steele, A. Schwarzkopf, J. J. McClelland, and B. Knuffman. *Nano Futures*. **1**, 015005 (2017)

C18: ToF-SIMS on a Plasma FIB: Dos and Don'ts

Jamie Ford[1]
[1] Singh Center for Nanotechnology, University of Pennsylvania, Philadelphia, PA, USA

While time-of-flight secondary ion mass spectrometry (ToF-SIMS) is a well-established analytical technique, it is uncommon to perform it with a Xe plasma focused ion beam microscope (XePFIB). Introducing a new technique to a central user facility with novice users leads to valuable lessons learned. In this talk, I will share some of those lessons, best practices for introducing a new technique to users, how to set expectations for unknown samples, and results from the wide variety of polymers, metals, and ceramics that come through a central academic facility.

C19: Novel LaserFIB Sample Preparation of Pillar Arrays For Synchrotron Imaging

Cheryl Hartfield[*1], Aubrey Funke[1], Heiko Stegmann[2], Joerg Lindenau[2]*

[1]Carl Zeiss Microscopy, LLC, White Plains, USA
[2]Carl Zeiss Microscopy GmbH, Oberkochen, Germany

Science is driven by good sample preparation, and the recent emergence of fs-lasers integrated into FIB-SEM instruments [1] produces a new class of instruments known as LaserFIB. These new FIB-SEM are enabling greater insights in materials and life sciences through new sample preparation approaches. The use of fs-laser for targeted synchrotron sample preparation of an epoxy-embedded biological sample has been previously described [2]. The pillars produced in that work were of high quality with structure visible on the laser-cut surface and displayed the characteristic sloping sidewalls that result from top-down laser ablation under standard parameters. There are two challenges to this sample preparation. First, an ideal synchrotron or nanoscale X-ray sample should ideally be a uniform cylinder. Second, a large volume of material is typically removed to create the pillars, potentially destroying material containing unique or important features and information.

In this talk, a new and innovative top-down fs-laser processing strategy will be presented, whereby arrays of closely spaced high-aspect-ratio pillars having nearly vertical sidewalls are produced in a matter of minutes. This solves the above-mentioned challenges, and further enables synchrotron analysis from a larger volume of interest than was previously possible. It will be shown how submicron 3D X-ray microscopy is used in a streamlined correlative workflow with the LaserFIB to ensure pillars contain desired targeted features. The application of this new sample preparation for study of ultrastructural changes important to the study of retinopathies, as recently published [3], will be discussed along with the potential for addressing diverse samples and applications by this new sample preparation method.

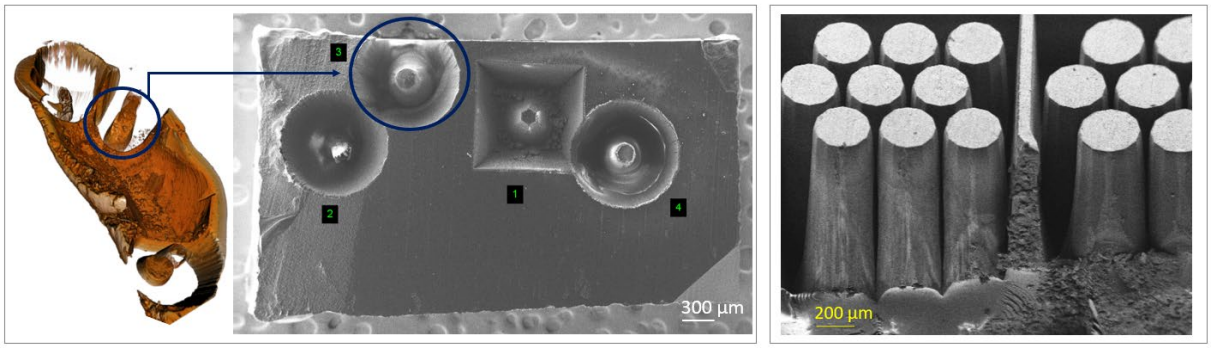

Previous work targeted a site based on 3D X-ray microscopy data (left image). Further parameter optimization makes it possible to extract multiple pillars of 500 µm in height from samples in a mm or more area (right image).

References

1. Tordoff et al. Appl Microsc. 2020 Oct 26;50(1):24. doi: 10.1186/s42649-020-00044-5.
2. Hartfield et al., invited talk at FIB-SEM User Meeting 2021, accessible at https://www.zeiss.com/microscopy/en/resources/insights-hub/life-sciences/the-pivotal-role-of-fib-sem.html
3. Bosch et al. 2023 bioRxiv preprint at https://doi.org/10.1101/2023.01.10.523473

C20: Automated preparation of high-quality lamellae using artificial intelligence assessed by 4D-STEM multimodal analysis

Jaroslav Kastyl, Tomas Moravek, Lukas Omasta, Andrej Baldovsky, Rostislav Vana, Zsolt Radi
TESCAN Brno s.r.o., Brno, 623 00, the Czech Republic

Significant progress was made over the last decade in sample preparation for transmission electron microscopy (TEM) where gallium-based focused ion beam (FIB) devices together with scanning electron microscope (SEM) systems play a major role. [1, 2] At the same time, the growing complexity of microscopes and continuing miniaturization in nanotechnologies place increasing demands on human FIB-SEM operators. [3] The latest AutoSlicer™ tool by TESCAN, a material-independent software module utilizing artificial intelligence (AI) and neural networks was used to produce lamellae-like site-specific samples from various materials in automated way, with user-defined dimensions and in condition ready for TEM/STEM analysis. The AutoSlicer™ module was used with a predefined set of templates tuned up for the mostly analyzed groups of materials. Next, detailed multimodal analysis was performed using the newly developed near-UHV TESCAN TENSOR 4D-STEM [4]. Among the others, semiconductor samples, ceramics and metals got processed automatically with great repeatability and analyzed successfully.

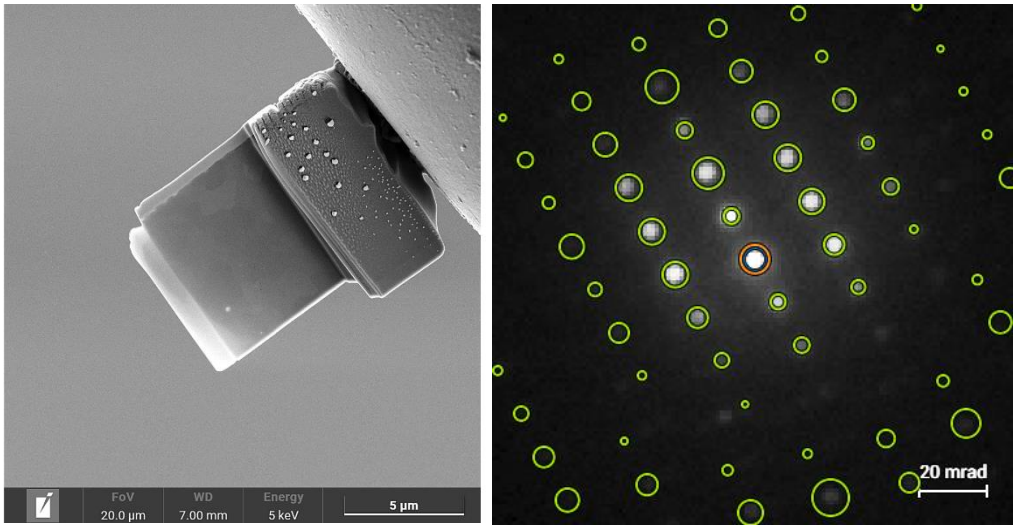

Left figure: The high quality of ZrO_2 ceramic lamella prepared by TESCAN AutoSlicer™ was achieved after Ga-FIB milling even at 30 kV@150 pA as the latest (final) step.
Right figure: Diffraction pattern provided by TESCAN TENSOR from ZrO_2 lamella prepared by AutoSlicer™ showing high signal-to-noise ratio and precise crystallographic matching (cubic symmetry).

References

[1] L. Gu, N. Wang, X. Tang, H. G. Changela. DOI: 10.1155/2020/8406917
[2] T. Zhou, R. P.Babu, Z. Hou, P. Hedström. DOI: 10.1080/10408436.2021.1941751
[3] M. Manoccio, M. Esposito, A. Passaseo, M. Cuscunà, V. Tasco. DOI: 10.3390/mi12010006
[4] Tescan unveils TENSOR STEM – Wiley Analytical Science, available on 9 November 2022, https://analyticalscience.wiley.com/do/10.1002/was.0002056997

C21: Practical Applications of the Multi-Ion Species Plasma Focused Ion Beam

Rick Passey[1], *Qian (Ken) Wu*[1], *Brandon van Leer*[1], *Adam Stokes*[1]
[1]Thermo Fisher Scientific, 5350 NE Dawson Creek Dr, Hillsboro 97124, USA

In 2020, the first multi-ion species plasma focused ion beam (PFIB) became commercially available. Combined with the scanning electron microscope (SEM), this new form of DualBeam (SEM+PFIB) provided four ion species: xenon, argon, oxygen, and nitrogen. These ion species enable several types of sample modification, including site specific cross-sectioning, lamella preparation for transmission electron microscope (TEM) analysis, forming atom probe tomography (APT) tips, and 3D tomography (using electron/ion imaging, energy dispersive x-ray analysis (EDS), or electron backscatter diffraction (EBSD)). The application of the original xenon PFIB in the early 2010s was obvious; higher beam currents equaled higher milling rates compared to gallium FIB; xenon eliminated any sample conflict when using a reactive gallium FIB source. The xenon PFIB was capable of nearly everything that had previously been performed using the gallium FIB. So why add access to argon, oxygen, and nitrogen plasma? What capabilities does argon, oxygen, and nitrogen provide that xenon and gallium do not? This presentation will highlight the unique applications for each ion species and review the latest results in the fields of material science, life science, and semiconductor production and development.

C22: The next generation FIB source: GaBiLi ions for 2D and 3D ion microscopy

Yang Yu[1], Andre Linden[1], Torsten Richter[2]
[1] Raith America Inc., Islandia 11749, NY, USA, [2] Raith GmbH, 44263 Dortmund, Germany

Liquid Metal Alloy Ion Source (LMAIS) is an emerging Focused Ion Beam (FIB) source technology. It has been established for nanofabrication over the last years [1]. Most recently, ion imaging with Lithium ions from GaBiLi eutectic alloy has become feasible [2]. Multiple ion species such as Lithium and Bismuth are emitted simultaneously from a single source and are separated in a downstream Wien filter. We have developed a FIB column that accomplishes automatic switching between different ions such as Li and Bi within a few seconds. Different ion species, light or heavy and fast or slow, can be selected quickly without any source change or column adjustment [3].
Lithium is the lightest ion available from LMAIS. It features the smallest virtual source diameter and lowest energy spread [4]. Hence Lithium offers the smallest probe size of all ions emitted from eutectic alloys, resulting in sub 2nm image resolution at lowest sample damage and highest surface sensitivity (Fig. 1, Fig.2).
Besides Lithium, Gallium and Bismuth ions, Bi clusters are also available from the same source. Bismuth ions and in particular Bi clusters have an excellent depth resolution to be utilized for sample delayering. Using Bi ions/clusters along with smart strategies for uniform sample delaying and Li ions for 2D imaging provides an outstanding scheme for in-situ 3D imaging and analysis of various samples. This engineering setup allows stable imaging of 3D structures and sample reconstruction (Fig. 3). Beside ion imaging and nanofabrication FIB is utilized as a primary beam for SIMS analysis [5]. GaBiLi ions enable application optimized SIMS at maximum sensitivity, optimized sputter yield and highest lateral resolution.
In this contribution we describe the working principle and capabilities of a top-down FIB system equipped with GaBiLi LMAIS. Results of 2D Lithium-ion microscopy and workflows for stable 3D tomography without stage or sample tilt by Bismuth milling and Li imaging will be presented.

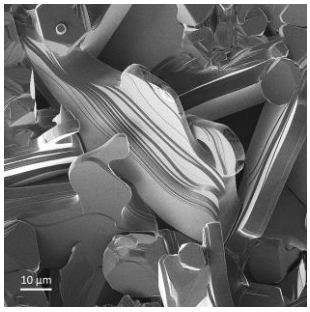

Fig.1: Bi_2-Ca_2-Co compound

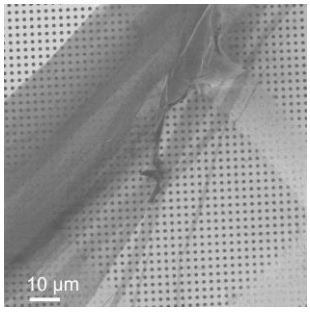

Fig 2: CNM

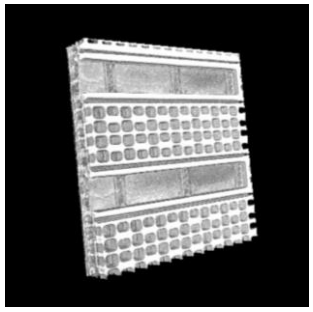
Fig.:3 3D reconstruction

References
[1] J. Gierak et al, Journal of Vacuum Science & Technology B 36, 06J101 (2018)
[2] N. Klinger et al, Beilstein J. Nanotechnology, 11, 1742–1749 (2020)
[3] W. Pilz et al, Journal of Vacuum Science & Technology B 37, 021802 (2019)
[4] L. Bischoff et al, Appl. Phys. Rev. 3, 021101 (2016)
[5] Jean-Nicolas Audinot et al, Rep. Prog. Phys. 84 105901 (2021)

C23: A new FIB/SEM for TEM sample preparation workflow

Patrick Phillips[1], *Hiroki Kato*[2]
[1] JEOL USA, Inc. Peabody, MA, USA
[2] JEOL Ltd. Akishima, Tokyo, Japan

The newly released JIB-PS500i from JEOL Ltd. focuses on ease-of-use in the materials science sample preparation space. In many fields of materials science, such as battery, semiconductor, thin film, quantum, etc., site-specific analysis is critical. Be it for chemical, structural, or electronic characterization of defects and interfaces, it is oftentimes necessary to identify a TEM sample region of interest on the nanometer scale. The dual-beam focused ion beam/scanning electron microscope (FIB/SEM) remains the typical instrument for this type of TEM sample preparation. The JIB-PS500i aims to streamline lamella preparation workflow while simultaneously improving the quality of the lamellae.

Owing to a large, high-tilt and flexible chamber design, a user is able to seamlessly switch between processing and imaging to observe the lamella quality (Fig. 1) during preparation. SEM and FIB column improvements enable low kV imaging and processing for damage reduction/sample thinning. Furthermore, a newly designed double tilt cartridge (Fig. 2) transfers between the FIB/SEM stage and TEM without requiring lamella grid removal or remounting.

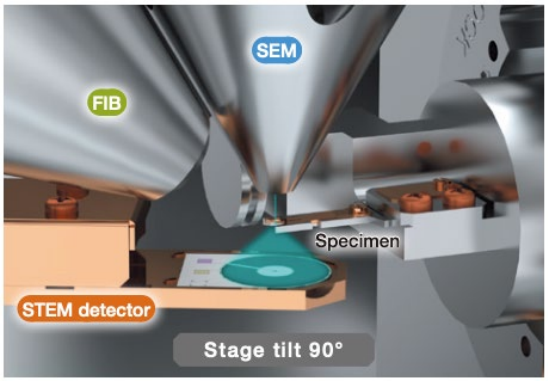

Figure 1. Inside the JIB-PS500i chamber, the stage is tilted to 90 degrees for immediate STEM imaging to determine sample quality.

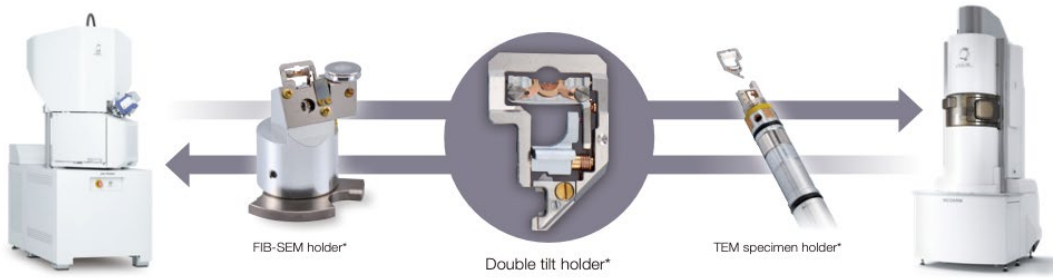

Figure 2. The double tilt cartridge transfers immediately between FIB/SEM and TEM with no need to remove the prepared lamella.

C24: The *Stenciling Principle* for Extracellular Matrix Mineralization

Marc D. McKee[1,2], Daniel J. Buss[2], Natalie Reznikov[1,2,3]

[1]Dental Medicine and Oral Health Sciences, [2]Anatomy and Cell Biology, [3]Bioengineering,

McGill University, Montreal, QC, Canada

Correlative, multi-scale imaging approaches are now in common use in structural biology studies. However, this is not generally the case for hard mineralized tissues such as bone, where the matrix is permeated with a mineral phase that renders them difficult to analyze. Given the nano-scale structure of apatite crystals within the fibrillar, collagenous extracellular matrix of bone, together with their micro-scale crossfibrillar tessellation – a packing pattern that contributes to bone's well-known mechanical properties – it is imperative to assess bone in a correlative and contextual 3D manner to study matrix-mineral relationships.

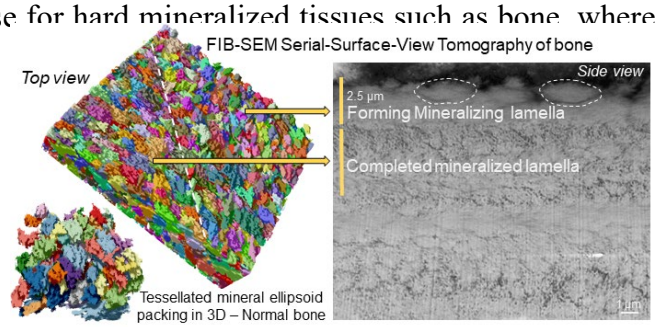

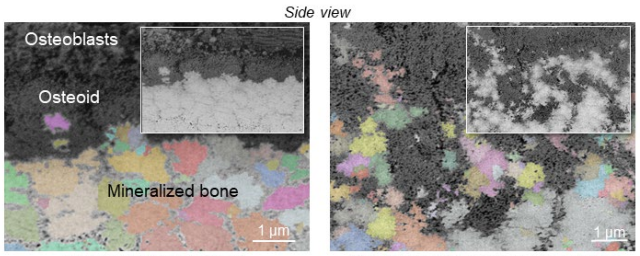

We use a variety of multi-scale imaging approaches to study normal (wildtype) and diseased (osteomalacic /hypomineralized, *Hyp*) mouse bone. These correlative approaches include light microscopy, TEM and SEM, and micro/nano-computed X-ray tomography and FIB-SEM electron tomography, the latter two with the additional implementation of feature segmentation aided through the use of deep-learning algorithms and image analysis protocols. From our microscopy findings, we present the *Stenciling Principle* for extracellular matrix mineralization which describes an enzyme-substrate pairing, double-negative regulatory process (inhibition of inhibitors) that promotes biomineralization. The principle relates to both small-molecule and protein inhibitors of mineralization, and promoters (enzymes) that degrade the inhibitors to permit and regulate mineralization. In this process, an organizational micro-scale motif for bone mineral arises that we call *crossfibrillar mineral tessellation* where mineral formations traverse multiple collagen fibrils (laterally), a patterning that is defective in the osteomalacic *Hyp* mouse. Tessellation of a same, small basic unit to form larger structural assemblies results in numerous 3D interfaces, allows dissipation of critical stresses, and enables fail-safe cyclic deformations in healthy bone. Incomplete mineral tessellation in osteomalacia may explain why soft osteomalacic bones buckle and deform under loading. *Funded by CIHR.*

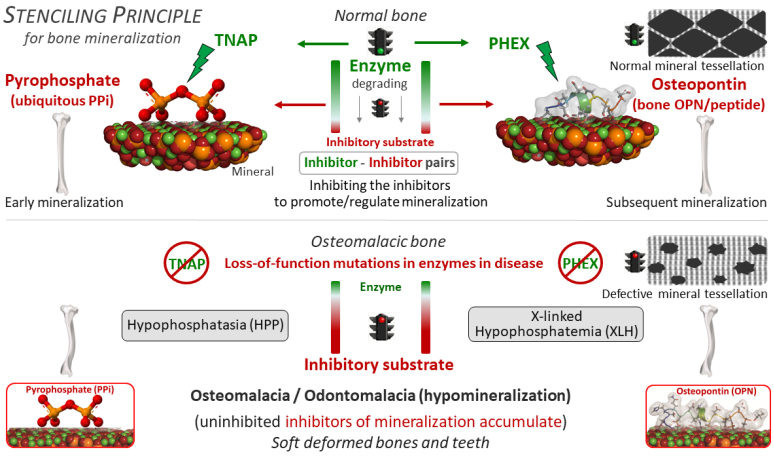

C25: The translating bacterial ribosome at 1.55 Å resolution by open access cryo-EM

Simon A. Fromm[1†], Kate M. O'Connor[2], Michael Purdy[3], Pramod R. Bhatt[2], Gary Loughran[2], John F. Atkins[2,4*], Ahmad Jomaa[3,5†*], Simone Mattei[1,6*]

Affiliation

[1]EMBL Imaging Centre, European Molecular Biology Laboratory, Heidelberg, Germany.
[2]School of Biochemistry and Cell Biology, University College Cork, Cork T12 XF62, Ireland.
[3]Department of Molecular Physiology and Biological Physics, School of Medicine, University of Virginia, Charlottesville, USA.
[4]MRC Laboratory of Molecular Biology, Cambridge CB2 0QH, UK
[5]Centre for Cell and Membrane Physiology, University of Virginia, Charlottesville, USA.
[6]Structural and Computational Biology Unit, European Molecular Biology Laboratory, Heidelberg, Germany.

*Corresponding to: simone.mattei@embl.de, ahmadjomaa@virginia.edu, J.Atkins@ucc.ie

† These authors contributed equally

Abstract

Our understanding of protein synthesis has been conceptualised around the structure and function of the bacterial ribosome. This complex macromolecular machine is the target of important antimicrobial drugs, an integral line of defence against infectious diseases. Here, we present the structure of the translating ribosome from *Escherichia coli* at 1.55 Å resolution. The obtained structures allow for direct determination of the rRNA sequence to identify ribosome polymorphism sites in the *E. coli* strain used in this study and enable interpretation of the ribosomal active and peripheral sites at unprecedented resolution. This includes scarcely populated chimeric hybrid states of the ribosome engaged in several tRNA translocation steps resolved at ~2 Å resolution. The current map not only improves our understanding of protein synthesis but also allows for more precise structure-based drug design of antibiotics to tackle rising bacterial resistance.

C26: Visualizing Cellulose Nanostructure with High Resolution Microscopy

Mouhanad Babi,[1] Ayodele Fatona,[1] Anthony Palermo,[1] Alyssa Williams,[2] Xiang Li,[1] Christine Cerson,[1] Victoria Jarvis,[3] Nabil Bassim,[4,5,6] Emily Cranston,[7,8] Tiffany Abitbol,[9] Jose Moran-Mirabal[1,2,6,10]*

[1] Department of Chemistry and Chemical Biology, McMaster University; [2] School of Biomedical Engineering, McMaster University; [3] McMaster Analytical X-ray Diffraction Facility, McMaster University; [4] Canadian Centre for Electron Microscopy, McMaster University; [5] Department of Materials Science and Engineering, McMaster University; [6] Brockhouse Institute for Materials Research, McMaster University; [7] Department of Wood Science, University of British Columbia; [8] Department of Chemical and Biological Engineering, University of British Columbia; [9] RISE Research Institutes of Sweden; [10] Center for Advanced Light Microscopy, McMaster University.

Abstract

Nanocelluloses are attractive materials for the production of biodegradable and renewable products. The use of nanocelluloses for such practical applications often requires visualizing their distribution within complex matrices. This can be achieved with fluorescence microscopy techniques if the nanocelluloses are fluorescent, as the sensitivity and specificity of these methods permit visualizing nanoparticles and nanofibers within complex systems. Yet, advanced imaging methods like multiphoton or super-resolution microscopy are rarely applied to cellulose. This is partly due to a lack of efficient and cost-effective methods to fluorescently tag nanocelluloses without altering their unique properties. We have developed modular surface chemistry, based on triazinyl linkers, that allows us to tune the reactivity of cellulosic materials, leading to efficient ways of fluorescently tagging nanocelluloses.[1]

In this presentation, I will describe our work on labeling nanocelluloses for use in high resolution fluorescence microscopy studies. I will present a versatile and efficient two-step approach based on triazine and azide–alkyne click-chemistry to label nanocelluloses with a variety of dyes.[2] This method was used to label a range of nanocelluloses to high degrees of labeling using minimal amounts of dye while preserving their native morphology and crystalline structure. The ability to tune the labeling density with this method allowed us to prepare optimized samples that were used to visualize nanostructural features of cellulose through super-resolution microscopy. Using this approach, we directly visualized and measured alternating crystalline and disordered regions within individual fluorescently labelled bacterial cellulose (BC) fibrils.[3] To study the structural origins of the disordered regions along BC fibrils, we used correlative super-resolution light/electron microscopy and observed that the disordered regions seen in super-resolution correlate with the ribbon twisting observed in electron microscopy.[4] Through efficient labeling and high-resolution microscopies, unraveling the hierarchical assembly of bacterial cellulose provides insight into its biosynthesis and susceptibility to hydrolysis.

References

[1] Fatona A, *et. al.* (2018) *Chemistry of Materials*. 30: 2424-2435.
[2] Babi M, *et al.* (2022) *Biomacromolecules*. 23: 1981-1994.
[3] Babi M, *et al.* (2022) *ChemRxiv.* https://doi.org/10.26434/chemrxiv-2022-0jqng
[4] Babi M, *et al.* (2023) *Biomacromolecules*. 24: 258-268.

C27: NanoMi: an Introduction to an Open-Source Electron Microscope

Marek Malac[1,2], Mark Salomons[1], Darren Homeniuk[1], Makoto Schreiber[1,2], Sam Ruttiman[1,2], Xuanhao Wang[3], Olivier Adkin-Kaya[4], Mohammad Kamal[4], Jesus Alejandro Marin Calzada[2], Patrick Price[1], Martin Cloutier[1], Misa Hayashida[1], Ray Egerton[2], Ken Harada[5], Yoshio Takahashi[6], Heiko Muller[7]

[1] NRC-NANO, Edmonton, Alberta, Canada
[2] Dept. of Physics, U. of Alberta, Edmonton, Alberta, Canada
[3] Dept. Comp. Sc., U of Alberta, Edmonton, Alberta, Canada
[4] Dept. Electical and Comp. Eng., U. of Alberta, Edmonton, Canada
[5] RIKEN, Center for Emergent Matter Science, Hatoyama, Saitama 350-0395, Japan
[6] R&D group, Hitachi, Ltd., Hatoyama, Saitama 350-0395, Japan
[7] CEOS, GmbH, Heidelberg, Germany

We are developing a public-license electron microscopy platform, referred to as NanoMi [1,2]. NanoMi provides modular components for SEM, STEM, TEM, and electron diffraction (ED) capabilities, Fig. 1. An important aspect of the NanoMi design is ease of manufacturing of its components, their affordability, and ease of assembly and alignment making it suitable for educational purposes. NanoMi intended imaging performance is modest, e.g. 10 nm minimum probe diameter in SEM and STEM mode, 10 nm image resolution in TEM and maximum intended electron energy of 50 keV. NanoMi components are ultra-high vacuum compatible for implementation of custom instruments, electron optics test-beds and for attachments to an existing aparatus. The electron optics of NanoMi is independent of its vacuum envelope, the latter utilizing off the shelf ConFlat™ hardware. The first NanoMi uses elecrostatic einzel lens, deflectors and stigmators eliminating the need for water cooling. We are now focusing on implementation of TEM, STEM and ED capabilities. The Python control software, is completed and real-time display and live data processing are facilitated using Panta-Rhei Image Viewer by CEOS GmbH on a Linux PC. Data are collected using a Canon M50 digital camera pointed at a scintillator screen that communicates with the Image Viewer.

Further information and links to electronic resources, such as source code of the control software, can be found at nanomi.org and github.com/NRC-NANOmi/NanoMi.

References

[1] M. Malac et al., NanoMi: An open source electron microscope hardware and software platform, Micron 163 (2022), 103362.

[2] Support for the project was provided by NRC-NANO and by NSERC RGPIN-2021-02539.

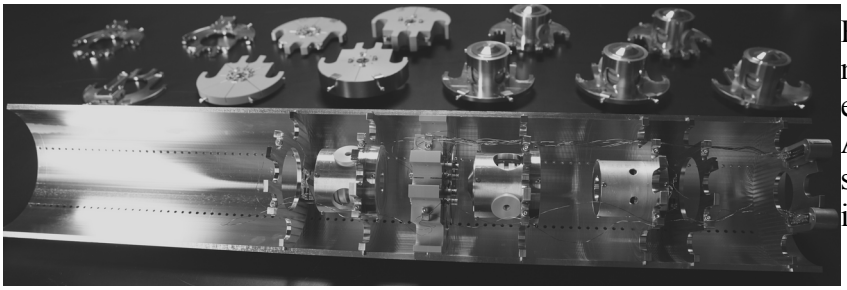

Fig 1. 5-inch diameter mounitng half pipe with three einzel lens and a deflector. Additional deflectors, stigmators and lens are shown in the background.

C28: Quantification of Entanglement Between Aloof Swift Electrons and Geometrically Fractal Nanoprisms

Peter Neathway[1,], Isobel Bicket[2], and Gianluigi Botton[1,3]*

[1] Department of Materials Science and Engineering, McMaster University, Hamilton, Ontario L8S 4L7, Canada

[2] Canadian Centre for Electron Microscopy, McMaster University, Hamilton, Ontario L8S 4M1, Canada

[3] Canadian Light Source, Saskatoon, Saskatchewan S7N 2V3, Canada

Electrons can become entangled with surface plasmons (SPs) in nanoparticles through their mutual interactions. A framework for describing these interactions was recently proposed and applied to several important cases analytically[1]. Other schemes have been proposed for using entanglement as a means of circumventing beam-related irradiation damage to samples through ghost-imaging[2]. Here, the entanglement between swift electrons in aloof impact parameters and SPs has been studied numerically for the case of geometrically fractal nanoprisms (GFNs). This framework was used to investigate whether hybridization between SPs on these individual GFNs[3] would favour more than a single possible exchange per unit energy, which would potentially result in entangled post-interaction electron states with non-unity purity[1].

Density matrices for evaluating the purity of the post-interaction electrons were calculated from dyadic Green's functions[1] based on electric fields[4] solved for using the MNPBEM toolbox[5] for MATLAB[6]. Our results indicate signatures of very weak entanglement in the density matrices of simulated post-interaction electrons. This could be an analogue of relatively small scattering-cross sections and the lack of energetic degeneracy between multiple SPs for the simulated GFNs[1], despite modal hybridization[3]. No correlation was found between the generation of the GFN generation and likelihood of entanglement. Purity of the post-interaction electrons approached unity (e.g., no entanglement) for impact parameters beyond a few tens of nanometers from the GFNs. Study of electron-SP entanglement effects in aloof impact should perhaps be kept within this range. Some testing revealed non-physical results likely rooted in our approach to discretization of the analytical method which inspired this work[1].

References

1. Mechel, C. *et al.* Quantum Correlations in Electron Microscopy. *Optica*. **8.1**, 70-78 (2021).
2. Rotunno, E. *et al.* One-Dimensional Ghost Imaging with an Electron Microscope: a Route Towards Ghost Imaging Inelastically Scattered Electrons. *arXiv preprint arXiv.* 2106.08955 (2021).
3. Bicket, I. *et al*. Hierarchical Plasmon Resonances in Fractal Structures. *ACS Photonics*. **7.5**, 1246-1254 (2020).
4. Hohenester, U. Nano and Quantum Optics. *Springer* (2020).
5. Hohenester, U., Trügler, A. MNPBEM - a MATLAB Toolbox for the Simulation of Plasmonic Nanoparticles. *Comput. Phys. Commun.* **183**, 370-381 (2012).
6. MATLAB, *version 9.6 (R2019a)*, The MathWorks Inc., Natick, Massachusetts (2019).

C29: The Holy Trinity of Microanalysis: Standards, K-ratios and Physics

John Donovan[1], Aurélien Moy[2], Will Nachlas[2] and John Fournelle[2]

[1] CAMCOR, University of Oregon, Eugene, Oregon, USA
[2] Department of Geoscience, University of Wisconsin-Madison, Wisconsin, USA

Standards (reference materials), k-ratios (measurements) and physics (matrix corrections) are essential components of accurate quantitative microanalysis. However, even with historic advances now yielding relative accuracy around 2%, there are several aspects of quantitative microanalysis that can still be improved upon.

Standard reference materials have not improved substantially since the early 1980s, primarily because there a limited number of high purity minerals that are homogeneous and of known (stoichiometric) composition that are also available in quantities sufficient for global distribution. All too often microanalysis standards are locally sourced, naturally heterogeneous, contain a variety of inclusions and have a range of composition which results in a significant lack of consensus between different laboratories [1]. To place the field on a more sound scientific footing we ideally require, ~kilogram quantities of single crystal (or polycrystalline) synthetic minerals of high purity and exact stoichiometric composition which should be distributed globally so that every microanalytical laboratory in the world can reference the exact same primary standard reference materials.

K-ratios are the basis of wavelength dispersive spectroscopy (WDS) measurements in microanalysis. However, acquisition of k-ratios depends on the accuracy of several instrumental calibrations including the software dead time correction and picoammeter linearity, especially at high count rates which are easily attainable with modern instruments and large area Bragg crystals. The traditional linear dead time expression does properly account for single and multiple photon coincidence, however various non-linearities are introduced at high count rates due to details of pulse sensing electronics. These must be corrected for, by using a non-linear logarithmic expression for improved accuracy [2].

Physics provides the basis for our analytical matrix corrections to account for differences in the electron-photon interactions between our standards and unknowns. However, relying on mass normalizations we introduce unphysical biases into our calculations, especially when the A/Z ratios of the elements in compounds are significantly different, which introduces large uncertainties in the areas of the backscatter correction and for continuum modeling [3].

References

[1] Wieser, PE, Kent, AJR, Till, CB, Donovan, JJ, Neave, DA, Blatter, DL, Krawczynski, MJ "Barometers behaving badly: Assessing the influence of analytical and experimental uncertainty on clinopyroxene thermobarometry calculations at crustal conditions", Journal of Petrology in review

[2] Donovan, J, Moy, A, Handt, A, Gainsforth, Z, Maner, JL, Nachlas, W and Fournelle, J "A New Method for Dead Time Calibration and a New Expression for Correction of WDS Intensities for Microanalysis", Microscopy & Microanalysis in preparation

[3] Donovan, JJ, Schwab, JJ, Gainsforth, Z, Moy, A, Wade, B, Ducharme, A, McMorran, B "An Improved Average Atomic Number Calculation for Estimating Backscatter and Continuum Production in Compounds", Microscopy & Microanalysis in review

C30:Progress on applications of event-driven direct electron detectors to electron microscopy

Francisco de la Peña[1], Yves Auad[2], Mario Peláez Fernández[1], Adrien Teurtrie[1], Maya Marinova[1], Damien Jacob[1], Corentin Le Guillou[1], Hugues Leroux[1], Luiz H. G. Tizei[2], Jean-Denis Blazit[2], Odile Stéphan[2], Mike Walls[2], Mathieu Kociak[2], Marcel Tencé[2]

[1] UMET, University of Lille, Villeneuve d'Ascq, France
[2] LPS, University Paris-Saclay, Orsay, France

Direct electron detectors (DEEs) are becoming commonplace in electron microscopes thanks to their advantages with respect to scintillator-based detector systems, namely a better point spread function, dynamic range, sensitivity, and speed [1]. Most DEEs utilize frame-based readouts, i.e., all the pixels are read out at once. Recently, a new kind of DEE has emerged that utilizes an event-based readout instead [2]. In event-based readout systems, the pixels are read out only when they are hit, with a time-of-arrival resolution of 1.6 ns (195 ps in the next generation of detectors). The high time resolution makes them ideal detectors to study beam sensitive samples. For example, in TEM mode, one can acquire data for an image during a certain time. If the sample damages during the data acquisition, one can use the detector's time resolution to only use the data acquired before the onset of damage to generate the final image. In STEM mode, since there is no frame exposure time to set, the scanning speed is no longer limited by the detector but by the scanning unit, enabling EELS [3] and 4D-STEM [4] at fractions of a microsecond per pixel. Event-driven detectors involve a paradigm change in the way in which we acquire and analyze our data. Here we will discuss our ongoing efforts in this regard and their application to the analysis of beam sensitive samples such as samples from a carbonaceous asteroid collected by the HAYABUSA2 space mission.

References

[1] MacLaren, Ian, et al. "Detectors—The ongoing revolution in scanning transmission electron microscopy and why this important to material characterization." Apl Materials 8.11 (2020): 110901.
[2] Poikela, Timepix, et al. "Timepix3: a 65K channel hybrid pixel readout chip with simultaneous ToA/ToT and sparse readout." *Journal of instrumentation* 9.05 (2014): C05013.
[3] Auad, Yves, et al. "Event-based hyperspectral EELS: towards nanosecond temporal resolution." *Ultramicroscopy* (2022): 113539.
[4] Jannis, Daen, et al. "Event driven 4D STEM acquisition with a Timepix3 detector: Microsecond dwell time and faster scans for high precision and low dose applications." *Ultramicroscopy* 233 (2022): 113423.

This project has been partially supported by the National Agency for Research under the program of future investment TEMPOS-CHROMATEM (reference no. ANR-10-EQPX-50), the TEM-Aster project funded by I-SITE ULNE and the MEL.

C31: A Method for Spatial Sampling of Metallic Glass Structure and Evolution Using 4-D STEM and Time Resolved 4-D STEM

Carter Francis[1], Shuoyaun Huang[1], Paul Voyles[1]
[1] Materials Science and Engineering, University of Wisconsin, Madison, Wi, USA

Metallic glasses have small structures on the range of 0.5 – 2nm which have been shown to be very important to the physical properties (strength, ductility etc.) as well as the kinetic properties (stability vs crystallization and glass formability).[1] 4-D Scanning Transmission Electron Microscopy (4-D STEM) excels at measuring these glassy structures as the size of the probe is similar in size to the size of the structures in the glass. Methods including Fluctuation Electron Microscopy [2], Angular Correlations analysis [3] and Correlation Symmetry analysis [4] all use 4-D STEM datasets to measure structure both spatially and averaged over the entire area probed. These methods are powerful in measuring the size, symmetry and atomic spacing of structures but are very sensitive the thickness of the sample as well as the ratio of signal to background. With the correlative nature of the methods, these effects lead to uncertainty.[4]

Here we show a new method for measuring glassy structure using a novel direct peak finding approach. The method is specifically designed to be robust to datasets with a low signal to background ratio, and to reduce the complexity of analysis. This is done by first filtering the data using a Laplacian of Gaussian filter in 4 dimensions. A properly defined kernel for the filter acts as a spatial bandpass filter, accentuating real diffraction features which exist in both real and reciprocal space. Then peaks are found in the 4-dimensional space. The resulting list of peaks gives the center of the important features in all four dimensions (x, y, kx, ky). Manipulating this list of peaks we can extract information about symmetry, size, atomic spacing with high fidelity and with good spatial accuracy.

This method has been used to measure the structure of a PdCuSi metallic glass using a large 1024x1024 probe position 4-D STEM scan. As well as shows promise in measuring the structural evolution of a ZrCuNiTi glass using a time resolved series of 4-D scans.

References

[1] Cheng, Y. Q. & Ma, E. Atomic-level structure and structure-property relationship in metallic glasses. *Progress in Materials Science* vol. 56 379–473 Preprint at https://doi.org/10.1016/j.pmatsci.2010.12.002 (2011).
[2] P.M. Voyles & D.A. Muller. Fluctuation microscopy in the STEM. *Ultramicroscopy* **93**, 147–159 (2002).
[3] Im, S. *et al.* Direct Determination of Structural Heterogeneity in Metallic Glasses Using Four-Dimensional Scanning Transmission Electron Microscopy. *Ultramicroscopy* (2018) doi:10.1016/j.ultramic.2018.09.005.
[4] Huang, S., Francis, C., Ketkaew, J., Schroers, J. & Voyles, P. M. Correlation symmetry analysis of electron nanodiffraction from amorphous materials. *Ultramicroscopy* **232**, 113405 (2022).

C32: Watching Phase Transformations with a Dynamic Transmission Electron Microscope

Kenneth R. Beyerlein[1]

[1] Centre Énergie Matériaux Télécommunications, Institut National de la Recherche Scientifique, Varennes, Québec, Canada

Abstract:
Computational initiatives like the Materials Project have amassed structure and energetic information of nearly 150,000 materials with the goal of accelerating the discovery of materials with enhanced properties. However, it remains a challenge to synthesize many of the predicted phases, largely due our inability to control the phase transformation process. Better understanding of the energy transfer mechanisms and kinetic pathways involved is critical for accurate prediction of the product phase and microstructure. This insight requires studying the early stages of the structural evolution on the atomic and nanometer scale. However, measurements of this kind are limited due to the extreme temporal and spatial resolution required. The Dynamic Transmission Electron Microscope (DTEM) has been recently developed to address this challenge, and is capable of imaging irreversible transformations in materials with nanosecond and nanometer resolution. In this talk, an introduction to the operating principle of this microscope and the challenges of snapshot imaging with electrons will be given. A current benchmark of the capabilities of the DTEM at INRS will be presented, along with planned future developments.

C33: Sub-Ångström Resolution Imaging at 20 keV in a Scanning Electron Microscope from Ptychography with Integrated Projection Lens Distortion Correction

Arthur M. Blackburn[1], Cristina Cordoba[2], Matthew Fitzpatrick[2], Robert McLeod[3]

[1] Department of Physics and Astronomy, and the Centre for Advanced Materials and Related Technologies, University of Victoria, Victoria, BC, Canada

[2] Hitachi High-Tech Canada Inc., Toronto, ON, Canada

The desire to obtain sub-Ångström (< 10^{-10} m) information from general purpose, low energy (<30 keV) scanning electron microscopes (SEMs) has existed for many years [1]. Imaging at this resolution at these energies has previously only been possible through using complex aberration correctors, which introduce additional expense, labour to operate, and installation space. Here, through combination of adding a simple diffraction projector lens to a non-aberration corrected SEM operating in transmission mode; incorporating calibration and correction of projector lens pincushion distortion with a multi-slice ptychographic reconstruction algorithm; and using un-coated hybrid direct electron detector [2], we show a resolution of at least 0.7 Å with a 20 keV beam in experimental sample image reconstructions. Test samples include Au particles on amorphous carbon, with an example reconstructed phase and amplitude given in Figure 1(a). Analyzing the Fourier ring correlation between independent reconstructions shows that features of 0.7 Å are resolvable (Figure 1(b)). Furthermore, we see excellent alignment between the experimental image fast Fourier transform (FFT) and model diffraction patterns, showing that distortion from our simple projector lens has been successfully corrected. Analyzing reconstructed images of MoS_2 based samples shows this resolution is achievable in more practical materials even in the presence of some sample contamination, through using background removal routines. Thus, low-energy sub-Å resolution imaging, previously only possible in aberration corrected S/TEM instruments, is now demonstrated as feasible at typical SEM instrument acceleration voltages.

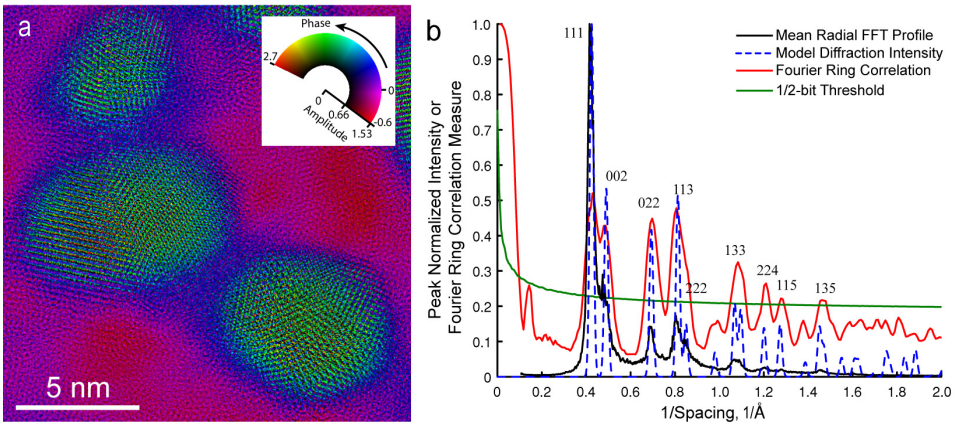

Figure 1 – (a) Reconstructed exit wave for electron transmission through a gold particle supported on carbon imaged at 20 keV; (b) Fourier ring correlation characteristic with experimental and model radial FFT profiles of a reconstructed image containing many particles.

References

[1] MJ Humphry, B Kraus, *et al.* (2012), Nature Comms, **3**:730

[2] G Tinti, H Marchetto, *et al*. (2017), J. Synchrotron Rad. **24**, 963

C34: High Resolution X-ray Ptychography at the Cryo STXM endstation, Soft X-ray Spectromicroscopy (SM) Beamline, Canadian Light Source.

Venkata S.C. Kuppili[1], James J. Dynes[1], Yingshen Lu[1], Chithra. Karunakaran[1], Jian Wang[1]

[1] Canadian Light Source, 44 Innovation Boulevard, Saskatoon

Ptychography is a lensless X-ray diffraction microscopy technique [1,2,3] in which the sample is scanned at pre-defined positions collecting far-field diffraction patterns at each of these scanning positions. The diffraction patterns along with the information regarding the scan positions are then processed using iterative phase retrieval algorithms resulting in high resolution complex transmission function of the sample. Unlike techniques like transmission X-ray microscopy (TXM), Fourier transform holography (FTH) or scanning transmission X-ray microscopy (STXM), the resolution doesn't depend on the focusing optics or the reference aperture, but on the detectable signal contained in the measurable inverse space. While other parameters such as beam stability and stage accuracy play an important role, the fundamental limitation on obtain-able resolution is the measurable inverse space. We have implemented an experimental geometry wherein the detector in the Cryo STXM endstation can be positioned at 35 mm behind the sam-ple. This enabled us to carry out high resolution ptychography at the Cryo STXM endstation of the soft X-ray spectromicroscopy beamline, Canadian Light Source [4]. We will report on the ex-perimental and algorithmic details of the imaging setup along with the results obtained. We will also take this opportunity to report on the newly acquired in-situ, in-operando capabilities of the SM beamline.

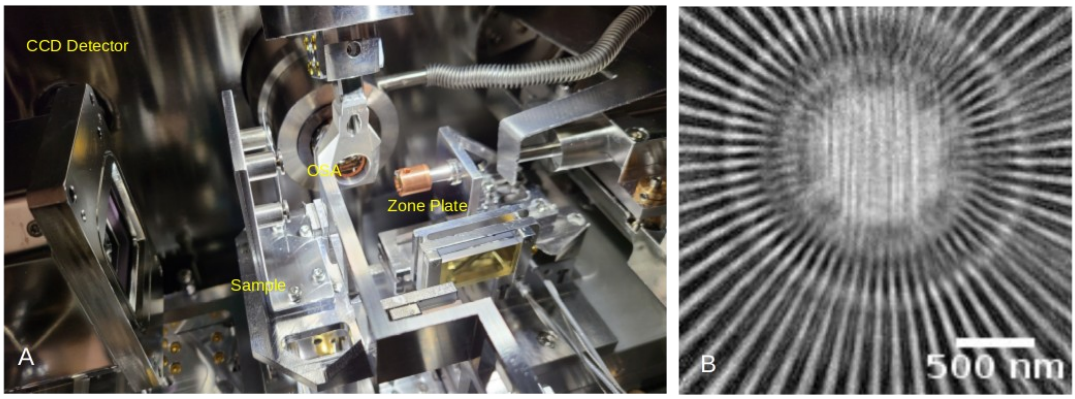

(A) Shows the high resolution ptychography experimental geometry, the detector can be positioned as close as 35 mm from the sample. (B) Shows a ptychographic reconstruction of a Siemens star imaging standard, we were able to resolve features as small as 25 nm.

References

[1] J. M. Rodenburg., et al., Physical Review Letters, 98(3):1–4, (2007)
[2] P. Thibault., et al., Science 379 379–383 (2008)
[3] V.S.C. Kuppili., et. al., Journal of Physics: Conference Series (2017)
[4] A.F.G. Leontowich., et. al., Review of Scientific Instruments 89, 093704 (2018)

C35: Functional chemistry of extraterrestrial organic matter revealed by high spatial resolution synchrotron spectroscopy – electron microscopy techniques

Christian Vollmer[1], Jan Leitner[2], Charlotte L. Bays[3], Ashley J. King[3], Paul F. Schofield[3], Tohru Araki[4], Aleksander B. Mosberg[5], Demie Kepaptsoglou[5], and Quentin M. Ramasse[5]

[1]Universität Münster, Institut für Mineralogie, Corrensstr. 24, Münster, Germany
[2]Max-Planck-Institut für Chemie, Hahn-Meitner-Weg 1, 55128 Mainz, Germany
[3]Planetary Materials Group, Natural History Museum, London SW7 5BD, UK
[4]Diamond Light Source, Didcot OX11 0DE, UK
[5]SuperSTEM Laboratory, Keckwick Lane, Daresbury, WA4 4AD, UK

Organic Matter (OM) is an important constituent in a variety of extraterrestrial samples such as carbonaceous meteorites [1] or dust grains returned by space missions [2]. The morphology, structure, elemental composition, and functional chemistry of this OM record a combination of presolar, nebular, parent-body, and terrestrial processes, leaving a complex fingerprint on the OM. These manifold processes can be disentangled by high-spatial resolution studies, which have the advantage that they also allow study of the petrographic relationship to the surrounding matrix and require only minimal chemical treatment. The analysis of this material also gives important insight into the make-up of the first biomolecules delivered to the early Earth [3]. Here we have investigated OM properties within the recent observed fall Winchcombe. This carbonaceous chondrite was classified as CM2 and is the first recovered observed fall in the UK for 30 years [4]. The OM was documented within a meteorite thin section by scanning electron microscopy (SEM) and then sectioned by the focused ion beam (FIB) technique using a Hitachi Ethos NX5000. Scanning Transmission X-Ray Microscopy (STXM) was performed at the I08 beamline of Diamond Light Source. Low-kV (60 kV) Electron Energy Loss Spectroscopy (EELS) in the vibrational and core loss regimes was performed with a monochromated, aberration-corrected Nion UltraSTEM 100MC [5]. OM identified in different lithologies of the Winchcombe meteorite shows globular, multi-globular, diffuse, and vein-like morphologies. Phyllosilicates and carbonates are intimately associated with the OM. STXM analyses at the carbon K-edge demonstrate that OM in Winchcombe has strong absorption at the aromatic C=C (~285 eV) and the ketone/aldehyde (~286.6 eV) bands, similar to OM in other primitive meteorites. Fine structure at the nitrogen K-edge shows two dominant bands at 398.8 eV and 399.8 eV, which can be attributed to C-N double (imine) and triple (nitrile) bonding environments. The functional chemistry of nitrogen in meteoritic OM is very sensitive to aqueous alteration reactions, with the abundance of oxygenated [6] and hydrogenated [7] nitrogen bonds correlating with advancing alteration. The presence of the highly reactive double and triple C-N bonding is therefore a strong indicator that the Winchcombe OM is still pristine.

References: [1] Pizzarello S. and Shock E. (2017) *Origins Life Evolution Biosphere* 47:249-260. [2] Yada T. et al. (2022) *Nature Astronomy* 6:214-220. [3] Martins Z. et al. (2020) *Space Science Reviews* 216:54-77. [4] King A. J. et al. (2022) *Science Advances* 8(46):abq3925. [5] Vollmer C. et al. (2020) *Scientific Reports* 10:20251-20260. [6] Cody G. D. and Alexander C. M. O`D. (2017) *Lunar and Planetary Science Conference* 48:A2747. [7] Vollmer C. et al. (2020) *Meteoritics & Planetary Science* 55(6):1293-1319.

C36: Corium materials characterizations through electron microscopy and X-ray diffraction

Emmanuelle Brackx[1], Mohamed Jizzini[1,2], Hirotomo Hikeuchi[3], Pascal Piluso[4], René Guinebretière[2]

[1] CEA, DES, ISEC, DMRC, Univ. Montpellier, Marcoule, France
[2] IRCER, Univ. Limoges, Limoges, France
[3] JAEA, 4-33 Muramatsu, Tokai-mura, Ibaraki-ken, Japan
[4] CEA, DES, IRESNE, DTN, Saint Paul lez Durance, France

In case of severe accident conditions in a nuclear reactor, corium, a complex material coming from the melting of the core at a very high temperature (2500-2800 K), is formed. The cooling process of this material from the liquid state can be rapid in the case of contact with water (from a few milliseconds to a few seconds for the so-called Fuel Coolant Interaction (FCI)), or slow in the case of contact with concrete (from a few minutes to a few hours for the so-called Molten Core Concrete Interaction (MCCI)). The knowledge of the structure and microstructure of corium according to the severe accident scenario is fundamental to understand severe accident progression and to guide dismantling operations.

The first studies focused on the investigation of the solidification behavior of a melt representative of the in-vessel conditions of Fukushima Daïchi Unit 1-F2. Boron was initially present in Unit 1-F2 under B_4C phase (control rod). Small-scale experiments were carried out at CEA Cadarache – IRESNE (PLINIUS/VITI) to characterize and model the solidification of the melt for materials containing B-C-Fe-O elements. The material were analysed by Electron Probe MicroAnalysis under the wavelength dispersion mode (EPMA /WDS) taking into account the chemical shift of boron and carbon in the different states measured. X-ray diffraction (XRD) was used to determine the nature of the crystalline phases.

The second study was carried out on prototypical corium obtained Fuel Coolant Interaction experiments performed in the KROTOS facility at CEA Cadarache. The fragmented or exploded corium debris under consideration are corresponding to a ternary compound according to the $U_{1-x}Zr_xO_{2\pm y}$ solid solution. Typical size of 200 µm or less than 50 µm have been studied to determine microstructure, elemental composition and structural state [1]. EPMA was used to determine with high accuracy the local variation of the composition. A specific methodology will be presented and the results will be compared with the phases compositions obtained through Rietveld refinement of both X-rays and neutrons diffraction patterns. These analyses were completed by micro texture analyses with SEM/EBSD and Laue microdiffraction experiments. We observed at local state intra-crystalline local cationic composition fluctuation related to the different cooling processes and the corium particles sizes.

The last study concerns EPMA performed in the frame of a corium round robin on tools and methodology for post test analyses on a sample of typical MCCI experimental tests. The results evidence the ability of the methods that we used to determine the corium global and local compositions characterised by presence of uranium and a large number of major light elements.

References

[1] Jizzini. M, Brackx. E, Piluso. P, Menut D, Guinebretière. R, *Nucl. Mat. and Energy, vol 32, 2022, 101183.*

C37: Carbon Nanohorn Assembly and Structure Revealed by Aberration-Corrected Transmission Electron Microscopy

Fanny Casteignau[1], Louka Yilmaz[1], Armand Soldera[2], Christian Ricolleau[3], Richard Martel[4], Nadi Braidy[1,5]*

[1] Department of Chemical and Biotechnological Engineering, Université de Sherbrooke, Quebec, Canada

[2] Department of Chemistry, Université de Sherbrooke, , Quebec, Canada

[3]Laboratoire Matériaux et Phénomènes Quantiques, Université de Paris, Paris, France

[4] Department of Chemistry, Université de Montréal, Montréal, Canada

[5] Institut Interdisciplinaire d'Innovation Technologique 3IT, Université de Sherbrooke, Quebec, Canada

Carbon nanohorns (CNHs) are ~50 nm long graphenic conical structures typically capped by a C_{60} and arranged in inseparable aggregates of about 100 nm in diameter with a sea urchin structure[1]. Thanks to their structure analogous to graphene and carbon nanotubes, CNHs are considered for a wide range of applications[2]. The growth mechanism of CNHs is virtually unexplored, although some studies have suggested that growth is initiated from the C_{60} tip or by winding graphene sheets. Here, we couple spherical aberration-corrected high-resolution electron microscopy (Cs-HRTEM), atomistic simulations, and TEM multi-slice methods to help interpret the atomic structure of these CNHs and investigate their growth mechanism.

We demonstrate the existence of a relation between fullerenes, small graphitic capsules (onion-like), and CNHs produced by RF plasma torch synthesis. CNHs aggregates systematically exhibit in their center ~10 nm-diameter onions or graphitic capsules. The last layer of these small capsules grows out to form CNHs. From these observations, we propose that the nucleation of CNHs starts from the base of the CNH, following the last graphitic layer of the onion-like structure. The co-production of fullerenes is observed together with the growth of the CNH. The occasional encapsulation of fullerene-like structures in CNHs during their growth is demonstrated and supported by TEM image simulations.

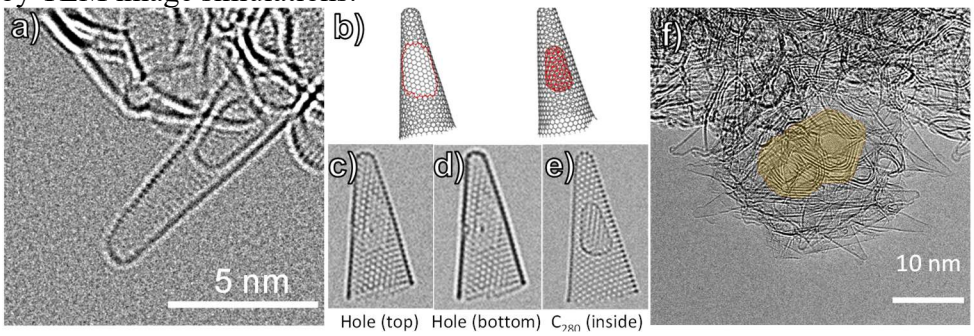

Figure 1. (a) CNH with internal structure. (b) CNH with a hole or with an encapsulated C_{280} fullerene atomistic model (c)-(e) Multislice simulation of the atomistic model f) Carbon onions found in the core of a CNH aggregate.

References

[1] Iijima S et al *Chem Phys Lett* (1999) **309** (3-4)165

[2] Karousis N et al *Chem Rev* (2016) **116** (8) 4850

[3] Harris PJF et al J Chem Soc (1994) **90** (18) 2799

[4] Zhang D et al. *Carbon* (2019) **142** 278

C38: Single-shot Photoluminescence Lifetime Imaging Microscopy using Compressed Sensing

Jinyang Liang
Laboratory of Applied Computational Imaging, Institut National de la Recherche Scientifique, Université du Québec, 1650 boulevard Lionel-Boulet, Varennes, Québec J3X 1P7, Canada

Photoluminescence lifetime imaging microscopy (PLIM) is increasingly featured in recent progress in material science and life science. The success of PLIM depends on two essential constituents: photoluminescent materials and optical imaging instruments. Despite many advances in photoluminescent materials, the development of optical imaging instruments is not kept up. In particular, to detect photoluminescence on the time scale of microseconds to milliseconds (e.g., from rare-earth nanoparticles), most PLIM techniques use point-scanning or wide-field time-correlated single-photon counting [1,2]. Although possessing high signal-to-noise ratios, these methods require large numbers of repetitive measurements to form a two-dimensional (2D) lifetime map. Meanwhile, the frequency-domain wide-field PLIM [3] techniques are strained by their limited measurable lifetime ranges and their requirement of a long integration time. For both types of techniques, the sample must remain stationary during acquisition. Thus, existing PLIM techniques fall short in 2D temperature sensing of moving samples.

To surmount these limitations, we develop a new PLIM system [4]. Synergistically combining dual-view optical streak imaging with compressed sensing, this system can capture photoluminescence intensity decay over a 2D field of view in a single acquisition (Fig. 1a). The captured ultrahigh-speed movie thus allows directly calculating the photoluminescence lifetime map. Using this system, we record wide-field luminescence decay of Er^{3+}, Yb^{3+} co-doped $NaGdF_4$ upconverting nanoparticles (UCNPs). We also apply this system to optical thermometry by leveraging the temperature-dependent lifetimes in these UCNPs (Figs. 1b–c). This system enables longitudinal 2D temperature monitoring beneath a thin scattering medium and dynamic temperature tracking of a moving biological sample at single-cell resolution (Figs. 1d–e).

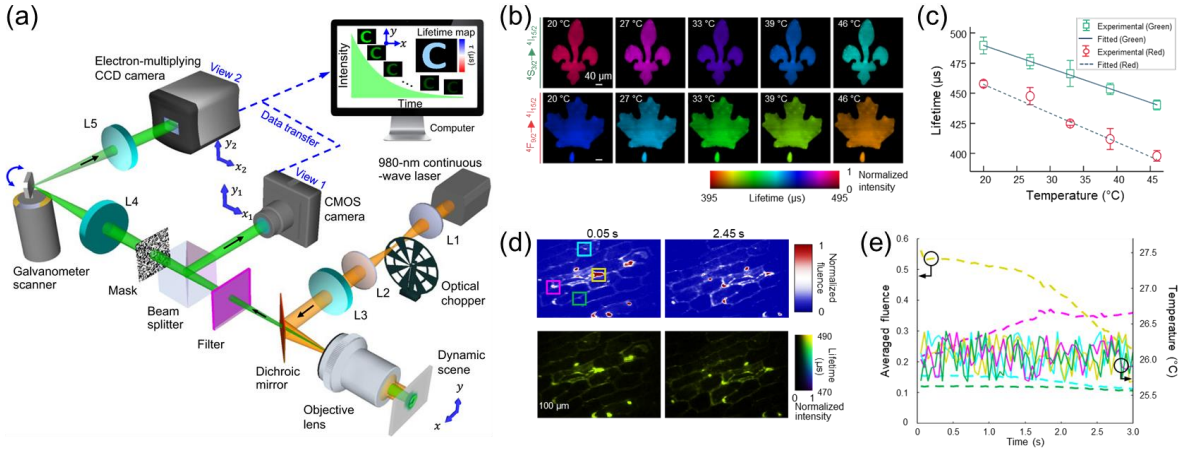

Fig. 1. Single-shot PLIM using compressed sensing. (a) System schematic. (b) Lifetime images of upconversion emission under different temperatures. (c) Relationship between temperature and lifetimes. (d) Representative fluence and lifetime frames of a biological sample. (e) Time traces of intensity and lifetime-determined temperature at selected areas. Adapted from [4].

References

[1] *Sci Rep* **8**, 12683 (2018).
[2] *Rev Sci Instrum* **88**, 013104 (2017)
[3] *Opt Lett* **45**, 81-84 (2020)
[4] *Nat Comm* **12**, 6401 (2021)

C39: Outer membrane biogenesis in *Acetonema longum*

Polina Beskrovnaya[*1], Elitza Tocheva*[1]

[1] Department of Microbiology and Immunology, University of British Columbia, Vancouver, BC, Canada

Endospore formation is a complex bacterial stress response strategy that involves asymmetric cell division to produce a daughter cell (prespore) enveloped by two lipid bilayers, the inner (IsM) and outer (OsM) spore membranes, derived from the inner membrane (IM) of the mother cell. Through subsequent maturation and dehydration, endospores gain the ability to preserve their genetic material under harsh environmental conditions. Although this process has traditionally been associated with the monoderm bacteria within the phylum Firmicutes, recent studies have also identified diderm spore-formers, such as the Negativicute *Acetonema longum*. Cryo-electron tomography (cryo-ET) analysis further reveals that both monoderm (*e.g. Bacillus subtilis*) and diderm (*A. longum*) spore formers indeed produce a diderm prespore [1]. While endospores of monoderms have been observed to shed the OsM in germination, diderm organisms instead appear to remodel the OsM into a true outer membrane (OM), hallmarked by asymmetric lipid leaflets and integral beta-barrel proteins (OMPs) [1]. However, the exact progression and the molecular mechanisms behind the remodeling of an IM-like lipid bilayer into an OM have not been elucidated. Previous phylogenetic analyses indicate that spore-forming Negativicutes like *A. longum* may represent an evolutionary missing link between the traditional monoderm and diderm bacteria, highlighting potentially novel processes behind the OM biogenesis [2]. In this study, we rely on a combination of biochemical and high-resolution imaging approaches to track *A. longum* OMPs throughout the sporulation cycle. Additionally, by generating polyclonal antibodies to BamA, the main porin of the Beta-Barrel Assembly Machinery, as well as the Firmicute-specific OM-peptidoglycan (PG) tethering protein OmpM, we were able to localize these key OMPs *in vivo* using fluorescence light and confocal microscopy, transmission electron microscopy, and cryo-ET. Altogether, we show that recruitment of BamA and OmpM to the OsM occurs during the outgrowth stage in germinating endospores.

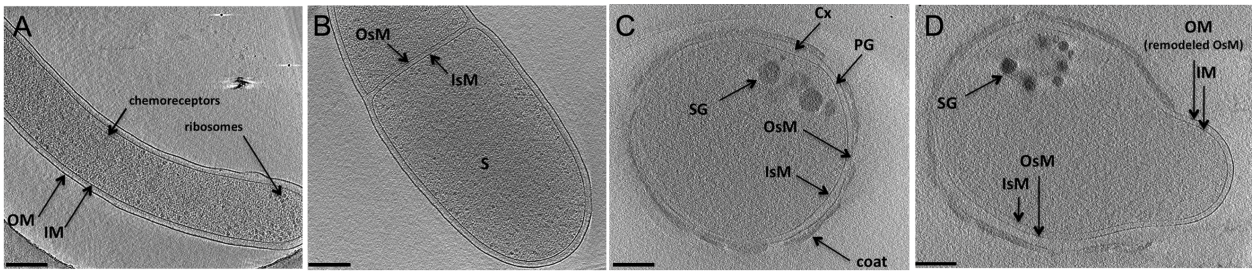

Figure 1. Sporulation cycle of *Acetonema longum*. Vegetative cell **(A)** undergoes asymmetric division **(B)**, producing a diderm spore **(C)**. In germination **(D)**, OsM is remodeled into a mature OM. Cx, cortex; SG, storage granules. Scale bar, 200nm. Modified from Tocheva *et al.* (2011) [3].

References

1. Tocheva, E. I., Ortega, D. R. & Jensen, G. J. Sporulation, bacterial cell envelopes and the origin of life. *Nat. Rev. Microbiol.* **14**, 535–542 (2016).
2. Taib, N. *et al.* Genome-wide analysis of the Firmicutes illuminates the diderm/monoderm transition. *Nat Ecol Evol* **4**, 1661–1672 (2020).
3. Tocheva, E. I. *et al.* Peptidoglycan remodeling and conversion of an inner membrane into an outer membrane during sporulation. *Cell* **146**, 799–812 (2011).

C40: International Union of Microbeam Analysis Societies Joint with the Annual Microscopical Society of Canada and FIB SEM Meetings

Cooperativity of ribosome associated GTPases in the assembly of the bacterial ribosome

Dominic Arpin[1,2], *Armando Palacios-Chaparro*[1,2], *Amal Seffouh*,[1,2] and *Joaquin Ortega*[1,2].
[1] Department of Anatomy and Cell Biology, McGill University, Montreal, Quebec, Canada.
[2] Centre de Recherche en Biologie Structurale (CRBS), McGill University, Montreal, Quebec, Canada.

The bacterial ribosome assembly is a complicated process involving a broad array of factors, including GTPases. RbgA, YphC and YsxC are three highly conserved essential GTPases in *Bacillus subtilis* implicated in the assembly of the large subunit (1). To investigate their roles, the genes were placed under the control of an inducible promoter since gene inactivation is not viable. Large subunit assembly intermediates accumulate in depletion conditions, and characterization by cryo-electron microscopy (Cryo-EM) and quantitative mass spectrometry (qMS) of the intermediates resulting from RbgA ($45S_{RbgA}$), YphC ($45S_{YphC}$) or YsxC ($44.5S_{YsxC}$) depletion revealed that they are strikingly similar (2, 3). Moreover, studies in mitoribosomes have shown that the homologs of the three proteins are simultaneously bound to assembly intermediates (4). Using a combination of biochemical and biophysical approaches, our research aims to elucidate the molecular function and cooperativity of RbgA, YphC and YsxC during the assembly of the large ribosomal subunit. Microscale thermophoresis (MST) experiments show that all three enzymes irrespectively bind the assembly intermediates with high affinity (K_D ~ 100 nM). Furthermore, RbgA and YphC show positive cooperativity in their binding, i.e., when one enzyme is bound, the affinity and stability of the other are significantly increased. According to the results obtained by MST, a complex was formed with the $45S_{RbgA}$ with RbgA and YphC bound and analyzed by Cryo-EM. RbgA and YphC, respectively bind in the P and E sites of the functional core, forming stabilizing interactions with each other. Our model shows that the binding of YphC causes the breakage and distortion of Helix 89 to flip out U2521. This uridine is held exposed by hydrogen bonding with R353 of YphC. In the mature 50S, this nucleotide is isomerized to pseudouridine by an uncharacterized protein proposed to be YlmL, a prediction that we are experimentally validating (5). Thus, RbgA and YphC seem to orchestrate the maturation of the functional core as well as the recruitment and binding of other assembly factors. These results provide new insight into the network of factors required for proper stepwise maturation of the bacterial ribosome and allow us to propose that they are critical targets for the rational development of a new generation of antibiotics aiming to hamper ribosomal assembly in bacteria.

References

1. R. A. Britton, Role of GTPases in bacterial ribosome assembly. *Annu Rev Microbiol* **63**, 155-176 (2009).
2. X. Ni *et al.*, YphC and YsxC GTPases assist the maturation of the central protuberance, GTPase associated region and functional core of the 50S ribosomal subunit. *Nucleic Acids Res* **44**, 8442-8455 (2016).
3. A. Seffouh *et al.*, Structural consequences of the interaction of RbgA with a 50S ribosomal subunit assembly intermediate. *Nucleic Acids Res* **47**, 10414-10425 (2019).
4. M. Jaskolowski *et al.*, Structural Insights into the Mechanism of Mitoribosomal Large Subunit Biogenesis. *Mol Cell* **79**, 629-644 e624 (2020).
5. V. de Crecy-Lagard *et al.*, Survey and Validation of tRNA Modifications and Their Corresponding Genes in Bacillus subtilis sp Subtilis Strain 168. *Biomolecules* **10** (2020).

C41: Multiscale imaging of microtubules

Lia Paim[1], Thomas McAlear[1], Tatiana Lyalina[1], Mike Strauss[1], Susanne Bechstedt[1]*
[1] Department of Anatomy and Cell Biology, McGill University, Montreal, Quebec, Canada

The eukaryotic cytoskeleton is a complex dynamic network that provides mechanical support, enabling cells to perform essential functions like division and movement. Microtubules are long-hollow filaments that give structure and stability to cells, serve as tracks for motor-mediated transport of organelles, build the mitotic spindle, and form motile axonemes and sensory cilia. My lab uses single-molecule reconstitution microscopy assays, live cell super-resolution imaging, and electron microscopy to study microtubule architecture and dynamics.
We will present data on the novel microtubule growth factor (CKAP2) [1] and how the protein dictates microtubule dynamics in cells and in vitro.

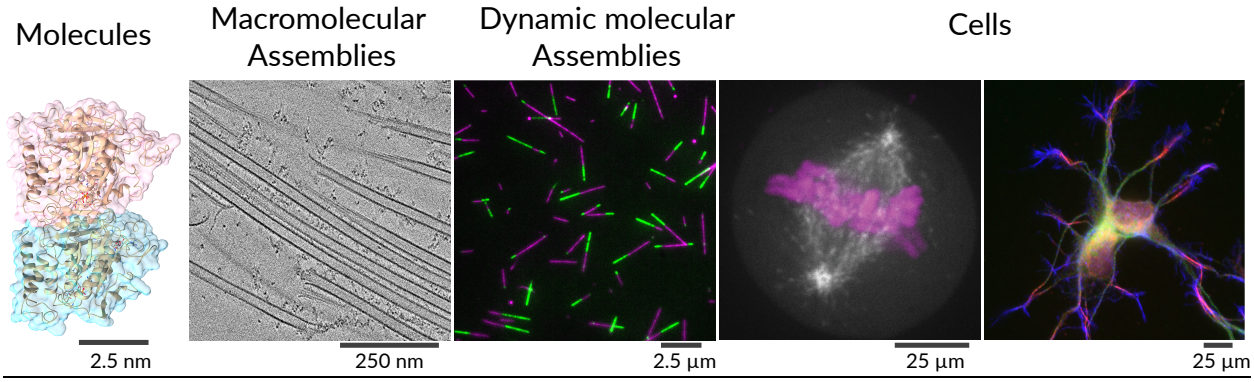

References
[1] T. S. McAlear, S. Bechstedt, The mitotic spindle protein CKAP2 potently increases formation and stability of microtubules. Elife 11 (2022).

C42: INTERROGATING THE PROPERTIES OF A MICROTUBULE (+) END-ASSOCIATED NANOSCALE CONDENSATE IN LIVING CELLS USING SUPER-RESOLUTION MICROSCOPY

*Morelli K[1], Meier SM[2], Zhao A[1], Willis M[1], Barral Y[2], *Vogel J[1]*

[1]Department of Biology, McGill University, Montreal, Canada
[2]Institute of Biochemistry, Department of Biology, ETH Zürich, Switzerland

Interactions between microtubules and actin guide many important functions in cells including positioning of the mitotic spindle in budding yeast. To position the spindle, the dynamic (+) ends of astral microtubules probe the cytoplasm, forming interactions with polarized actin filaments network through the (+)-end tracking protein (+TIP) Kar9 (1). Meier *et al*. (2) have now demonstrated that in vitro, Kar9 and two additional +TIPs, the EB1 ortholog Bim1 and the CLIP170 ortholog Bik1, form a liquid-like condensate through multivalent interactions. These interactions are proposed to maintain the condensate on the (+) end as the microtubule grows and shrinks. However, the nanoscale dimension of these condensates in living cells makes direct observation of predicted behaviors challenging.

We use lattice structured illumination super-resolution microscopy (lattice SIM) to study the behaviors and properties of the Kar9 condensate in living cells and investigated how this condensate may enable microtubule-actin interactions in vivo. We show that in living cells Kar9 condensates have diameters of ~200 nanometers. At this length scale, the emergent material properties of the Kar9 condensates, if consistent with those measured in vitro, have the potential to generate forces on the relevant scale of actin and microtubule-based motor proteins. Using a time series >15 frames per second resolution, we observe fusion events consistent with the contact between liquid-like droplets. Using a machine-learning classifier to extract condensate shapes, we observe that fusion events occur on the timescale predicted by in vitro reconstitution. Furthermore, we developed a method to annotate dynamic microtubule behavior according to dynamic instability parameters using Kar9 as a (+) end marker. Strikingly, shorter metaphase microtubules appear to grow and shrink along the contour of longer microtubules projecting from the same SPB. These astral microtubules undergo rapid angular motions relative to the SPB which are consistent with actin-bound myosin V pulling on Kar9 at the microtubule (+) end. Remarkably parallel microtubules remain linked during these motions. We conclude that microtubules are bundled by a mechanism that persists during phases of microtubule dynamic instability and rapid motion through the cytoplasm. In this work we demonstrate that biophysical measurements of biomolecular condensates are possible at nanoscale in living cells and propose that this length scale is an important frontier in condensate biology.

References

1. Liakopoulos D, Kusch J, Grava S, Vogel J, Barral Y. Asymmetric loading of Kar9 onto spindle poles and microtubules ensures proper spindle alignment. *Cell* 112, 561-74. 2003

2. Meier SM, Farcas AM, Kumar A, Ijavi M, Bill RT, Stelling J, Dufresne ER, Steinmetz MO, Barral Y. Multivalency ensures persistence of a +TIP body at specialized microtubule ends. *Nat Cell Biol. 2022*. doi: 10.1038/s41556-022-01035-2.

C43: Lactation-induced changes in bone cellular and sub-cellular networks: indication for altered bone mineral transport

T. Tang[1], A. Munoz[2], J. Huo[1], A. Gourrier[3], A. Carriero[2], K. Grandfield[1]
[1] Department of Materials Science and Engineering, McMaster University, ON, Canada
[2] Biomedical Engineering Department, The City of College of New York, New York, USA
[3] University Grenoble Alpes, CNRS, LIPhy, Grenoble, France

Over 90% of the calcium in the human body is deposited as mineral within bones of our skeleton and teeth. A balanced calcium exchange between extracellular fluid and bone cells is essential for maintaining structural and functional integrity of our skeleton. Any disturbance to this mineral homeostasis may lead to severe clinical consequences, such as osteoporosis. (1) In this context, the extracellular matrix of our bones is perfused with a fluid-filled unmineralized structure, lacunocanalicular network (LCN), which harbors bone cells (osteocytes) with their cytoplasmic processes and transports extracellular fluid and its constituents. This network is believed to play a role in facilitating mineral homeostasis through a process known as osteocytic osteolysis (OO). (2,3) However, after decades of research, the mechanisms underlying OO have remained poorly understood. Previous research have largely focused on the inherent cellular and molecular signalling pathways associated with OO, (4) yet there is limited information and direct evidence of calcium exchange and transport in the bone LCN in three-dimension (3D).

In the current study, 3D focused ion beam-scanning electron microscopy (FIB-SEM) with a spatial resolution of ~5 nm and imaging volume of tens of microns (~15 × 5 × 5 μm^3) was used to investigate the 3D cellular and sub-cellular architecture in mouse femoral cortical bone from pregnancy, lactation, and postlactation recovery groups. Lactation has been associated with an increased demand for calcium and a rapid skeletal turnover and maternal bone loss, (5) thus it can be a good model to explore the mechanisms, extent, and reversibility of OO. The present work has revealed altered and disorganized osteocyte network on the anterior aspect of endosteal cortical bone in the lactation and recovery groups compared to the pregnancy group. (6) Further, an extensive sub-canalicular, nanochannel network that is significantly smaller than the well-known osteocyte canaliculi (~ 30 nm vs 300 nm in diameter) was found penetrating the mineralized matrix of mouse cortical bone in all three groups. Similar interconnected nanochannel structures (~30 to 50 nm in diameter) have been reported recently in mineralizing turkey leg tendon, (7) at the mouse bone-cartilage interface, (8) and in human femoral cortical bone. (9) This sub-cellular network was proposed to provide conduits and pathways in permitting ion and small molecule diffusion throughout the extracellular matrix complementary to those of the LCN. (7–9) Interestingly, endosteal cortical bone showed increased volume of nanochannel porosity compared to the mid cortical bone region in all three groups, and the lactating mice demonstrated overall elevated nanochannel porosity compared to the other two groups. Collectively, these data yield new insight into the alterations in multiscale porosity networks and their potential role in mouse bone tissue mineralization that is fundamental to OO.

References

1. Sambrook P, et al. Lancet. 2006;367(9527):2010–8.
2. Tsourdi E, et al. J. Musculoskelet. Neuronal Interact. 2018;18(3):292–303.
3. Teti A, et al. Bone. 2009;44(1):11–6.
4. Robling AG, et al. Annu. Rev. Physiol. 2020;82:485–506.
5. Kovacs CS. J. Clin. Endocrinol. Metab. 2001;86(6):2344–8.
6. Kaya S, et al. J. Bone Miner. Res. 2017;32(4):688–97.
7. Zou Z, et al. Proc. Natl. Acad. Sci. 2020;117(25):14102–9.
8. Tang T, et al. Adv. NanoBiomed Res. 2022;2(8):2100162.
9. Tang T, et al. J. Bone Miner. Res. 2022;

C44: RbgA Ensures the Correct Timing in the Maturation of the 50S Subunits Functional Sites.

*Amal Seffouh[1,2], Chirstian Trahan[3], Tanzila Wasi [1,2], Nikhil Jain[4,5], Kaustuv Basu[1,2], Robert A. Britton[4,5], Marlene Oeffinger[3,6,7]and Joaquin Ortega[1,2]**

[1]Department of Anatomy and Cell Biology, McGill University, Montreal, Quebec H3A 0C7, Canada, [2]Centre for Structural Biology, McGill University, Montreal, Quebec H3G 0B1, Canada, [3] Center for genetic and neurological diseases, Institut de Recherches Cliniques de Montréal (IRCM), Montréal, Quebec H2W 1R7, Canada, [4]Department of Molecular Virology and Microbiology, Baylor College of Medicine, Houston, TX 77030, USA, [5]Center for Metagenomics and Microbiome Research, Baylor College of Medicine, Houston, TX 77030, USA, [6]Département de Biochimie et Médecine Moléculaire, Université de Montréal, Montréal, Quebec H3T 1J4, Canada and [7]Division of Experimental Medicine, McGill University, Montréal, Quebec H4A 3J1, Canada.

RbgA is an essential protein for the assembly of the 50S subunit in Bacillus subtilis. Depletion of RbgA leads to the accumulation of the 45S intermediate. A strain expressing a RbgA variant with reduced GTPase activity generates spontaneous suppressor mutations in uL6. Each suppressor strain accumulates a unique 44S intermediate. We reasoned that characterizing the structure of these mutant 44S intermediates may explain why RbgA is required to catalyze the folding of the 50S functional sites. We found that in the 44S particles, rRNA helices H42 and H97, near the binding site of uL6, adopt a flexible conformation and allow the central protuberance and functional sites in the mutant 44S particles to mature in any order. Instead, the wild type 45S particles exhibit a stable H42-H97 interaction and their functional sites always mature last. The dependence on RbgA was also less pronounced in the 44S particles. We concluded that the binding of uL6 pauses the maturation of the functional sites, but the central protuberance continues to fold. RbgA exclusively binds intermediates with a formed central protuberance and licenses the folding of the functional sites. Through this mechanism, RbgA ensures that the functional sites of the 50S mature last.

References: Seffouh et al. RbgA Ensures the Correct Timing in the Maturation of the Functional Sites in the 50S Ribosomal Subunit. (2022). *Nucleic Acids Research*. 50(19):10801-10816.

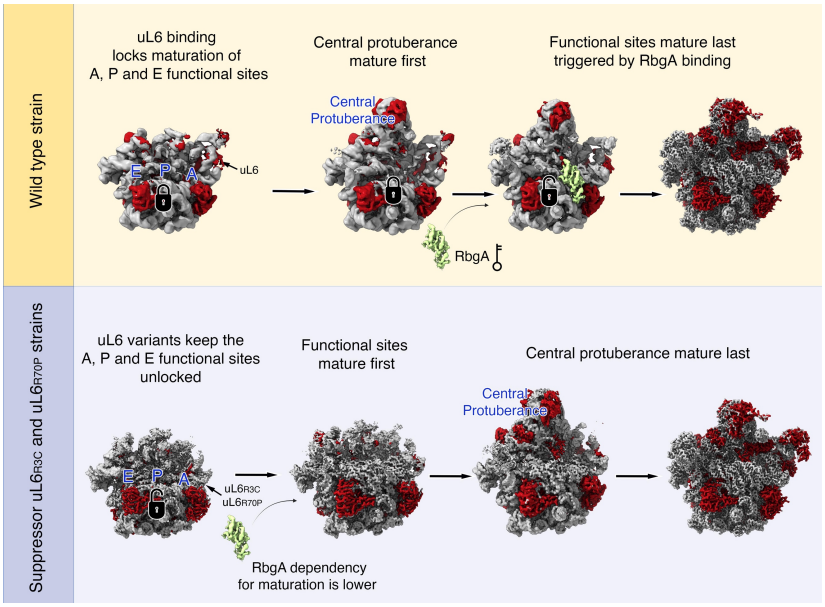

C45: Studying the hierarchical structure and nanoscale dislocations of bacterial cellulose using sr-CLEM

Mouhanad Babi[1,2], Alyssa Williams[3], Marcia Reid[4], Kathryn Grandfield[2,5,6], Nabil D. Bassim[2,3,5] and Jose M. Moran-Mirabal[1,2,3,6,]

[1] Department of Chemistry and Chemical Biology, McMaster University, Hamilton, ON, Canada
[2] Center for Advanced Light Microscopy, McMaster University, Hamilton, ON, Canada
[3] School of Biomedical Engineering, McMaster University, Hamilton, ON, Canada
[4] Canadian Centre for Electron Microscopy, McMaster University, Hamilton, ON, Canada
[5] Department of Materials Science & Engineering, McMaster University, Hamilton, ON, Canada
[6] Brockhouse Institute for Materials Research, McMaster University, Hamilton, ON, Canada

Cellulose is a structural biopolymer that is produced by all plant organisms and is also found in bacteria, tunicate and fungi. The hierarchical assembly of bacterial cellulose into ribbons and the structural origin of its alternating disordered and crystalline structure are tied to the biosynthesis and processing of cellulose materials, yet they remain to be fully understood. In this work, we used atomic force and transmission electron microscopy (TEM) to unravel the supramolecular structure of bacterial cellulose ribbons at the sheet, bundle and microfibril levels. The non-persistent twisting of cellulose ribbons was characterized in detail and cryo-TEM allowed the visualization of nanostructural defects within the twisted regions. Through super-resolution fluorescence microscopy, we visualized the alternating disordered and crystalline structure of cellulose fibrils in the form of a labeling pattern that represent areas of differing susceptibility to fluorescent labeling.[1] Combining this technique with TEM in a correlative super-resolution light and electron microscopy (sr-CLEM) workflow revealed that the disordered regions of cellulose are associated with the twisted segments of the ribbon.[2] These findings shed light on the biosynthesis of bacterial cellulose and the origin of the disordered regions, with implications on the processing and breakdown of cellulose to produce renewable materials and biofuels.

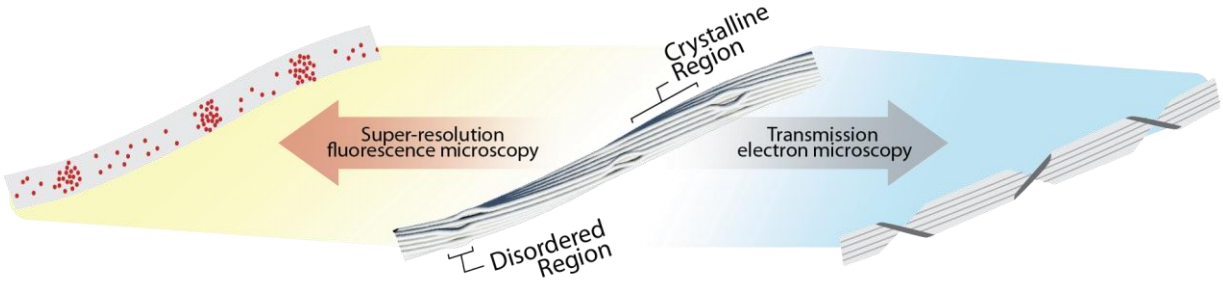

References

1. Babi, M., Palermo, A., Fatona, A., Jarvis, V., Nayak, A., Cranston, E.D., and Moran-Mirabal, J.M. Direct imaging of the alternating disordered and crystalline structure of cellulose fibrils via super-resolution fluorescence microscopy. *ChemRxiv,* 2022 (accessed 2023 01 12). Doi: 10.26434/chemrxiv-2022-0jqng

2. Babi, M., Williams, A., Reid, M., Grandfield, K., Bassim, N.D., and Moran-Mirabal, J.M. Unraveling the supramolecular structure and nanoscale dislocations of bacterial cellulose ribbons using correlative super-resolution light and electron microscopy. *Biomacromolecules* **2023**, *24(1),* 258-268. Doi: 10.1021/acs.biomac.2c01108

C46: The Three-Dimensional Structure of the Gecko Eggshell

Joseph Deering[1], Valentin Nelea[1], Marc D. McKee[1,2]

[1]Dental Medicine and Oral Health Sciences, McGill University, Montreal, QC, Canada
[2]Anatomy and Cell Biology, McGill University, Montreal, QC, Canada

Eggshells have evolved as protective encasements for embryonic development across avian and reptilian species. Along with providing a rigid exterior to protect the embryo, eggshells facilitate the transport of water and gas and provide resistance to pathogen ingress [1]. In some species, eggshell mineral partly dissolves to provide mineral ions for embryonic skeletal mineralization. The structure of the chicken eggshell is particularly well-described, being composed of an inner layer of organic membrane fibers and a columnar layer of organized calcium carbonate mineral, typically calcite [2]. Ranging from soft to semi-rigid to hard shells, reptilian eggshells often have major and diverse structural differences from avian eggshells [3] – with a mineral (calcite) distribution and fiber density that contributes to differing mechanical properties [4]. Even among gecko species, the structural pattern and continuity of the calcareous layer varies between species [5]. Until now, examination of reptilian eggshells has largely been through scanning electron microscopy and other 2D characterization techniques. In this work, we perform a *multiscale analysis of the leopard gecko eggshell* adding 3D methods including X-ray micro-computed tomography (µCT) and focused ion beam-scanning electron microscopy (FIB-SEM) tomography.

By light microscopy, staining with toluidine blue (for organics) and Von Kossa reagent (black/gray, for mineral) revealed discrete clusters of mineral at the outer surface of the eggshell that we newly define as *mineral scutes*. The mineral phase was surprisingly sensitive to aqueous sample preparation protocols, necessitating anhydrous methods whenever possible. SEM of the eggshell exterior revealed that the outer surface of the scutes contained an abundance of tightly aggregated mineral nanospheres. SEM and atomic force microscopy of the scute interior revealed organic fibers embedded within the mineral. In some locations, the core of these membrane fibres was cavitated. Segmentation of mineral scutes using deep learning after 3D imaging by µCT of critical point-dried eggshells, and dual-beam FIB-SEM run in serial-surface-view mode following cryogenic sample preparation (high-pressure freezing), allowed for a quantitative description of scute morphometry. In conclus ion, this multiscale structural characterization provides a baseline structural description in 3D for the eggshell of the leopard gecko, a structure defining its semi-rigid properties and also providing a template for monitoring eggshell response to climate change.

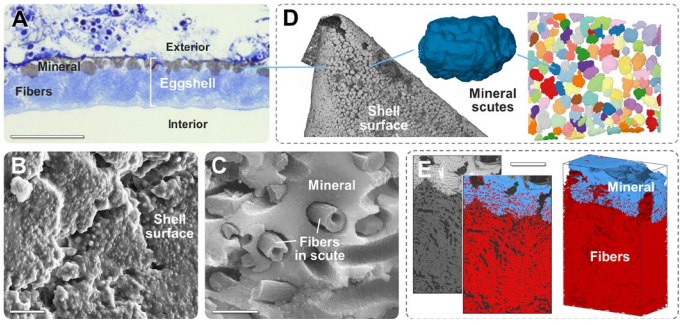

Figure: (A) Light microscopy of cross-sectioned leopard gecko eggshell stained for organics (blue) and mineral (gray). (B-C) Scanning electron microscopy of mineral scutes, surface and cross-sectional views. (D) 3D µCT of mineral scutes, with segmentation and reconstruction. (E) FIB-SEM reconstruction of mineral and fibers. Scale bars: (A) 150 µm, (B) 5 µm, (C) 1 µm, (E) 20 µm.

References: [1] Hincke et al. (2012). *Front. Biosci. 17,* 1266-1280. [2] Board (1982). *Biol. Rev. 57,* 1-28. [3] Legendre et al. (2022). *J. Anat., 241(3)*, 641-666. [4] D'Alba et al. (2021). *J. Morphol. 282(7),* 1066-1079. [5] Choi et al. (2018). *PLoS One, 13(6),* e0199496.

C47:Determination of magnetic exchange stiffness by measuring magnetic domain wall width

Kodai Niitsu[1]

[1] Research Center for Advanced Measurement and Characterization, National Institute for Materials Science (NIMS), Tsukuba, Ibaraki, Japan

[Introduction]

Magnetic exchange stiffness A is a parameter that describes the magnetic exchange coupling, which is crucial in the calculation of Micromagnetics. However, the traditional method of measuring A through an experiment of spin wave dispersion is limited to a small range of materials and temperatures. On the other hand, in this study, the author constructed a method to evaluate A from the width δ of domain walls introduced into the TEM sample. The proposed method allows for easy measurement by changing the temperature, making it possible to measure A in a wide range of temperatures from cryogenic to just below the Curie temperature (T_C). The calculated A using this method was found to be in good agreement with the values obtained from spin wave dispersion measurements across all temperatures. The method is demonstrated using the ferromagnetic elements Fe and Ni as examples.

[Experiments]

TEM foils of Fe and Ni single crystals were cut using FIB (focused ion beam) processing so that the axis of easy magnetization was oriented in the plane of the thin film. In-plane magnetic imaging were performed across a temperature range of 5 to 1080 K using split-illumination electron holography.

[Results]

Fig. 1 shows the magnetic phase profiles across the domain wall obtained for the Fe thin film at various temperatures and the temperature dependence of A derived from these profiles [1,2]. The presence of domain walls was confirmed up to 1040 K (=0.997 T_C), and A was able to be calculated. The resultant values were found to be in good agreement with literature values obtained through spin wave dispersion measurements across the whole temperature range below T_C. This suggests that the method established in this study can be an alternative to the conventional method of measuring A through spin wave dispersion.

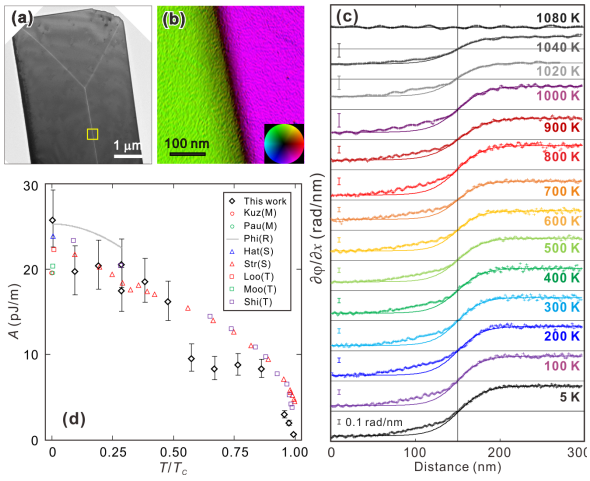

Fig. 1 (a,b) Lorentz and magnetic phase images of Fe thin foil. (c) Magnetic phase profile across a magnetic domain wall at various temperatures [1]. (d) Derived A as a function of normalized temperature T/T_C [2].

References

[1] K. Niitsu, T. Tanigaki, K. Harada, D. Shindo. *Appl. Phys. Lett.* **113**, 222407 (2018).

[2] K. Niitsu, *J. Phys. D: Appl. Phys.* **53**, 39LT01 (2020).

C48: Imaging and Spectroscopy of Kagome Lattice YCr_6Ge_6

Babafemi S. Agboola[1], Jonah Gautreau[2], Graeme Luke[2], Maureen J. Lagos[1,3]

[1] Material Science and Engineering, McMaster University, Hamilton, Ontario, Canada.

[2] Department of Physics, McMaster University, Hamilton, Ontario, Canada

[3] Canadian Centre for Electron Microscopy, McMaster University, Hamilton, Ontario, Canada.

The Cr and Ge atoms in YCr_6Ge_6 crystal lie on a kagome lattice that exhibits exotic electronic properties[1]. Material realization and characterization of structural and electronic properties are challenging and are still under progress. We grew single crystals of YCr_6Ge_6 with the flux method, then a small thin specimen was created using a focused ion beam microscope. We use TEM/STEM methodologies (e.g., diffraction and imaging) to obtain structural information and EELS spectroscopy technique to access relevant chemical information. The diffraction patterns obtained from different micrometer-sized regions in the crystal revealed crystalline configuration, which suggest that the whole synthetized material is monocrystalline. We also verified that the crystal has HCP crystal structure. Atomic-resolution imaging was performed in STEM mode to spatially identify the atomic arrangement. Figure 1a show a ADF STEM of the YCr_6Ge_6 crystal along the $[11\bar{2}0]$ direction, in which interatomic distance of 2.7 Å, 2.68 Å, and 1.07 Å between the Y, Ge and Cr atoms, respectively, can be seen. We also conducted core loss EELS spectroscopy to identify the chemical composition of the crystal. The spectrum image was collected at different ionization edge energies, revealing different degrees of scattering delocalization. Figure 1b shows a spectrum image of chromium, revealing the highly localized signal from the chromium atomic planes. Our work represent progress towards the atomic/nanoscale characterization of exotic quantum materials using electron microscopy.

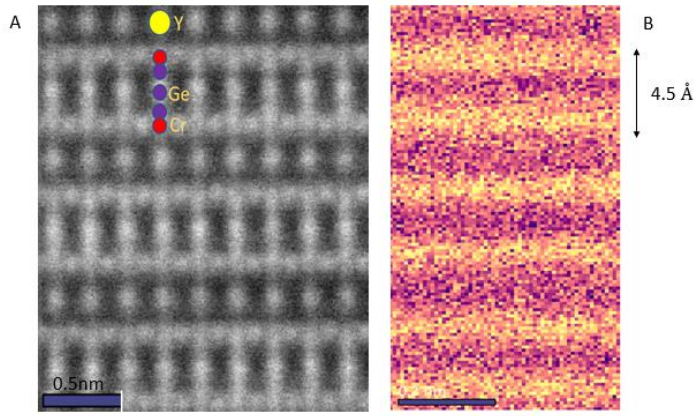

Fig. 1 (a) ADF-STEM image of YCr_6Ge_6 along the $[11\bar{2}0]$ direction. Y, Ge and Cr atomic column positions are indicated by yellow, purple and red discs, respectively. (b) Elemental map of YCr_6Ge_6 indicating Cr atomic planes.

References

[1] Y. Ishii, et al. Jour. Phys. Soc. Jap. 82 (2013) 023705.

[2] We acknowledge NSERC under a Discovery Grant and CCEM for access to microscopy facilities.

C49: Elucidating Structural and Chemical Modification of Ambient-Conditioned $LiNi_{0.8}Mn_{0.1}Co_{0.1}O_2$ with a Lithium Boron Carbon Oxide Coating with Analytical Electron Microscopy and X-ray Absorption Spectroscopy

Jingyi Qu[1,], Zoya Sadighi[2], Hui Yuan[3], Gillian Goward[2], and Gianluigi Botton[1,4]*

[1] Department of Materials Science and Engineering, McMaster University, Hamilton, Ontario L8S 4L7, Canada

[2]Department of Chemistry and Chemical Biology, McMaster University, Hamilton, Ontario L8S 4L7, Canada

[3]Canadian Centre for Electron Microscopy, McMaster University, Hamilton, Ontario L8S 4M1, Canada

[4]Canadian Light Source, Saskatoon, Saskatchewan S7N 2V3, Canada

Lithium-ion Batteries (LIBs) are an essential solution for addressing severe environmental issues, such as climate change and energy sustainability. All over the world, researchers are dedicated to optimizing LIBs materials, understanding and improving their performance.

As a significant cathode candidate, $LiNi_{0.8}Mn_{0.1}Co_{0.1}O_2$ (NMC811 for short) stands out for its high capacity and wide potential window. Unfortunately, this material still needs to be improved due to the limited air stability and fast capacity fade. During the preparation, storage, and transportation, it is a practical and inevitable issue that the cathode will be exposed to ambient conditions. However, NMC811 is very sensitive and unstable when exposed to humidity and carbon dioxide in the air. Some lithium compound residuals, e.g., LiOH, and Li_2CO_3[1], have been demonstrated to form on the surface. As one of the solutions, coating strategies have been widely utilized for surface and interface modifications. In this work, we coated a lithium boron carbon oxide on ambient-conditioned NMC811 with the sol-gel method[2]. With the Focused Ion Beam (FIB), the cross-section of the secondary particles was prepared. The coating material was confirmed as lithium boron carbon oxide (LBCO) with analytical electron microscopy – Electron Energy Loss Spectroscopy- and supported with synchrotron X-ray Absorption Spectroscopy. This nm-level LBCO coating effectively enhances the electrochemical performance, helps recover the specific capacity, and increases the capacity retention, elucidated from structural and chemical perspectives by the advanced characterization techniques. Our results show that the FIB and analytical electron microscopy are essential and irreplaceable tools to investigate the local surface and interface structure at the nanoscale and unveil the correlation between chemistry, structure and LIBs' performance.

References

1. Zou, L. *et al.* Unlocking the passivation nature of the cathode–air interfacial reactions in lithium ion batteries. *Nat Commun* **11**, 3204 (2020).
2. Zhang, Y. *et al.* Direct Visualization of the Interfacial Degradation of Cathode Coatings in Solid State Batteries: A Combined Experimental and Computational Study. *Adv. Energy Mater.* **10**, 1903778 (2020).

C50: Discovery of 1-dimensional TiO_2 lepidocrocite

Robert F Klie and Francisco Lagunas
Department of Physics, University of Illinois, Chicago, IL, USA

Nanostructured (NS) titanium dioxides, TiO_2, have been, and remain, of significant research interest due to their unique physical and chemical properties, as well as their potential application in a wide range of fields including paint pigment, catalysis, photocatalysis, photoluminescence, gas sensors, and solar and fuel cells, among many others. One dimensional (1D) and two-dimensional (2D) materials possess characteristics and properties that their three-dimensional (3D) counterparts do not. In this contribution, we present our recent discovery 1-dimensional TiO_2 nanofilaments with lepidocrocite structure. Using a combination of high-resolution scanning transmission electron microscopy, Raman spectroscopy, obtained using low laser power, and density functional theory modeling, we find that the 1D titania lepidocrocite-based structure has a minimal cross sections of $\approx 5 \times 5$ Å^2. The nanofilaments, shown in Figure 1, grow along [100] with *a* and *c* lattice parameters of 3.78 ± 0.01 Å and 3.04 ± 0.06 Å. They tend to self-assemble/stack in two directions along the *b* and *c* axes. [1] We will demonstrate that these nanofibers can be readily decorated with H_3O^+, Li^+, Na^+, Mg^{2+}, Mn^{2+}, Fe^{2+}, Co^{2+}, Ni^{2+} and Zn^{2+} cations. And while in-plane and out-of-plane interfilamentous distances are functions of the nature of the cations surrounding the NFs, the band gap, at z 4 eV, is not. Using atomic-resolution scanning transmission electron microscopy (STEM), in-situ cryo-STEM, electron energy-loss spectroscopy (EELS) and first principles density funcational theory modeling, we will show how the different functional groups affect the filament stacking, spacing and thermal properties. [2]

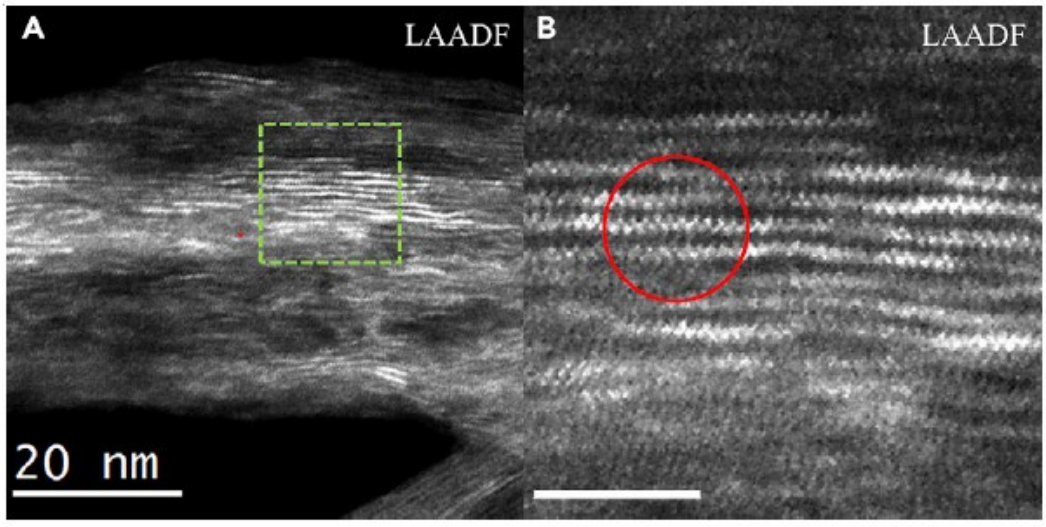

Figure 1: Low-angle annular dark field STEM micrographs of TiO_2 nanofibers at (A) low magnification and (B) higher magnification of region enclosed in green square in (A). Scale bar in 5 nm. Zigzag and 2-layered nature of Ti atoms in the NFs in area enclosed by red circle are clearly shown.

References

[1] H.O. Badr, F. Lagunas, D.E. Autrey, J. Cope, T. Kono, T. Torita, R.F. Klie, Y.-J. Hu, and M.W. Barsoum, *Matter*, **6**, 128-141 (2023)

[2] This work was funded by the National Science Foundation (NSF DMR-1831406).

C51: Nanomineralogy in mining and environmental research

Martin Couillard[1], Andre Zborowski[1], Daniel Tyo[1], Oltion Kodra[1], Bussaraporn Patarachao[1]

[1] Energy, Mining and Environment Research Centre, National Research Council Canada, Ottawa, ON, Canada

Nanomineralogy explores the wealth of information contained in mineral systems at a scale well below the micrometer. By combining surveys and analytical tools with transmission electron microscopy, it becomes possible to extend mineralogical assessments from the field scale down to the atomic scale. Nanomineralogy allows the study of interfacial interactions of nanominerals, mineral nanoparticles, and nanopore structures. In this presentation, by discussing our experiments, we demonstrate how nanomineralogy support the mining sector in three areas:

(1) *Exploration*: By analyzing a gold deposit at the sub-µm scale [1], we have deduced that water-oil micro-emulsions were the geological explanation for the concentration of uranium and gold (figure 1, top). A key experimental evidence was the observation of nanoparticles in thin pyrobitumen layers on pores' surface. A second example that will be presented is the identification, relying on nanoscale spectroscopy, of several mineral phases containing rare-earth elements that were found as micro-inclusions in zircon.
(2) *Extraction*: Micro-emulsions stabilized by contaminants are a common issue in resource extraction. For instance, ultrafine clay platelets stabilize water-in-oil emulsions, impacting bitumen extraction from oil sands. By combining EELS mapping with mineral separation experiments, we have shown that organic coatings affect the wettability of platelets [2]. In particular, a "patchy" coating results in biwettable clays, which tends to accumulate at the surface of water bubbles in bitumen.
(3) *Environmental impact*: To understand remobilization pathways of metals in mine wastes, it is often necessary to visualize at the nanoscale the mixture of fine-grained secondary phases that are formed following the exposure of primary minerals to the environment. Our study of lead-containing waste rocks [3] highlights a spatial heterogeneity of secondary phases down to the nanoscale (figure. 1, bottom) that points to potential storage as well as potential release of lead from mine wastes to the surrounding environment.

Finally, we will present a brief overview of future work on critical minerals and carbon capture by mineralization, where nanomineralogy will be an essential component of the research.

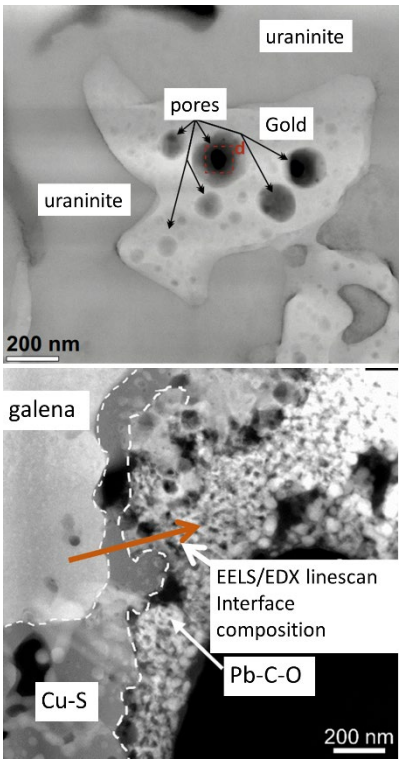

Figure 1 (top) Gold ore, (bottom) Lead-bearing mine waste rocks.

References
1. Fuchs *et al*. (2021) , *Ore Geology Reviews* **138**, 104313
2. Couillard *et al*. (2020), *Minerals* **10**, 1040
3. Bao *et al*. (2021), *Journal of Hazardous Materials* **412**, 125130

C52: Phase Imaging Dislocation Strain Annihilation at Crystal Surface Forming Pit

Rodney Herring

MENG, UVic, Victoria, Canada V8W 2J2

Recently two new imaging capabilities, i.e., phase imaging the strain existing at the core of dislocations and phase imaging the bottom surface of a crystal TEM specimens [1, 2], has made it possible to image and measure the strain of a dislocation passing from the top surface to the bottom surface of a TEM crystal specimen. As the dislocation approaches the free surface, which cannot support the strain, i.e., strain is zero at free surfaces, it becomes unstable, cross-slips and splits into two equivalent dislocations creating a triple point. The three dislocations at the triple point further split into partial dislocations forming three stacking faults that form the surfaces of a three dimensional pit existing at the free surface. This is the first time this mechanism has been imaged. The energy required for the formation of the pit is determined to be ½ E/B where E is the elastic modulus of the material and B is the Burgers vector of the dislocation.

1. Herring, R.A., "Phase Imaging Dislocations using Diffracted Beam Interferometry" Microscopy (2020) MICRO-2020-00047.
2. Herring, R.A., "Diffracted beam interferometry – Differential phase contrast image of an amorphous thin film material" Micron Volume 160, September 2022, 103317. doi.org/10.1016/j.micron.2022.103317

C53: Hyperbolic Phonon Polaritons in Twisted Bilayers Revealed by Electron Energy Loss Spectroscopy

Ka Yin Lee[1], *Joaquin E. Reyes-Gonzalez* [1], *Marcelo D. Martinho*[1], *Babafemi Agboola*[1], *Maureen J. Lagos*[1,2]

[1] Department of Materials Science and Engineering, McMaster University, Hamilton, ON, Canada

[2] Canadian Centre for Electron Microscopy, McMaster University, Hamilton, ON, Canada

Monochromated electron probe with high energy (~ 3-5 meV) and spatial (~ 1 Å) resolution enables access to infrared (IR) photonic information at the nanoscale using electron energy loss spectroscopy (EELS). For instance, the spatial distribution of phonon polariton modes (PhPs) in nanoscale objects [1] and plasmon-phonon coupling behavior [2] were studied with nanometer resolution. Recently, it was shown that α-MoO_3 twisted bilayers (TBls) sustain highly confined, low loss PhPs in which possess attractive properties such as hyperbolic to elliptical transition [3], and canalization of polaritonic propagation [4]. Here, we present an EELS study on the role of twisting in localized PhPs in α-MoO_3 TBls. Our results showed that there are multiple polaritonic modes over wide range from ~ 30-120 meV along three directional Reststrahlen bands in a single α-MoO_3 flake (1µm x 3µm). Figure 1a shows the spatial distribution of three hyperbolic modes, which is dictated by the anisotropy of the material. A comparison (Fig. 1b) of EELS spectra for a α-MoO_3 single flake and TBls revealed the complexity in tuning the various directional, far infrared PhPs and demonstrated potentials in developing new approaches for tuning far IR responses at the nanoscale. This study highlights strong interlayer coupling in bilayer systems with high IR anisotropies, which offers new opportunities in manipulating strong light–matter interactions in nano devices in the far IR range.

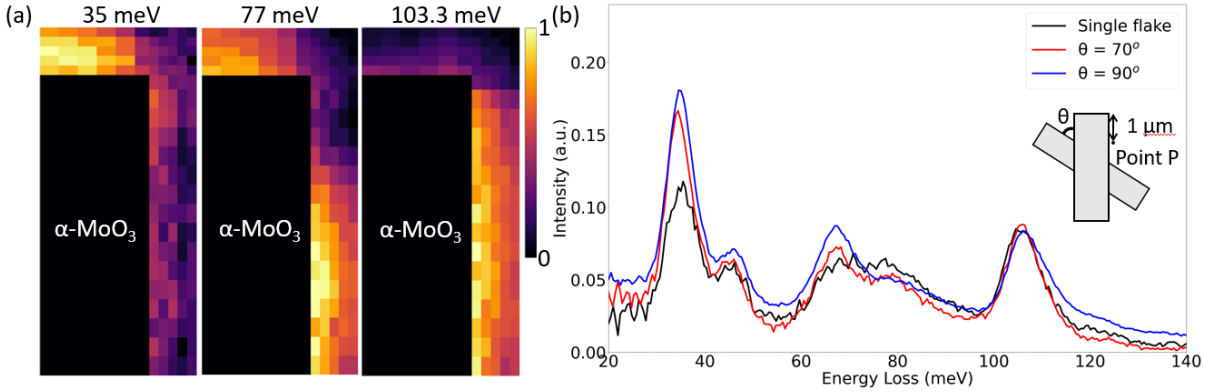

Fig.1 (a) EELS intensity maps obtained around a corner of an α-MoO_3 single flake (labelled black rectangle). Figures' spatial aspect ratios are modified for better illustration. (b) EEL spectra obtained in aloof geometry at 60 nm from the vertical edge (Point P inset).

References

[1] M. J. Lagos et al., Nature, 543(7646) (2017), 529-532.

[2] M. J. Lagos et al., ACS Photonics 8 (2021), 1293–1300

[3] G. Hu et al., Nature 582, 209–213 (2020)

[4] P. Li et al., Nature communications, 11, (2020) 1-8

[5] We acknowledge NSERC under a Discovery Grant and CCEM for access to microscopy facilities.

C54: Vibrational Spectroscopy of Single Molecular Nanocrystals in the Electron Microscope

Marcelo Martinho[1], *Maureen J. Lagos*[1,2]

[1] Department of Materials Science and Engineering, McMaster University, Hamilton, ON, Canada

[2] Canadian Centre for Electron Microscopy, McMaster University, Hamilton, ON, Canada

Vibrational spectroscopy studies of nanoscale materials are now possible in the electron microscope using Electron Energy Loss Spectroscopy (EELS). Recent studies have reported vibrational information from single organic nanostructures, including bonds with light atoms such as hydrogen[1,2]. This exploration of vibrational studies of organic nanomaterials in electron microscopes has just started and a deeper understanding of the inelastic scattering data is needed. We present a study related to the detection of vibrational modes of molecular nanocrystals (e.g. paracetamol crystal (PC)) using an electron probe fabricated in a Nion HERMES electron microscope, which offers 5 meV energy resolution and 1 Å spatial resolution. We probed PC in a non-intersecting geometry to minimize beam damage. We found a large variety of peaks associated with the excitation of several intramolecular modes over a wide range of the IR region (20–420 meV), as indicated in Figure 1. Some modes (e.g. C-H, N-H, O-H) are assigned to certain peaks, clearly indicating the chemical presence of light atoms. The physical origin of the mode excitation is driven by dipole scattering rules. To verify our results, we conducted Fourier-Transform Infrared (FTIR) Spectroscopy and found an excellent agreement between our FTIR and EELS data. We also analyzed the dipolar response of PC under different orientations with respect to the travelling electron trajectory, finding significant scattering variations of scattering which suggest a strong dependence of the dipole scattering on the oscillating dipoles. Moreover, modes below 40 meV were also detected (~26 meV) which are not accessible by conventional FTIR. Our work represents advances towards the characterization of vibrational behavior of organic nanomaterials over the IR range with higher spatial sensitivity, and towards the understanding of the complex physics of inelastic electron scattering from vibrational modes in molecular crystals.

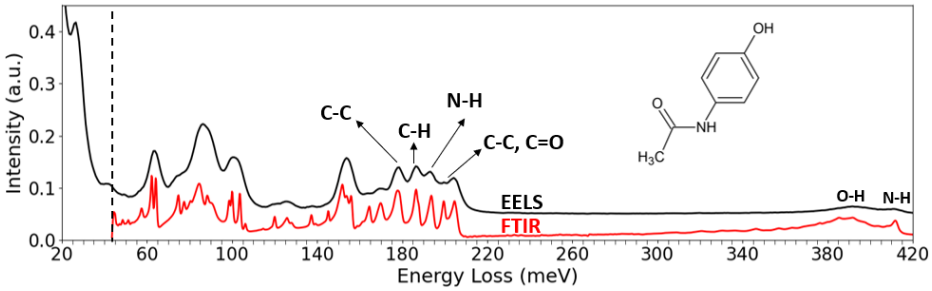

Figure 1 – EELS spectrum of monoclinic paracetamol single crystal compared with FTIR spectrum. CH, NH (stretch and deformation), CO, CC and OH peaks match with FTIR spectra position. Vibrational modes are related to paracetamol molecule structure depicted in the schematic.

References

1. Rez, P. *et al*. *Nat Commun* **7**, (2016).
2. Krivanek, O. L. *et al*. *Nature* **514**, 209–212 (2014).
3. We acknowledge NSERC under a Discovery Grant and CCEM for access to Microscopy facilities.

C55: Quantitative electron probe microanalysis of lithium in different materials including battery compounds

Pia Schweizer[1], Emmanuelle Brackx[1], Philippe Jonnard[2]

[1] CEA, DES, ISEC, DMRC, Univ Montpellier, Marcoule, France

[2] Sorbonne Université, Faculté des Sciences et Ingénierie, UMR CNRS, Laboratoire de Chimie Physique - Matière et Rayonnement, 4 Place Jussieu, F-75252 Paris Cedex 05, France

Electron probe microanalysis (EPMA) is a reliable and widely used technique to do non-destructive, accurate material characterisation for scientific and industrial applications. Nevertheless, despite of the great interest in lithium (Li) and the urgent need to do accurate non-destructive analysis at a micron scale, quantification of Li using EPMA has not been performed successfully yet. Recently developed periodic multilayers allow spectroscopy in the energy range around the characteristic Li K emission ~50 eV [1] but the detection and quantification of Li by a microprobe equipped with a bent crystal spectrometer and standard commercialised multilayers without diffraction gratings still is challenging.
The difficulties of Li detection are caused by different factors: the fluorescence yield of Li is extremely low, few characteristic photons are produced by the decays of the Li 1s core hole, favoring the emission of Auger electrons. Because of their low energy, the photons are strongly absorbed before even leaving the sample and its eventual coating. The signal therefore is principally coming from a thin surface layer that can be subject to contamination and that may be sensitive to electron bombardment. Further photon absorption by the microprobe components, especially by separation windows, will additionally decrease the measured intensity. As the Li K emission (2p – 1s transition) involves valence electrons, the shape of the Li emission band is highly dependent on the density of states (DOS) of the valence band and so highly dependent on the chemical state of the sample. Chemical shifts of some eV and strong peak shape alterations can occur and should be expected for EPMA of light elements [2], complicating quantitative analysis.

This work shows, to our knowledge for the first time, quantitative EPMA of Li in different materials including battery compounds and metal alloys with Li concentrations down to 2 %. This was made possible after the integration of a new detection system. Further work on the quantification procedure using real standards and correction programs suited for low voltage EPMA has also been accomplished. We show that EPMA is a powerful tool to do quantitative analysis of Li even if it is contained in heavy matrices with elements showing characteristic emission bands in the same spectral range as Li. This novel Li quantification method is more accessible than other techniques using synchrotron radiation and less expensive than detection using a SEM equipped with multilayer gratings.

References

[1] Polkonikov, V., Chkhalo, N., Pleshkov, R., Giglia, A., Rividi, N., Brackx, E., Le Guen, K., Ismail, I., Jonnard, P. , *Appl. Sci.* 2021, *11*, 6385. https://doi.org/10.3390/app11146385

[2] Schweizer, P., Brackx, E., Jonnard, P., *X-Ray Spectrom*. 2022, *51 (4)*, 403. https://doi.org/10.1002/xrs.3290

C56: Cathodoluminescence Response of Barite at Room and Liquid Nitrogen Temperatures

Heather Lowers[1], Colin MacRae[2], Nick Wilson[2], Phil Verplanck[1], and Aaron Torpy[2]
[1.] U.S. Geological Survey, Geology, Geophysics, and Geochemistry Science Center, Denver, CO, USA
[2.] CSIRO Minerals, Microbeam Laboratory, Clayton, Victoria, Australia

The cathodoluminescence (CL) response of barite at room (RT) and liquid nitrogen (LN) temperatures was studied. CL data collection and data reduction were performed with the xCLent Analysis software package [1]. Quartz optics from the RT analysis at USGS allow collection of signals beyond 4 eV whereas the glass optics used at CSIRO have a strong absorption starting around 3.54eV (Fig. 1). The background of the room temperature spectrum is higher at lower energies than the LN spectrum and the position of the peak near 3 eV is different for the two temperatures. These changes are likely due to reduced thermal vibrations caused by the LN environment thus accentuating the main transitions [2]. The ~3.9 eV peak at RT may be attributed to either an intrinsic $(SO_4)^{2-}$ or the presence of Ti^{3+} [3]. The peak at ~2.25eV is most likely associated with Mn^{2+}originally attributed by Tarashchan [4] and subsequently confirmed by Gaft et al. [4]. The peak observed at ~ 3.02eV in the LN CL spectra may be attributed to Ca replacement in the barite structure [3].

References

[1] MacRae. C.M. et al., 2005, Hyperspectral mapping—combining cathodoluminescence and X-ray collection in an electron microprobe, Microscopy Research and Technique Vol. 67 Issue 5, pp. 271-277
[2] MacRae C.M. et al., 2017, EPMA Characterisation of Quartz and Quartz-Cement from a Triassic Sandstone, Microscopy and Microanalysis, 23 S1: 1072-1073
[3] Gaft, M.L. et al., 1985, Luminescence Centers in Anhydrite, Barite, Celestite and Their Synthesized Analogs, Phys Chem Minerals 11: 255-260
[4] Tarashchan A.N., 1978, The luminescence of minerals, Naukova dumka (in Russian)

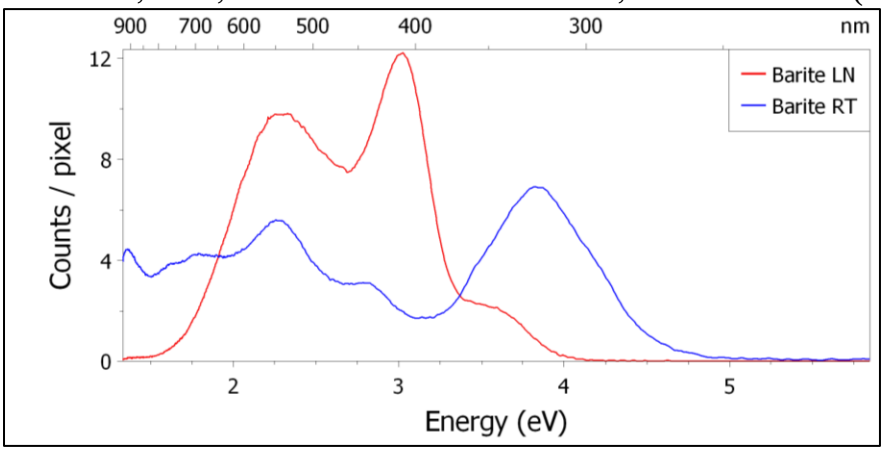

Figure 1. The sum CL spectra of barite for the liquid nitrogen (red, standard optics) and room temperature (blue, quartz optics) acquisitions.

C57: Probing Near- and Far-Field Responses of the Magnetic Dipole Mode in a Plasmonic Split Ring Resonator

Isobel C. Bicket[1], Edson P. Bellido[1], Sophie Meuret[2], Toon Coenen[3,4], Albert Polman[3], Gianluigi A. Botton [1,5]

[1] Dept of Materials Science and Engineering, McMaster University, Hamilton, ON, Canada
[2] CEMES-CNRS, Toulouse, France
[3] Center for Nanophotonics, AMOLF, Science Park, Amsterdam, The Netherlands
[4] Delmic BV, Delft, The Netherlands
[5] Canadian Light Source, Saskatoon, SK, Canada

Plasmonic nanostructures support coherent resonant oscillations of conduction electron density known as localized surface plasmon resonances (LSPR). LSPR produce evanescent electromagnetic (EM) near-fields with which a focused electron beam can interact, and can produce radiating far-fields which can be accessed through optical means. The characteristics of the fields produced are defined by the size, shape, and material of the nanostructure and its surrounding environment, providing great freedom in engineering the near- and far-field EM response towards applications such as enhanced sensing, nano-optoelectronics, or optical metamaterials.

One structure of particular interest for its ability to support a magnetic dipole moment is the split ring resonator (SRR). These devices support degenerate, but orthogonal, electric and magnetic dipole moments at low energies. Typical studies are done on SRRs lying flat on the substrate due to the relative ease of fabrication, but in this geometry the ability of the SRR to couple to the magnetic field of incoming radiation is reduced [1]. We present the fabrication and characterization of a vertically-oriented SRR (VSRR), in which both the electric and magnetic dipole moments are oriented parallel to the substrate [2]. Using electron beam lithography, we have fabricated a VSRR with dimensions on the order of 300 nm, supporting a low energy magnetic dipole mode at a free-space wavelength of approximately 1800 nm, as confirmed through monochromated electron energy loss spectroscopy. We further characterize the magnetic dipole mode using infrared cathodoluminescence (CL) polarimetry [3, 4], complemented with boundary element method simulations [5] and custom Python analysis code [6]. Through this analysis, we are able to derive the approximate phase and amplitude relationship between these two dominant dipole moments. By spatially mapping out the polarized CL emission, we also discover that there is a non-negligible amount of circular polarization emitted from the VSRR, dependent on the electron beam excitation location, suggesting interesting opportunities for exploring the chiral near-fields of plasmonic nanostructures.

References

[1] Gay-Balmaz & Martin, *J. Appl. Phys.*, **92**, 5, 2002.
[2] Bicket *et al.*, *Microscopy*, **67**, suppl_1, 2018.
[3] Bicket *et al.*, Manuscript in preparation.
[4] Coenen & Polman, *Opt. Express*, **20**, 7, 2012.
[5] Hohenester, *Comput. Phys. Commun.*, **185**, 3, 2014.
[6] Bicket (2020), [Python 3], https://github.com/icbicket/CLFields.
DOI: 10.5281/zenodo.3739563.

C58:Investigation of structure and chemical properties of core/shell germanium/germanium-tin nanowires

Milenka Andelic[1*], A. Pofelski[1], S. Assali[2], S. Koelling[2], L. Luo[2], O. Moutanabbir[2], and G.A. Botton[1*]

[1.] Department of Materials Science and Engineering, McMaster University, Hamilton, ON, Canada
[2.] Department of Engineering Physics, Ecole Polytechnique Montreal, Montreal, QC, Canada
* Corresponding authors: andelicm@mcmaster.ca, gbotton@mcmaster.ca

The development of IV group semiconductor devices based on nanowires heterostructures depends strongly on their controlled fabrication and careful structural and chemical characterization. The ability of group IV GeSn semiconductors to confine active carriers offers the possibility of increasing radiative recombination, which proves that they can be used as building blocks in the functional nanoscale silicon-compatible optoelectronic operating at the nanoscale [1]. Furthermore, the bandgap tunability of GeSn makes them attractive materials for photodetector's operation extending the emission wavelength to the mid-infrared energy range (0.4-0.9 eV). [2]

Here the composition and structure of the core/shell Ge/GeSn nanowires are studied using core-loss electron energy loss spectroscopy (EELS) in atomically resolved high-resolution scanning transmission electron microscopy (HR-STEM). The characterization has been done on the nanowires with different concentration of Sn content incorporated in the shell. Employing core loss EELS we discovered not-uniform Sn distribution in the GeSn shell, and its concentration varies with the selected area of interest. Likewise, it was found that a high amount of defects occur when increasing the Sn content followed by the strain relaxation present in these structures. The defect's diversity in nature and location of formation strongly depends on the Sn concentration as has been demonstrated in this work. Moreover, these effects were investigated along [111] growth direction.

Resolving pressing questions such as already noticed strain effects and phase separation, faceting during nanowire growth due to the anisotropy of the surface energy, will lead us towards a better understanding of these alloyed materials with unique geometry. While utilizing these advanced techniques with the addition of Moiré interferometry we will here further investigate in detail and with precision, the occurrence of diverse structural features on these nanowires, explore their origin and question their behaviour and characteristics. [3]

[1] Luo, L., Assali, S., Atalla, M. R., Koelling, … & Moutanabbir, O. (2022). Extended-SWIR Photodetection in All-Group IV Core/Shell Nanowires. *ACS Photonics*, *9*(3), 914-921.

[2] Moutanabbir, O., Assali, S., Gong, X., O'Reilly.., ... & Nam, D. (2021). Monolithic infrared silicon photonics: the rise of (Si) GeSn semiconductors. Applied Physics Letters, 118(11), 110502

[3] This work was carried out at the Canadian Centre for Electron Microscopy, a national facility supported by the CFI under the MSI program, McMaster, and NSERC.

C59: EELS Characterization of Niobium Oxide Memristor Devices

Bradley T De Gregorio[1*], Evgeniya Lock[1], Keith Knipling[1] and Hans Cho[1]

[1.] U.S. Naval Research Laboratory, Washington, DC, USA.
* Corresponding author: bradley.degregorio@nrl.navy.mil

Memristor devices are being developed as a key component of neuromorphic computing systems, where the device may be switched between multiple conduction states dependent on external factors. NbO_2 is a promising phase-change material that has recently been demonstrated in memristor prototypes, having a reversible transition between an insulating rutile crystal structure (R-NbO_2; E_g = 1 eV) and a conducting tetragonal structure (T-NbO_2). These conduction states may be tunable by modifying the Nb:O composition by H reduction steps during ALD deposition of NbO_x thin films. STEM-EELS of Nb and O absorption edges can be used to identify structural transitions between phases during growth/annealing, electroforming, and device testing. We find that compositional stratification of NbO_x thin film creating by ALD are retained after annealing. However, we also observe pore formation that can lead to device failure. Correlated x-ray photoelectron spectroscopy and atom probe tomography provide a full picture of the internal composition of these materials.

C60: Dissecting the role of the universally conserved protein KsgA in the maturation process of 30S ribosomal subunit

Jingyu Sun[1,2], Laurel Fay Kinman[3], Dushyant Jahagirdar[1,2], Joaquin Ortega[1,2*] and Joseph H. Davis[3*]*

[1]Department of Anatomy and Cell Biology, McGill University, Montreal, Quebec, Canada,
[2]Centre for Structural Biology, McGill University, Montreal, Quebec, Canada,
[3]Department of Biology, Massachusetts Institute of Technology, Cambridge, MA, USA.

The methylation of two adjacent adenosines (A1518 and A1519) located in helix 45 is universally conserved in ribosomes from all three life kingdoms[1]. These methylations are catalyzed by the universally conserved KsgA/Dim1p enzyme family. *Escherichia coli* lacking KsgA displays a temperature-sensitive phenotype and reduced translational fidelity[2]. The loss of KsgA also attenuates the virulence of specific human pathogens[3]. Early studies established the belief that these phenotypes result from the KsgA methylase activity. However, recent studies lead to a hypothesis that there is an additional role of ksgA in facilitating the 30S ribosomal subunit assembly beyond its methylase activity[4,5]. Here, we leverage the power of cryo-EM and machine learning to discover that the bacterial methyltransferase KsgA acts as a novel "proofreading factor" in the assembly of 30S ribosomal subunit by recognizing and partially disassembling particles that have matured but are not competent for translation. We propose that the novel function of KsgA allows those inactive 30S particles an opportunity to reassemble and transition to the active state, thereby ensuring the fidelity of the assembly process. These results provide for the first time a mechanistic understanding of the novel function of KsgA as a "proofreading factor" governing ribosome biogenesis and showcase the power of heterogeneity analysis in cryo-EM to unveil functionally relevant information in biological systems.

References:

1 Mangat, C. S. & Brown, E. D. Ribosome biogenesis; the KsgA protein throws a methyl-mediated switch in ribosome assembly. *Molecular Microbiology* **70**, 1051-1053, doi:10.1111/j.1365-2958.2008.06484.x (2008).

2 Desai, P. *Adenosine dimethyltransferase KsgA : biochemical characterization of the protein and its interaction with the 30s subunit*, <http://scholarscompass.vcu.edu/etd/1915> (2009).

3 Kyuma, T., Kizaki, H., Ryuno, H., Sekimizu, K. & Kaito, C. 16S rRNA methyltransferase KsgA contributes to oxidative stress resistance and virulence in Staphylococcus aureus. *Biochimie* **119**, 166-174, doi:10.1016/j.biochi.2015.10.027 (2015).

4 Inoue, K., Basu, S. & Inouye, M. Dissection of 16S rRNA methyltransferase (KsgA) function in Escherichia coli. *J Bacteriol* **189**, 8510-8518, doi:10.1128/JB.01259-07 (2007).

5 Connolly, K., Rife, J. P. & Culver, G. Mechanistic insight into the ribosome biogenesis functions of the ancient protein KsgA. *Mol Microbiol* **70**, 1062-1075, doi:10.1111/j.1365-2958.2008.06485.x (2008).

C61: Novel insights into the role of the YsxC GTPase in the assembly of the 50S ribosomal subunit revealed by Cryo-EM

Amal Seffouh[1,2], Kaustuv Basu[1,2], Dominic Arpin[1,2], Robert A. Britton[3,4] and Joaquin Ortega[1,2]

[1] Department of Anatomy and Cell Biology, McGill University, Montreal, Quebec H3A 0C7, Canada. [2] Centre for Structural Biology, McGill University, Montreal, Quebec H3G 0B1, Canada.

[3] Department of Molecular Virology and Microbiology, Baylor College of Medicine, Houston, TX 77030, USA. [4] Center for Metagenomics and Microbiome Research, Baylor College of Medicine, Houston, TX 77030, USA.

The assembly of the ribosome is assisted by biogenesis factors that are not part of the ribosome's final structure. Ribosome biogenesis GTP-binding protein YsxC is an evolutionarily conserved GTPases widely distributed in bacteria, higher eukaryotes and mitochondria. It is an essential GTPase for most pathogenic bacteria and is involved in the assembly of the large subunit. Depletion of YsxC causes a slow-growth phenotype and accumulation of immature ribosomal 50S particles called $44.5S_{YsxC}$ particles [**1**]. These particles show disordered functional rRNA helices and are severely depleted of late binding ribosomal proteins (r-protein) [**2**]. To explore the YsxC function in the 50S assembly process, we determined the high-resolution Cryo-EM structure of the $44.5S_{YsxC}$ particle in complex with the YsxC protein. Unexpectedly, YsxC occupies the binding site of the core r-protein uL2. Microscale thermophoresis shows that it binds with high affinity to the ribosomal subunit (Kd ~107 ± 36 nM). Analysis of this complex allowed us to examine the conformational changes that occur during the interaction with the ribosomal subunit and the structural elements involved in nucleotide and ribosome binding. YsxC active site shows that the spatial arrangement of residues surrounding the β and γ-phosphate groups is similar to that observed in related GTPase. However, the resolution of existing structures does not provide enough detail of the water molecules in the immediate environment of the γ-phosphate group of the GTP-analogue [**3 - 4**]. Our high-resolution cryo-EM model identifies the position in the structure of the attacking nucleophilic water molecule and the catalytic residue, which, together with the divalent cation ion, are thought to play a significant role in the catalysis by YsxC (unpublished data). This work provides new insights into the molecular mechanisms of GTP hydrolysis by YsxC and its role in assisting the assembly of the 50S ribosomal subunit.

References

[1] Schaefer, Laura et al. Multiple GTPases participate in the assembly of the large ribosomal subunit in Bacillus subtilis. Journal of bacteriology vol. 188,23 (2006): 8252-8.

[2] Ni, Xiaodan et al. YphC and YsxC GTPases assist the maturation of the central protuberance, GTPase associated region and functional core of the 50S ribosomal subunit. Nucleic acids research vol. 44,17 (2016): 8442-55.

[**3**] Privé, G G et al. X-ray crystal structures of transforming p21 ras mutants suggest a transition-state stabilization mechanism for GTP hydrolysis. Proceedings of the National Academy of Sciences of the United States of America vol. 89,8 (1992): 3649-53.

[**4**] Ruzheinikov, SN et al. Analysis of the open and closed conformations of the GTP-binding protein YsxC from Bacillus subtilis. Journal of molecular biology vol. 339,2 (2004): 265-78.

C62: Cell Envelope Architecture of Chloroflexi Revealed by Cryo-Electron Tomography

Ameena Hashimi[1*], *Elitza I. Tocheva*[1]
[1] Department of Microbiology and Immunology, The University of British Columbia, Vancouver, BC, Canada

The bacterial cell envelope is a multi-layered structure that provides a critical barrier against changing environmental conditions and facilitates interactions between the cell and its surroundings. So far, only two major types of bacterial cell envelopes have been fully characterized: monoderm and diderm [1]. Monoderms are enveloped by a single lipid bilayer and a thick layer of the structural polymer peptidoglycan (PG), whereas diderms have two membranes: an inner membrane (CM/IM) and an outer membrane (OM) with a thin layer of PG between them. Though most characterized bacterial phyla typically share the same envelope type, recent studies from our lab and others have demonstrated that there are diderm members within phyla previously understood to be monoderm [1-3].

Chloroflexi is an ancient bacterial phylum that is often placed near the root of the tree of life. As such, members of this phylum can help elucidate the evolution and diversity of bacteria, including their cell envelopes. The architecture of the cell envelope in Chloroflexi remains unclear, however our preliminary cryo-electron tomography (cryo-ET) data show that the phylum contains both monoderm and diderm species. Since the diderm species share no homology to the lipids and proteins of typical diderm bacteria, we hypothesize that diderm Chloroflexi evolved a novel OM. Ultimately, understanding the evolution and diversity of the bacterial cell envelope can provide valuable insight into how modern phyla evolved.

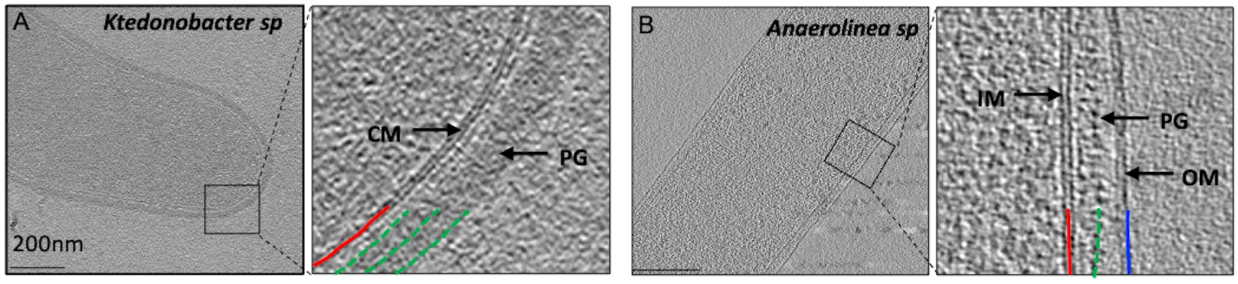

Figure 1. Cell envelope architectures in Chloroflexi revealed by cryo-ET. A) Monoderm species *Ktedonobacter*, and B) Diderm species, *Anaerolinea*. CM/IM shown in red, PG green, OM blue.

References

1 Taib, N. *et al.* Genome-wide analysis of the Firmicutes illuminates the diderm/monoderm transition. *Nature Ecology & Evolution*, 1-12, doi:10.1038/s41559-020-01299-7 (2020).
2 Tocheva, Elitza I. *et al.* Peptidoglycan Remodeling and Conversion of an Inner Membrane into an Outer Membrane during Sporulation. *Cell* **146**, 799-812, doi:10.1016/j.cell.2011.07.029 (2011).
3 Vincent, A. T. *et al.* The Mycobacterial Cell Envelope: A Relict From the Past or the Result of Recent Evolution? *Front. Microbiol.* **9**, 2341, doi:10.3389/fmicb.2018.02341 (2018).

C63: Phase Transformation Study of 2D Materials by in-situ STEM

Moon J. Kim,[1] S. Kwon,[1] Q. Wang,[2] X. Zhu[1]*

[1]Department of materials science and engineering, The University of Texas at Dallas, Richardson, Texas 75080, U.S.A.

[2]Materials Science and Engineering, King Abdullah University of Science & Technology (KAUST), Thuwal 23955, Saudi Arabia

The physical characteristics of many two-dimensional (2D) materials, such as transition metal dichalcogenides (TMDs) and transition metal carbides (TMCs), depend on their phase, atomic scale morphology, and defects. However, there is a lack of detailed studies of these 2D materials' stability and transformational behavior upon exposure to an external stimulus, which is critical for their practical applications.

We have used *in-situ* scanning transmission electron microscopy (STEM) to investigate the thermally-induced phase transformation and defect evolution of 2D materials down to the atomic scale. In this talk, I will present several examples of emerging 2D materials such as $Cr_2Ge_2Te_6$, $NbSe_2$, and high-entropy TMC. Details of various physical and chemical transformations observed, such as new phase formation, 2H to 1T phase transition, defects, atomic desorption, intercalation, etc., as shown in Figure 1, will be presented and discussed.

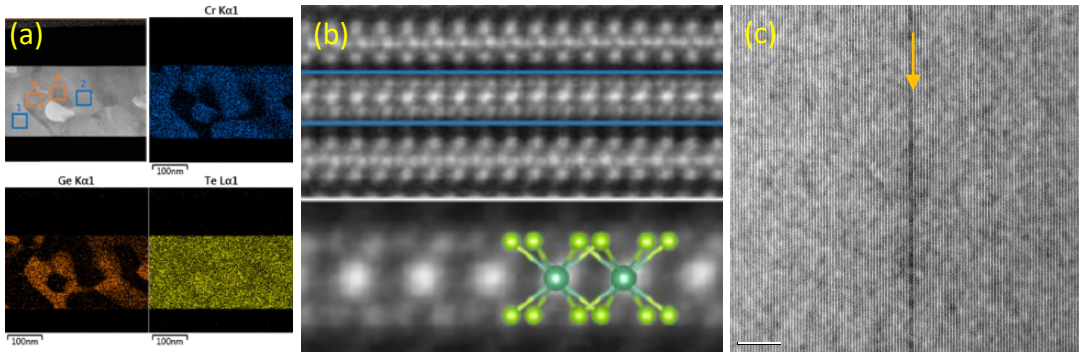

Figure 1. (a) $Cr_2Ge_2Te_6$ – STEM images showing elemental segregation occurring at 300°C. (b) $NbSe_2$ – Atomic resolution STEM image showing phase transition from 2H to 1T at 400°C. (c) HE MXene – STEM image showing an early stage of phase transformation observed at 700°C.

C64: Real-time Slip Planes Monitoring during In-situ Nanoindentation Enabled by Hollow-cone Dark-field Imaging

Yushun Liu[1], *Guo-zhen Zhu*[1*]

[1] Department of Mechanical Engineering and Manitoba Institute of Materials, University of Manitoba, Winnipeg, MB, R3T 5V6, Canada.
*Corresponding author. Email: Guozhen.Zhu@umanitoba.ca.

The mechanical responses of polycrystalline materials highly depend on their crystallographic orientations relative to the loading. The resulted mechanical anisotropy develops more in materials with less symmetric crystal structure like magnesium (Mg) having a hexagonal close-packed (HCP) lattice. Thus the linking of grain orientation to the mechanical responses, particularly the tracking of orientations during deformation, has been a key interest to numerous materials scientists. Although a few techniques like electron back-scattered diffraction (EBSD) [1], dark-field conical scanning [2] and precession electron diffraction (PED) [3] etc. have been invented to provide fully quantitative orientation data, one major drawback of these techniques is that all of them essentially require sampling the whole reciprocal space for each image pixel, which leads to excessively long acquisition time, making them not compatible to dynamic process like deformation. In current research, instead of sampling the whole reciprocal space, interested diffraction rings have been used for dark-field imaging under a hollow-cone illumination condition in transmission electron microscope (TEM) to track certain crystallographic traits. The collecting angle ranges from 8.4-11.7 mrad, covering the diffraction rings of three major slip planes ({0002}, {10$\bar{1}$0} and {10$\bar{1}$1}) of Mg. Given the Bragg's law of diffraction, any grains with their selected slip planes edge-on appear to be bright in the dark-field image. Thus by comparing the contrast changes in the in-situ movie, one can monitor in real-time the re-orientation of individual grains. Examples of the images recorded during the in-situ nanoindentation are shown in Fig. 1, from which clear contrast changes due to grain re-orientation can be observed after the deformation.

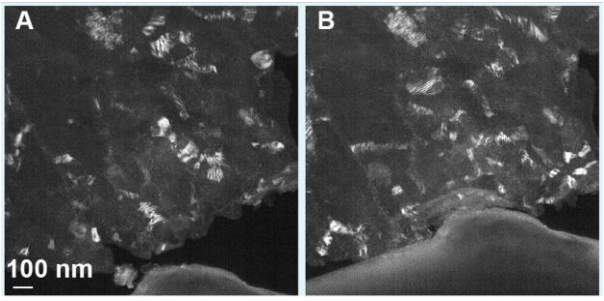

Figure 1. Snapshots taken from an in-situ nanoindentation movie (a) before and (b) after the indentation using hollow-cone dark-field imaging.

References

[1] Randle, V., & Engler, O. (2000). Introduction to Texture Analysis: Macrotexture, Microtexture and Orientation Mapping (1st ed.). CRC Press.

[2] S.I. Wright, D.J. Dingley, Orientation imaging in the transmission electron microscope, Mater. Sci. Forum. 273-275 (1998) 209-214.

[3] E. Rauch, M. Véron, J. Portillo, D. Bultreys, Y. Maniette, S. Nicolopoulos, Analysis-UK, Automatic crystal orientation and phase mapping in TEM by precession diffraction, Microsc. Anal. 22 (2008) S5-S8.

C65: In Situ EBSD Studies of Blocky Grain Growth in Welded Zircaloy-4

Ruth Birch[1,2], Ben Britton[1,2]

[1] Department of Materials, Imperial College London, London, UK
[2] Department of Materials Engineering, University of British Columbia, Vancouver, BC, Canada

Zirconium alloys, like Zircaloy-4, are popular nuclear fuel cladding materials due to their low thermal neutron absorption cross section, good mechanical performance, and weldability. Their performance is often enhanced through thermomechanical processing to optimise microstructure. During welding, the microstructure can be adjusted due to local fusion, generation of residual stress and plastic work. In this study, we employ in situ electron backscatter diffraction (EBSD) observations with heating to explore Zircaloy-4 microstructure and the formation of very large 'blocky' alpha grains (grain size >500 μm) in electron beam welds. Using parent grain reconstruction, we reveal that the while the prior beta grain structure is important in the evolution of the microstructure, the crystallographic texture, grain shape and grain structure is nucleation controlled. These findings are important when designing and improving the manufacturing routes of multipart zirconium components.

C66: Investigation of stress corrosion cracking in CMSX-4 turbine blade alloys using Deep Learning assisted X-ray microscopy

Hrishikesh Bale[1], Maadhav Kothari[1], Andy Holwell[1], Simon Gray[2], Johnathan Legget[3]

[1] Carl Zeiss Research Microscopy Solutions, Dublin, California
[2] Cranfield University, Cranfield, UK
[3] Rolls Royce, Derby, UK

Single crystal Ni superalloys are typically are used in power generation and aviation applications due to their unique properties. Recently, incidents of failure due increased temperature around root blade regions has caused Type II hot corrosion leading to cracking in blade roots resulting in catastrophic failure [1]. Understanding the failure mechanism and crack characterisation is vital in solving this industrial issue.

Here we demonstrate a unique workflow of characterization using X-ray microscopy (Figure 1) aided with deep-learning based algorithms for data reconstruction and segmentation, combined with FIB-SEM and electron microscopy in order to characterize cracks and crack tips developed during stress corrosion cracking. By extracting the fracture tip, both crystal plasticity and crystal deformity can be studied in detail resulting in orientation tomography of the corroded region of stress. Combining this correlative workflow we are able to demonstrate a unique technique in C-ring analysis and identifying structural defects not visible using typical microscopy techniques.

[1] : L. Brooking, J. Sumner, S. Gray & N. J. Simms (2018) Stress corrosion of Ni-based superalloys, Materials at High Temperatures, 35:1-3, 120-129, DOI: 10.1080/09603409.2017.1392414

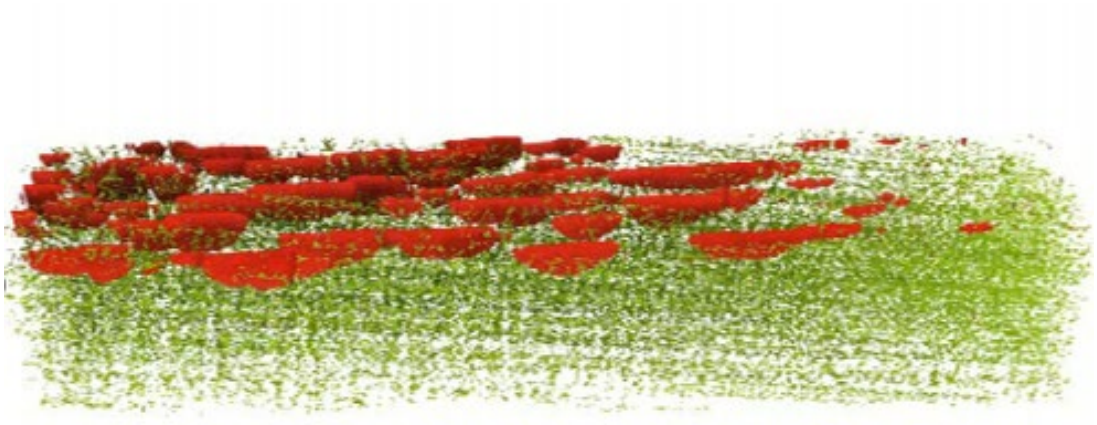

Figure 1 3D rendering of X-ray microscopy data reconstructed and segmented using deep-learning algorithms. Red features indicate semi-circular surface cracks formed due to stress-corrosion cracking. Green features represent voids seen along the dendritic direction of the single crystal CMSX-4 nickel based super alloy sample.

C67: Variational Convolutional Autoencoders for Anomaly Detection in Scanning Transmission Electron Microscopy

Robert F Klie, Arashdeep Thind, James P Buban
Department of Physics, University of Illinois, Chicago, IL, USA

Identifying point defects and other structural anomalies using scanning transmission electron microscopy (STEM) is important to understand a material's properties caused by the disruption of the regular pattern of a crystal. Thanks to the high spatial resolution of aberration-corrected transmission electron microscopes, atomic-resolution images with a field of view of several hundred nanometers can be taken [1]. In this contribution, we demonstrate that the performance of a convolutional variational autoencoder (VAE) [2] that is trained to learn the patterns of a bulk sample and generate a prediction (example) of a given input image based on the trained features [2]. We have shown that such a convolutional neural network (CNN) approach can be used to replicate an input image and to differentiate between bulk or defects.[3] In the case of a bulk input, the VAE can replicate well the input within a threshold value. For a defect input, the VAE will fail to output a prediction within the set threshold, allowing for a clear and automatic distinction of defects. Figure 1 shows how the VAE's predictions look compared to the respective inputs of $SrTiO_3$ [001]. The first row consists of the input samples: one bulk and three copies of it modified to reassemble three types of point defects, including anti-sites, vacancy, and ferroelectric distortions. The second row shows the respective prediction to the inputs above. The third row, the predictions are subtracted to the respective input and all pixels with a magnitude higher than 0.2 are isolated to obtain a heatmap of the difference. These "difference" images allow us to isolate the point defects in the input and can be used to differentiate between a bulk or defect sample. We will demonstrate that this approach can be applied to a wide variety of materials and the high fidelity in identifying point or extended defects. [4]

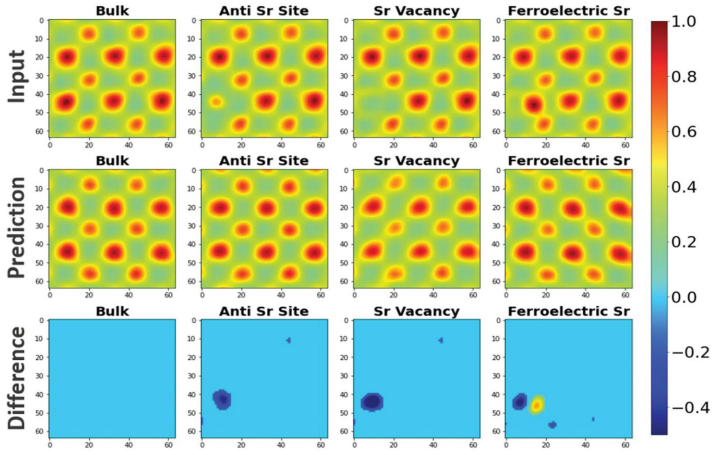

Figure 1: Input, prediction, and difference image for $SrTiO_3$ [001] bulk and various point defect structures.

References
[1] H Sawada et al., Journal of Electron Microscopy **58**(6) (2009), p. 357.
[2] DP Kingma and M Welling, ArXiv.org (2014)
[3] E Prifti, JP Buban, AS Thind and RF Klie, Small, 2205977 (2023)
[4] This work was funded by the National Science Foundation (NSF DMR-1831406).

C68: Interpretation of serial section 3D EDX maps: multivariate analysis and deep learning hybrid approach

Frédéric Voisard[1], Ryan Gosselin[2], Jiří Dluhoš[3], Hana Tesařová[3], Nadi Braidy[1,2]

[1] Institut Interdisciplinaire d'Innovation Technologique 3IT, Université de Sherbrooke, Sherbrooke, Québec, Canada

[2] Department of Chemical and Biotechnological Engineering, Université de Sherbrooke, Sherbrooke, Québec, Canada

[3] Tescan Orsay Holding, a.s., Brno, Czech Republic

Serial sectioning tomography (SST) in the focused ion beam-scanning electron microscope (FIB-SEM)[1] is a powerful tool to capture subsurface microstructure in 3D. When coupled to energy-dispersive spectral mapping (EDS), FIB-SEMs can generate analytical information on the sampled volume. However, despite day-long acquisition times, the low signal-to-noise ratio forces a compromise between spectral precision and spatial resolution. In addition, simple window integral algorithms are inappropriate to appreciate the complex and rich data generated by EDS-SST. On one hand, multivariate analyses can certainly tackle the data complexity but not the load. On the other hand, the low signal-to-noise ratio (SNR) severely impedes the generation of an acceptable training dataset for deep learning. There is therefore an opportunity to leverage the capability of multivariate analyses algorithm to classify low SNR data to produce the training dataset for the deep learning step. Here, we test this idea using a multi-phasic tribological coating made of tungsten carbides in an iron aluminide matrix. The coating was deposited using high-velocity oxyfuel jet of a ball-milled powder containing 30 % vol WC in Fe_3Al powder. The polyphasic and porous nature of the sample makes the sole BSE image segmentation difficult via simple thresholding methods.

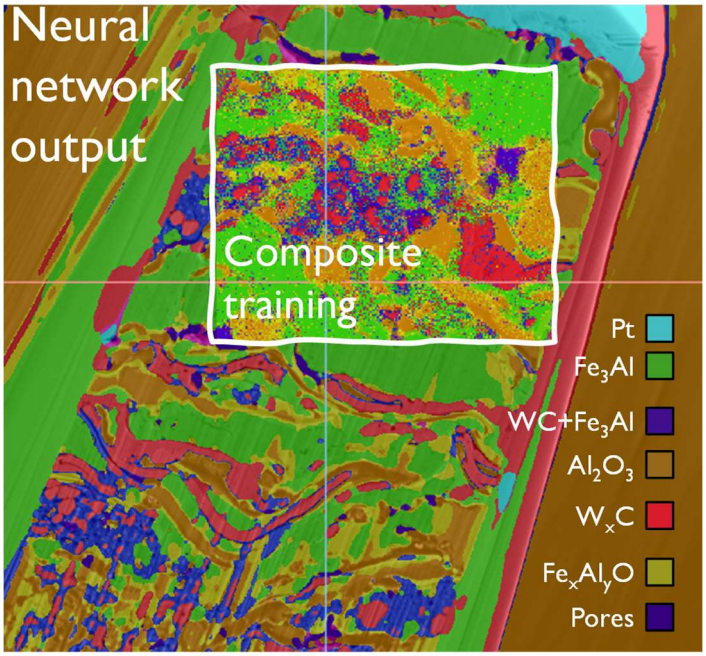

A training dataset was first produced using a hierarchal classification scheme[2] of the EDS dataset from 12 slices that helped identify 8 endmembers. The abundance maps for each slice by loglikelihood maximization[3] were then computed and converted to an 8-phase mask. These segmented BSE slices were then used as the training dataset for a deep learning step (2 or 3-level U-net, Dragonfly). The segmentation shows a crisp and complete phase separation which will greatly help understand the structure-properties relation of this composite.

References

1. Berger, S. D. et al. DualBeam metrology: a new technique for optimizing 0.13-um photo processes. in (ed. Sullivan, N. T.) 423 (2001). doi:10.1117/12.436768.
2. Fauteux-Lefebvre, C. et al R. Anal Chem 90, 13118–13125 (2018).
3. Lavoie, F. B., et al. Chem. Int. Lab. Sys. C, 40–50 (2016).

C69: Overcoming Phase Identification Ambiguity in the Analysis of SAED Patterns from Polymorphic Nanomaterials

Rasool Doostkam, Kenneth Beyerlein, Aycan Yurtsever
Energy, Materials and Telecommunications Research Center, Institute National de la Recherche Scientifique (INRS-EMT), Varennes, Quebec, Canada

Manufacturing new phases of materials with desired electronic, optical, and mechanical properties is a major goal in materials science. Ultrafast laser ablation can drive a material into pressure and temperature regimes that are otherwise inaccessible. A recent report by Rapp et al. [1] suggests the creation of rare high-pressure Silicon polymorphs resulting from high-power femtosecond laser ablation. The sample was analyzed using selected area electron diffraction (SAED) patterns collected from small volumes near the ablation crater. The candidate phases of bt8 and st12 were identified by matching d-spacing information obtained from the observed Bragg spots. However, the phase identification using this approach is ambiguous, as the d-spacings of many of the spots match both phases.

We have developed an algorithm to address this phase identification ambiguity in SAED patterns of polymorphic nanomaterials. It provides more confidence on the ascribed phase by taking into account the angular correlation between Bragg spots. We will demonstrate the fidelity of the algorithm on simulated patterns. Then, we will discuss the results of its application to experimental data collected by Rapp et al. We find that the st12 phase is more likely to be present in the material than bt8, overcoming the ambiguity in the previously reported analysis.

References

[1] Rapp L., Haberl B., Pickard C.J., Bradby J. E., Gamaly1 E.G., Williams J.S., Rode A.V., "*Experimental evidence of new tetragonal polymorphs of silicon formed through ultrafast laser-induced confined microexplosion*", Nature Communications, **6** 7555 (2015).

C70: Correlative energy dispersive X-ray spectroscopy (EDS/X) and electron backscatter diffraction (EBSD) analysis of

Chris Bilsland[1], Andrew Barrow[2], Ben Britton[1,3]*

[1] Department of Materials, Imperial College London, London, UK
[2] Rolls-Royce Submarines Limited, PO Box 2000, Raynesway, Derby, UK
[3] Department of Materials Engineering, University of British Columbia, BC, Canada

Analytical tools such as energy dispersive X-ray (EDS/EDS) and electron backscatter diffraction (EBSD) are commonly used semi-independently within a scanning electron microscope to reveal variations in chemistry (EDX) and crystal structure/orientation (EBSD) of complex microstructures, such as engineering alloys used in structural applications. In the present work, we directly combine simultaneous data-collection of EDX and EBSD data to enable a new correlative approach for precipitate distribution analysis. We use EDS to label Mo-/Nb-rich particles and link them to different boundary types of the Ni matrix in samples of Alloy 625 (a Ni-based alloy used in structural applications, including nuclear reactors). Measurement of many thousands of particles enables us to employ statistical tools, such as ANOVA analysis, to confidently assess whether the distribution of precipitates varies between different boundary types (e.g. special and non-special boundaries) within the same sample [1], as well as between different samples manufactured with different processing routes. Furthermore, as the particles are labelled well we can directly investigated the co-partitioning of different elements into particles from differing populations using Wurher and Moran [2] plots. These plots enable us to identify trends in multicomponent analyses of the pair-wise combinations of 12 different elements in the Alloy 625 samples. Our findings include statistical analysis of the distribution of particles, their chemistry and the statistical differences in population are thought to be important in understand the stress-corrosion cracking performance of these alloys in steam generation components within in a boiler.

References

[1] Bilsland, C., Barrow, A., and Britton, T.B. (2021) Materials Charaterization
[2] Wuhrer, R. and Moran, K. (2014) IOP Conference Series: Materials Science and Engineering

P01: Distribution and Speciation of Selected Elements in Insect Wings

James J. Dynes[1], Zachary Arthur[1], Viorica F. Bondici[1], Tom Z. Regier[1], Malgorzata Korbas[1], Tor Pedersen[1], Sean Prager[2]

[1] Science Department, Canadian Light Source, Saskatoon, SK, Canada
[2] Department of Plant Sciences, University of Saskatchewan, Saskatoon, SK, Canada

Insects developed wings at least 400 million years ago, exploiting a number of design and material properties (e.g., lightweight, flexible, morphology, strength) that make them the most versatile and maneuverable of all flying machines. Manipulation of the three-dimensional wing shape is all important for controlling wing motion to generate sufficient aerodynamic force to attain flight and for maneuverability. Insects, however, have little control over the shape of their wings as their flight muscles are attached to the wing base, unlike that of invertebrates such as birds and bats whose wings contain muscles that control many aspects of the wing shape. Therefore, unique morphological/structural and/or compositional features of insect wings are responsible for deformation (i.e., twisting, bending) of the wing and of unique properties such as hydrophobic surfaces. However, there is still a lack of crucial information on the elemental composition, particularly elemental distribution and speciation, of insect wings, which is required to fully understand the properties/design of insect wings [1,2].

Only a few studies have been published that determined the elemental composition, excluding carbon (i.e., organics), of insect wings. One study used SEM coupled with energy dispersive analysis (EDAX) to detect selected elements from selected spots on dragonfly, seven-spotted lady beetle, white grub and sphingid moth wings[3]. In another study synchrotron-based X-ray fluorescence (XRF) was used to map the distribution of selected elements in a damselfly wing [4]. No studies have looked at the speciation of elements in insect wings.

There are about 30 orders of insects, and about 20 contain winged species. The aim of this project was to gain a comprehensive understanding of the distribution and speciation of selected elements in insect wings from different insect orders and/or species within an order. We used the SGM and BIOXAS Imaging beamlines at the Canadian Light Source to speciate and map the distribution of selected elements, at a spatial resolution of about 20 um, from insects collected from Saskatchewan. We present our results here for a variety of insects (e.g., bumblebee, wasp, fly and butterfly). There were notable differences in the speciation and/or distribution of selected elements in the wings between the various insect species/orders. The findings are of fundamental significance in understanding the distribution and speciation of selected metals on wing design and material properties.

References

[1] T.B.H. Schroeder, et al., Advanced Materials 30, 1705322 (2018).
[2] M.J. Tobin, et al., J. Synchrotron Radiation 20, 482 (2013).
[3] M. Ragaei, et al., IJOSR, 1,10 (2013).
[4] Stuhr S., et al., Scientific Reports 8, 8413 (2018).

P02: Exploring Phase in Soft X-ray Spectroptychography

Joesph Stitsky[1,], Jian Wang[1,2], Stephen G. Urquhart[1]*
[1] Chemistry, University of Saskatchewan Saskatoon, SK Canada
[2] Canadian Light Source, University of Saskatchewan Saskatoon, SK Canada

Soft X-ray spectromicroscopy combines the high spatial resolution of X-ray microscopy with the chemical sensitivity of near-edge X-ray absorption fine structure (NEXAFS) spectroscopy. An example is scanning transmission X-ray microscopy (STXM) where a zone plate focused spot is raster scanned across the sample, providing chemical information with a spatial resolution down to 30 nm.[1,2] However, STXM performance is limited by the physical limits of zone plate nanofabrication and a poor absorption contrast for thin samples.[3] Recently, the development of X-ray ptychography, which combines aspects of STXM with diffraction-based methods, offers spatial resolutions as fine as 3 nm.[3-5] In ptychography, a coherent beam is raster scanned across the sample to create a dataset of overlapping diffraction patterns that is processed with an iterative reconstruction algorithm to yield amplitude and phase information for the sample and probe.[3] By varying the photon energy, the resulting spectroptychography technique provides chemical information at smaller length scales than possible with STXM.[2-5]

Previous soft X-ray spectroptychography studies show that Fe 2p edge phase images and spectra may have greater image contrast and greater chemical sensitivity than amplitude images and absorption spectra.[6,7] This chemical sensitivity is also revealed in a higher sensitivity of phase images to certain artefacts, such as photodeposition as indicated by the Fe $2p_{3/2}$ amplitude and phase images of Fe_2O_3 nanoparticles shown in Figure. 1.These questions are explored by experimental studies performed on model systems at the Spectromicroscopy Beamline at the Canadian Light Source, which are compared to simulated phase spectra generated using the Kramers-Kronig relation.

References

1. C. Jacobsen, X-ray Microscopy, Cambridge University Press, 2020.
2. A.P. Hitchcock. J. Electron Spectrosc. Rel. Phenom., 2015, 200, 49-63.
3. F. Pfeiffer, Nat. Photonics 2018, 12, 9–17.
4. D. A. Shapiro et al., Nat. Photonics 2014, 8, 765–769.
5. S.G. Urquhart, ACS Omega 2022, 7, 11521–11529.
6. X. Zhu et al., Proc. Natl. Acad. Sci. 2016, 113, E8219–E8227.
7. T. Olumorin, M.Sc. Thesis, University of Saskatchewan, 2021.

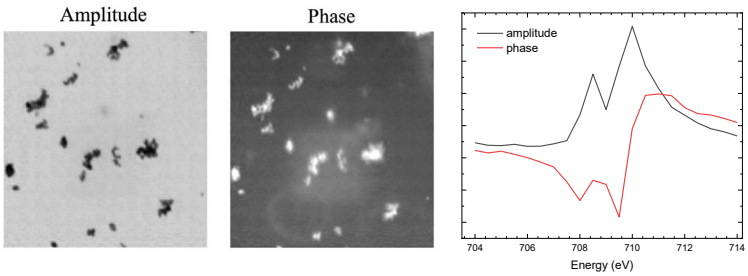

Figure 1: X-ray ptychography amplitude and phase images recorded at 710 eV (left; 3x3 micron) and amplitude and phase spectra (right) of 30 nm Fe_2O_3 nanoparticles.

P03: 3D EDS-EBSD and segmentation of battery materials

Stéphanie Bessette[1*], *Raynald Gauvin*[1]

[1] Department of Mining and Materials Engineering, McGill University, Montréal, Québec, Canada

Focused ion beam combined with scanning electron microscopy (FIB-SEM) expands the characterization possibilities of materials by revealing sub-surface microstructure and phase distributions over a volume reconstructed from a series of 2D SEM images. In this work, we will present the characterization of field-emission (FE)-SEM datasets of lithium-based cathodes with different state of charge with the addition of Energy-dispersive X-ray spectroscopy (EDS) and Electron Backscatter Diffraction (EBSD) data. The data is acquired using Hitachi Ethos NX5000 FIB-SEM built with cold field emission electron gun with a nominal resolution of 1.5nm at 1keV [1]. The FIB-SEM tool located at the Facility for Electron Microscopy Research at McGill University is equipped with Ultim Max 100 SDD detector and Oxford Instrument's Symmetry S2 EBSD that allows collection of up to 4500 patterns per second to ensure fastest acquisition with minimal time. The 3D volume reconstructions of the pristine and cycled materials give new insight on the changes in the distribution of phases following charge-discharge cycles. The effect of cycling on porosity, percolation and elemental distributions of prepared volumes of up to $(25\mu m)^3$ is studied.

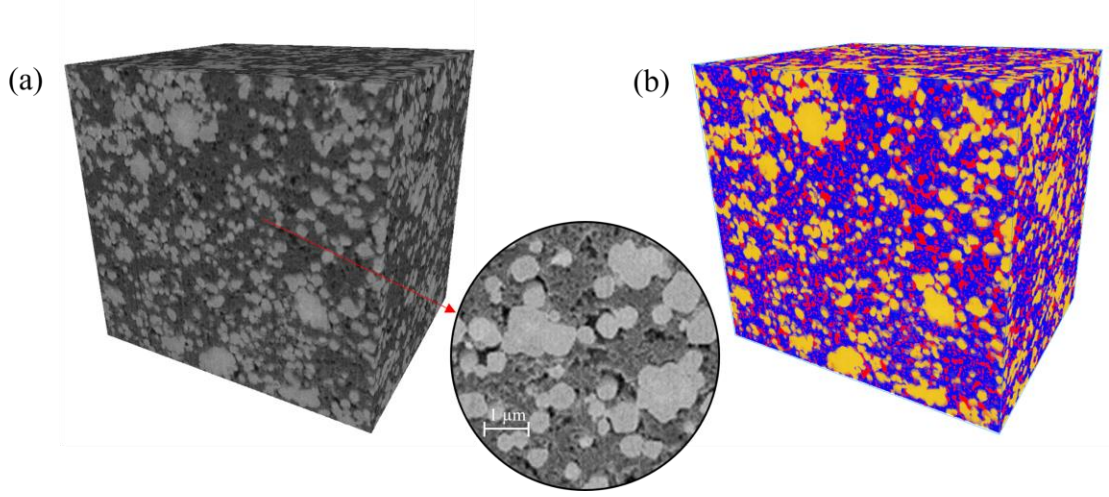

Figure 1. Preliminary results on pristine lithium cathode material with voxel size 50nm 50nm 40nm. (a) reconstructed volume from full stack of SEM images acquired at 2keV from mixed BSE U+L signals (b) Image segmentation using deep learning methods in Dragonfly of active material (yellow), carbon filler (blue) and porosity (red). Inset shows high magnification of a slice of the dataset acquired by FIB-SEM.

References

[1] H Suzuki, Hitachi Scientific Instrument News, 11 (2018) 110302.

Acknowledgements

The authors acknowledge Pr. Natalie Reznikov and Dr. Nicolas Piché for their help with this work.

P04: Low tension attachments are capable of chromosome capture

Khalid Al-Naemi[1], Jackie Vogel[1]
[1] Biology Department, McGill University, Montreal, Quebec, Canada

During mitosis, duplicated chromosomes (sister chromatids; SCs) must be separated and then segregated into daughter cells. After the spindle is formed, an error prone process of attaching microtubules (MTs) to the centromeres of SCs begins. MTs attach to outer kinetochore proteins, which is located at the centromere of each SC. When both centromeres of the SC are attached, tension is applied by depolymerization of the MT (+) end and the outer kinetochore proteins are displaced from the inner kinetochore. As a result, these attachments are stable as they are protected from aurora kinase, which releases the MT from the SC in the absence of tension. Previous work (1) using confocal microscopy predicted that the spindle must achieve a minimum equilibrium length of 1 μm to achieve sufficient tension to inhibit Aurora kinase. Here, we use a state-of the-art Zeiss Elyra 7.2 Lattice SIM microscope to observe the displacements of the two centromeres of a single SC at a resolution of 120 nm throughout metaphase and early anaphase. These measurements indirectly measure the application of tension to the kinetochore and can be used to quantify relative tension in relation to the equilibrium length of the spindle. Previously, we used a sliding deficient kinesin-5 mutant (cin8-R196K; kip1Δ) to reduce the equilibrium length of newly formed spindles (2). Using this mutation, we observed that tension is applied to centromeres below the 1 μm threshold, and that these attachments were unexpectedly stable. However, the transition to anaphase is dependent on an equilibrium length > 1 μm. We predict that low-tension attachments are sufficient to inhibit aurora kinase, while high tension attachments are required to inhibit the spindle assembly checkpoint (SAC) and allow the cell to undergo the metaphase-anaphase transition. Our findings provide new insight into the mechanism that provides both error correction and efficient chromosome attachment.

References

1. Stephens, A. D., Haggerty, R. A., Vasquez, P. A., Vicci, L., Snider, C. E., Shi, F., Quammen, C., Mullins, C., Haase, J., Taylor, R. M., Verdaasdonk, J. S., Falvo, M. R., Jin, Y., Forest, M. G., & Bloom, K. (2013). Pericentric chromatin loops function as a nonlinear spring in mitotic force balance. Journal of Cell Biology, 200(6), 757–772.
2. Leary, A., Sim, S., Nazarova, E., Shulist, K., Genthial, R., Yang, S. K., Bui, K. H., Francois, P., & Vogel, J. (2019). Successive kinesin-5 microtubule crosslinking and sliding promote fast, irreversible formation of a stereotyped bipolar spindle. Current Biology, 29(22).

P05: Phosphoregulation of γ-tubulin regulates anti-parallel microtubule bundling through kinesin-5

Shannon Sim[1], Angela Zhao[1], Jackie Vogel[1]
[1]Department of Biology, McGill University, Montreal, Quebec, Canada

The mitotic spindle ensures the accurate segregation of genetic material during cell division. The spindle is composed of microtubules (MTs) and of proteins that associate with them and influence their organization and function. The spindle MTs have two functions: either attaching to the chromosomes, or to each other as anti-parallel pairs to form interpolar MTs (ipMTs) that are crosslinked by kinesin-5. The ipMTs span the length of the spindle and function in spindle formation and in maintaining the bipolar structure of the spindle throughout mitosis. In the absence of the ipMTs, the spindle collapses and chromosome segregation cannot occur.
Using budding yeast as a model organism, we used a combination of confocal microscopy and EM tomography to show that the precursors of the ipMTs are present in monopolar spindles and drive spindle formation (1). Surprisingly, we now report that phosphorylation of γ-tubulin (2,3), which nucleates MT assembly at the spindle poles, appears to influence the organization/number of the ipMTs that are formed. This non-canonical function involves a conserved tyrosine residue (Y445) located in the unstructured carboxyl terminus (γCT). Mimicking phosphorylation in this residue (Y445D) results in a defect in kinesin-5 localization and spindle instability, and the Y445D mutation is lethal in the absence of Ase1, a PRC1 homolog that crosslinks ipMTs in anaphase. Ase1 is found at the spindle midzone in both WT and Y445D cells, indicating that it can partially substitute for kinesin-5 in metaphase. Using a fluorophore-switching technique that provides nm-scale resolution of the spindle poles, we find that spindle formation is not perturbed or delayed in Y445D cells, suggesting the formation of the ipMT precursors is normal in the mutant. We hypothesize that the Y445D mutation inhibits the recruitment of kinesin-5 after spindle formation, limiting the overlap between ipMTs. It is unclear how γ-tubulin, located at the MT (-) end, can influence the localization of kinesin-5 to the MT overlaps of ipMTs. We speculate that after a nascent bipolar spindle is formed, the relatively short overlaps of ipMTs cause kinesin-5 to walk towards the MT (-) end, where it can be sequestered by the phosphorylated γCT. The γCT containing the Y>D mutation adopts unique extended conformations not found in the WT γCT (4). We hypothesize that Y445 phosphorylation may regulate the exchange of kinesin-5 between unpaired and ipMTs and thus specify the number of ipMTs in newly formed spindles.

References

1. Leary, A. *et al*. (2019). Successive kinesin 5 microtubule crosslinking and sliding promote fast, irreversible formation of a stereotyped bipolar spindle. Current Biology. 29, 22, 3825-3837.
2. Vogel, J. *et al*. (2001). Phosphorylation of γ-tubulin regulates microtubule organization in budding yeast. Dev Cell 1(5):621-31
3. Keck, J. M. *et al*. (2011). A cell cycle phosphoproteome of the yeast centrosome. Science. 332, 6037, 1557-1561
4. Harris, J. *et al*. (2018). Concerted millisecond timescale dynamics in the intrinsically disordered carboxyl terminus of γ-tubulin induced by mutation of a conserved tyrosine residue. Protein Science. 27, 531

P06: The Cornea Conundrum: How to Balance High Resolution and Context While Preserving Native Tissue Architecture

Eran Ittah [1], Natalie Reznikov [1,2,3]

[1] Department of Bioengineering, Faculty of Engineering; [2] Department of Anatomy and Cell Biology, Faculty of Medicine and Health Sciences; [3] Faculty of Dental Medicine and Oral Health Sciences; McGill University, Montreal, Quebec, Canada

The cornea is a unique hierarchically structured connective tissue with exceptional optical transparency, mechanical properties, and macrostructure – all of which contribute to optimal light refraction. At the macromolecular level, these properties can be attributed to the long-range order of collagen fibrils which exhibit a hexagonal packing (*1*). To maintain this unique tissue ultrastructure, these fibrillar components are decorated with highly charged proteoglycans which enable electrostatic repulsion–exerting control over the hydration environment at the nanoscale (*2*). It is this hydration control which modulates the structure of the tissue and, by extension, its desirable optical properties (*3*). Although the relationship between nanostructure and hydration of the cornea has been well characterized by x-ray scattering (*4*), this is an "averaged" representation of the bulk tissue and does not account for local structural variations. Furthermore, the poor contrast of conventionally stained collagen fibrils in the cornea coupled with their relatively small diameter (30nm) limit the ability to resolve ultrastructural features with SEM over a large area. Accordingly, studies trying to elucidate the nanostructure of the cornea have been confined to 2D (TEM) or limited thickness tomographic methods (*2*) thus extricating the view of how this ultrastructural arrangement exists within the context of the broader tissue microstructure. Here, we present our work in progress in specimen preparation for FIB-SEM tomography. Our aim is to enhance contrast of the corneal ultrastructure whilst maintaining pristine/hydrated fibrillar spacing by modulating osmolarity throughout the specimen preparation process. Preliminary results reveal fine 3D fibrillar architecture within a broad contextual volume of interest. Prior observations have asserted that the fibrils between lamellar layers exist in a nearly perfect orthogonal arrangement to one another (*5*). Conversely, we observe from a correlation between light and electron microscopy, that the fibrillar orientation seems to resemble rather a "St Andrew's cross" motif. Ultimately, these findings illustrate the importance of adapting preparation methods to hydrated tissues to reliably contextualize meaningful features.

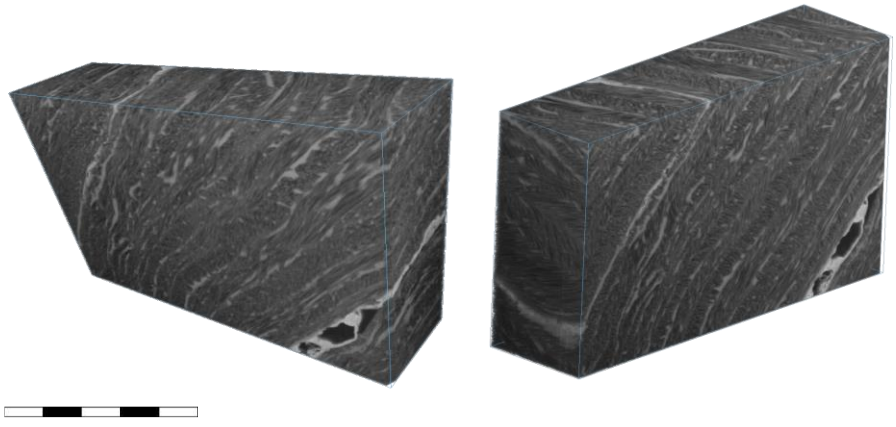

3D volume visualization of cornea exhibiting lamellar microstructure with well defined fibrils

1. K. M. Meek, *Biophys Rev*. **1**, 83–93 (2009).
2. P. N. Lewis *et al.*, *Structure*. **18**, 239–245 (2010).
3. S. Hayes *et al.*, *Journal of The Royal Society Interface*. **14**, 20170062 (2017).
4. K. M. Meek *et al.*, *Biophysical Journal*. **60**, 467–474 (1991).
5. R. D. Young *et al.*, *Experimental Eye Research*. **187**, 107772 (2019).

P07: High-resolution characterization of additively manufactured bimetal using focus ion beam milling

Sajad Shakerin[†1], *Mohsen Mohammadi*[1]

[1] *Marine Additive Manufacturing Centre of Excellence (*MAMCE), University of New Brunswick (UNB), Fredericton, *NB, E3B 5A1, Canada*

This study outlines the application of focus ion beam (FIB) milling to characterize the microstructure of an additively manufactured bimetal at the nanoscale. A nickel aluminum bronze (NAB) – stainless steel bimetal was produced using the wire arc additive manufacturing (WAAM) technique, and a very narrow interface was formed at the boundary between the two materials. The focus ion beam (FIB) milling was carried out at the interface area, and a FIB chunk with 10×4×1 µm dimensions was extracted. The thinning process was then performed on both sides of the FIB chunk to make a lamella with up to 100 nm thickness. Finally, the thinned chunk was used to take microstructure imaging in scanning transmission electron microscopy (STEM) mode. Then, energy dispersive spectroscopy (EDS) was used to analyze the nano precipitates within the interfacial microstructure. **Figure 1** shows the STEM mode micrograph of the interface with three distinct regions, including the stainless steel, interface, and NAB zones. The off-axis TKD EBSD technique was also applied to obtain high-resolution grain morphology at the interface. The results show that FIB milling is an effective technique for precise microstructural characterizations, where ultrafine features are involved.

Keywords: Focus ion beam milling, Additive manufacturing, nickel aluminum bronze, interface, TKD EBSD.

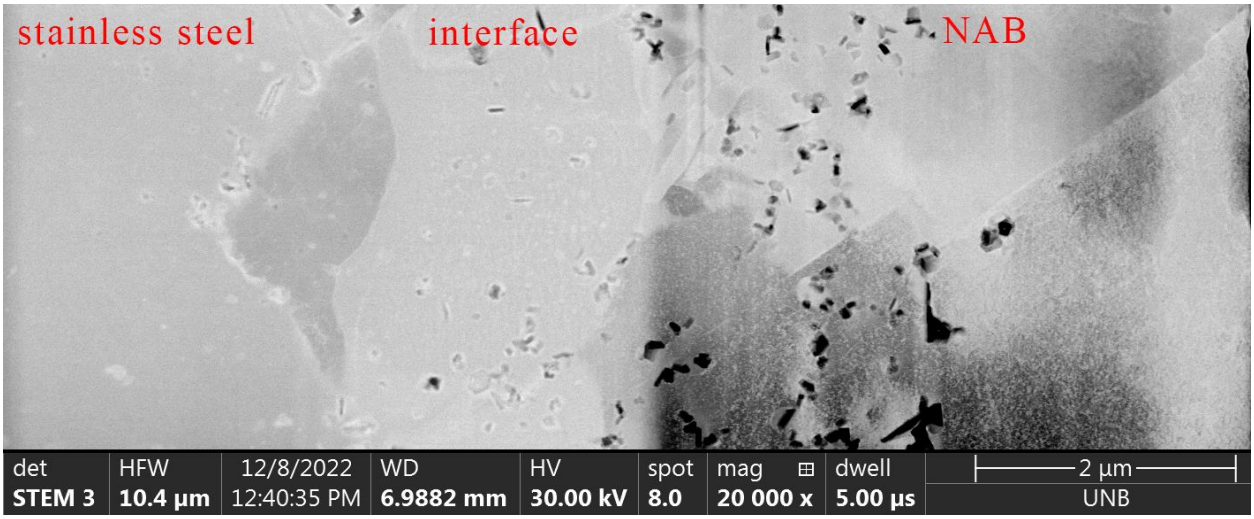

Figure 1. interfacial micrograph of the AM bimetal prepared using FIB milling

[†]Corresponding Author: Email: sshakeri@unb.ca

P08: Observation of Magnetic Bubbles in $BaFe_{12-x-\delta}Sc_xMg_\delta O_{19}$ by Lorentz Microscopy and Electron Holography

Ken Harada[1], Hiroshi Nakajima[2], Keiko Shimada[1], Shigeo Mori[2], and Yoshio Takahashi[3]

[1] CEMS, RIKEN (Institute of Physical and Chemical Research), Hatoyama, Saitama 350–0395, Japan
[2] Department of Materials Science, Osaka Metropolitan Univ., Sakai, Osaka 559–8531, Japan
[3] Research and Development Groupe, Hitachi, Ltd., Hatoyama, Saitama 350–0395, Japan

Hexaferrite magnets are well-known for exhibiting various magnetization structures. In particular, the M-type hexaferrites ($BaFe_{12-x-d}Sc_xMg_dO_{19}$ (BFSMO)) show magnetic bubbles (cylindrical domains and/or magnetization vortices) and stripe-shaped magnetic domains, and Lorentz microscopy has revealed their static structures and dynamical behaviors [1]. We have also developed some transmission electron microscopy techniques to visualize bubbles and stripe-shaped domains in order to clarify the magnetic properties of the materials [2]. Electron holography, however, has not yet been used to observe magnetic bubbles because high magnetic fields must be applied to specimens during observation experiments.

In the present study, we constructed a paired lens system by combining the objective lens and the first intermediate lens and applied it to relatively high magnetic fields up to 500 mT [3]. Figure 1 shows an example of the magnetic bubbles in BFSMO under the magnetic field of 153 mT, where (a) is a Lorentz micrograph of an underfocused Fresnel mode and (b) is a reconstructed phase distribution image. In both micrographs, the bright and dark contrast dots are type-I bubbles respectively indicating clockwise and counterclockwise magnetization vortices.

The developed optical system enabled us to observe and analyze the magnetic bubbles of the type-I, type-II (not shown here), and stripe-shaped domains by utilizing Lorentz microscopy and electron holography.

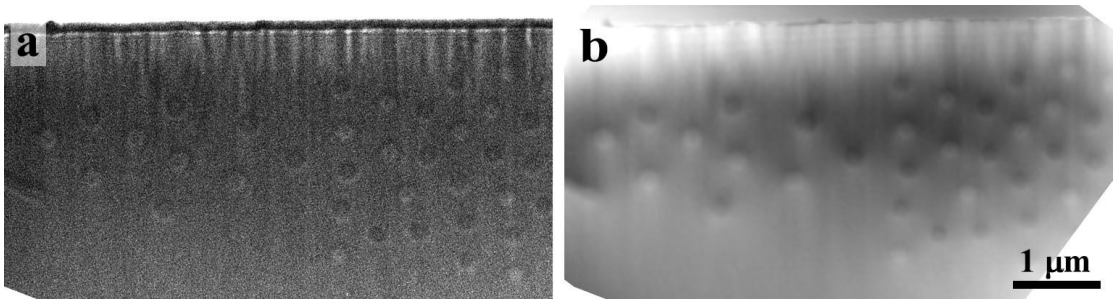

Fig. 1. BFSMO magnetic bubbles: (a) Lorentz micrograph of underfocused Fresnel mode and (b) reconstructed phase distribution image by electron holography.

References

[1] X. Z. Yu et al., PNAS, **109**, (2012) 8856.
[2] H. Nakajima et al., Jpn. J. Appl. Phys., **60**, (2021) 123003.
[3] K. Harada et al., Micron, **160**, (2022) 103306.

This work was supported by JSPS Grant-in-Aid for Scientific Research (KAKENHI) Grant Number JP20K20555.

P09: Investigation of InGaN/GaN NW p-i-n junctions using Electron Holography.

Anitha Jose[1], Maria Tchernycheva[2], Noëlle Gogneau[2], Cristina Cordoba[3], Arthur Blackburn[3], Martha McCartney[4], and Karen L. Kavanagh[1]

[1]Department of Physics, Simon Fraser University, Burnaby, British Columbia, Canada
[2]Centre for Nanoscience and Nanotechnology - C2N (CNRS / Université Paris-Sud), 91120 Palaiseau, France
[3]Department of Physics and Astronomy, University of Victoria, Victoria, BC, Canada
[4] Department of Physics, Arizona State University, Tempe, AZ 85287, USA
e-mail: anithaj@sfu.ca

GaN-based nanowire (NW) junctions have been applied in devices including light emitting diodes (LEDs) [1], photodetectors [2] and laser diodes [3]. We report the characterization of an n-GaN/InGaN/p-GaN structure using electron holography (EH) [4] for potential applications as LEDs. The NWs were grown by Molecular Beam Epitaxy using Si and Mg as the n-type and p-type dopant, respectively, on a Si substrate. SEM images of the sample on the substrate showed two kinds of wires distinguishable by their lengths. One set were more than a micron long and the other shorter, about 700-800 nm. They differed also in the effects of In on TEM image contrast, the rate of tapering in the diameters, and therefore, the expected junction positions. The longer wires had a sharp change in diameter on transitioning to the InGaN region whereas the shorter wires were of uniform diameter at the junction and tapered towards the bottom end of the wire. The longer n-type side on the top in the long wires had a high density of stacking faults when compared to the shorter wires. EH experiments were carried out on the two sets to estimate the electric potential distribution in the wires. This confirmed that the position of the junction was different in the two sets, with a higher built-in potential in the long wires when compared to the shorter wires. However, both values were smaller than that expected based on planar dopant calibrations. Modelling of the electric potential in the structure including effects of intrinsic polarization and piezoelectric effects, are underway to explain the observed potential profile.

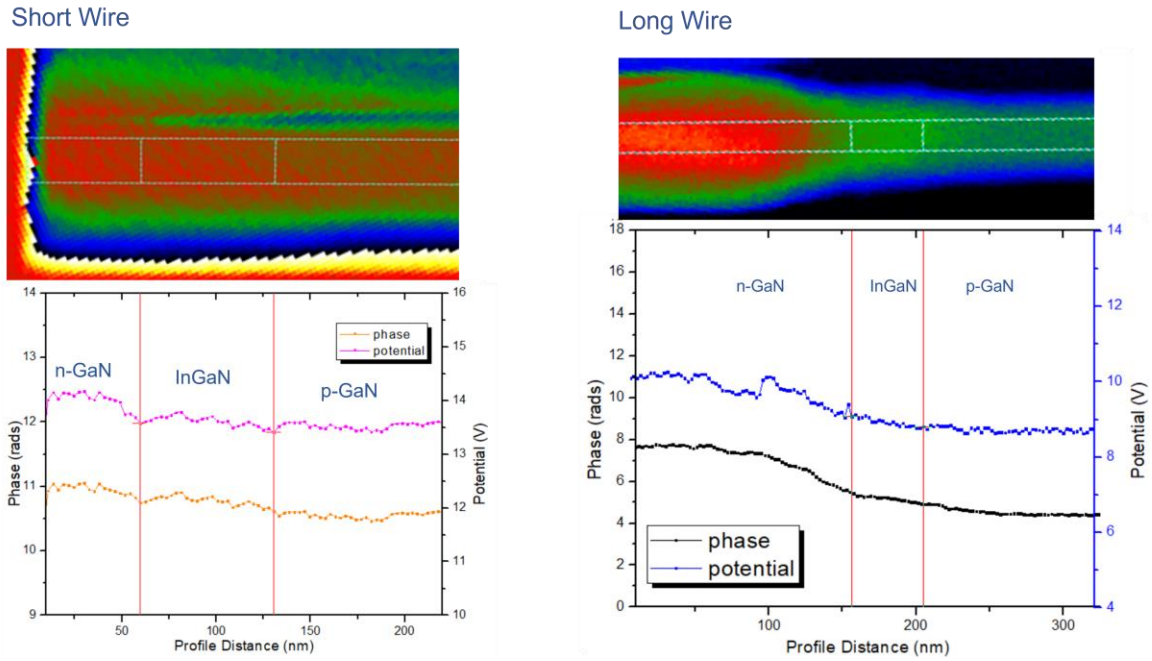

Fig 1. Phase images and corresponding phase and potential profiles of short and long wire

References

[1] C.-Y. Chen et. al, ACS Nano, **6**, 5687-5692 (2012).
[2] X. Zhang et al, J. Mater. Chem. C **5**, 4319-4326 (2017).
[3] J. Heo et al, Appl.Phys. Lett. **98**, 21110 (2011).
[4] M. Lehmann and H. Lichte, Microscopy and Microanalysis **8**, 447 (2002).